MODELING AND DEVELOPMENT OF THREE-DIMENSIONAL GEL DOSIMETERS

by

Abdullah T Nasr

A thesis submitted to the Department of Chemical Engineering

In conformity with the requirements for

the degree of Doctor of Philosophy

Queen's University

Kingston, Ontario, Canada

March, 2014

Abstract

A dynamic mathematical model was developed to simulate the response of polyacrylamide gel (PAG) dosimeters to a single spherical radioactive brachytherapy seed. Simulations were conducted for a high dose-rate (HDR) seed using ^{192}Ir and a low dose-rate (LDR) seed using ^{125}I. The model is able to predict the amount of polymer formed, the crosslink density, and the volume fraction of aqueous phase as a function of radial distance and time. Results show that PAG dosimeters can provide accurate HDR brachytherapy dosimetry at distances larger than 4 mm from the centre of the seed but will give poor results for LDR due to monomer diffusion.

Experiments were conducted to evaluate the potential for using pentacosa-10,12-diynoic acid (PCDA) as the reporter molecule in micelle gel dosimeters for optical computed tomography (CT) readout. Several gels containing PCDA that was solubilized using sodium dodecyl sulfate (SDS) responded to radiation by changing from colourless to blue. Unfortunately, all phantoms that showed colour changes were turbid, making them unsuitable for optical CT scanning. Several techniques were used to produce transparent gels containing PCDA but none of these gels responded noticeably to radiation. Only turbid gels with precipitated PCDA responded, indicating that the colour change was due to oligomerization within PCDA crystals and that PCDA molecules solubilized in micelles did not undergo oligomerization. As a result, PCDA is not suitable for use in radiochromic micelle gel dosimeters.

A new recipe for a radiochromic leuco crystal violet (LCV) micelle gel dosimeters with enhanced dose sensitivity was developed for optical CT readout. The recipe contains LCV, trichloro acetic acid (TCAA), Cetyl Trimethyl Ammonium

Bromide (CTAB), 2,2,2-Trichloroethanol (TCE), and gelatin. Experiments were conducted to improve understanding about interactions between the different components of LCV micelle gel, highlighting the importance of pH on dose sensitivity and transparency. Results also showed the effectiveness of chlorinated compounds in improving dose sensitivity. Statistical techniques were used to build empirical models that were used to optimize the gel recipe. Additional testing in larger phantoms will be required to assess the effectiveness of the proposed gel for clinical dosimetry.

Co-Authorship

The research that is presented in this thesis was conducted independently by me, under the supervision and guidance of Dr. K. B. McAuley of the Department of Chemical Engineering at Queen's University, and Dr. L. J. Schreiner of the Cancer Centre of Southeastern Ontario and the Departments of Physics and Oncology at Queen's University. A portion of the material in Chapter 1 has been published in *Journal of Physics: Conference Proceedings*. Material in Chapter 2 has been published in *Macromolecular Theory and Simulations*. Material presented in Chapter 3 has been published in *Physics in Medicine and Biology*. A journal article based on research material in Chapter 4 is in preparation and will be submitted in the future.

I prepared the first and subsequent drafts for all the manuscripts, performed all of the experiments and calculations and simulations, and generated all of the figures and tables. Dr. K. B. McAuley is co-author of the paper associated with Chapter 1. Dr. K. B. McAuley and Dr. L. J. Schreiner are co-authors of the journal articles in Chapters 2 to 4. They helped to formulate research objectives, they provided technical advice and they edited the thesis and suggested revisions. Dr. Tim Olding of the Cancer Centre of Southeastern Ontario and the Department of Physics at Queen's University assisted with irradiation of samples for the research material presented in Chapter 3 and is a co-author in the journal article presented in Chapter 3. Mr. Kevin Alexander of the Department of Physics at Queen's University assisted with irradiation of samples for the research material presented in Chapter 4 and will be a co-author in the journal article presented in Chapter 4.

Acknowledgements

First and foremost I thank ALLAH, the most gracious and the most merciful, who has guided me and bestowed his mercy and favours upon me and has helped me getting this far. Next, I would like to thank my parents for their prayers, patience and support, which I will never be able to pay back.

I would especially like to thank my supervisors, Dr. Kim McAuley and Dr. John Schreiner, for their support, advice and encouragement throughout my research at Queen's University. I was blessed to work with such smart, dedicated, and friendly people. I would exceptionally like to express my sincerest and deepest gratitude to Dr. Kim McAuley who is, above all, a sincere and understanding person for making a big difference in my life since the first time I met her on November 25th 2009.

I would like to thank my brothers and sisters for their continuous support and encouragement. I would especially like to thank my lovely wife Ghada, the closest to me. She was beside me in every step of the way towards this PhD. I could have not done this work without her. She is the best thing that happened to me. I would like to thank my two daughters, Batool and Sarah, for their smiles and laughter that kept me going.

I would like to thank Dr. Fouad Teymour from Illinois Institute of Technology and Dr. Said Al-Hallaj from University of Illinois at Chicago for their help and support. Many thanks to the faculty, staff and students of the department of Chemical Engineering at Queen's University, especially my officemates in G-36 who have made my stay at Queen's very enjoyable. Particular thanks are due to Jonathan Chain who showed me how to run the simulations and how to make gels. Finally, I would like to thank Dr. Tim Olding and Kevin Alexander who helped me in irradiating the gel samples.

Table of Contents

List of Figures

List of Tables

Chapter 1

Introduction

1.1 Background

Many patients requiring cancer treatment receive radiation therapy. Clinical radiation therapy uses powerful ionizing radiation to damage the DNA in cancer cells (National Cancer Institute 2013). Dose delivery techniques can involve either external beam radiation (e.g., high energy photons or electrons produced by a linear accelerator) or internal radiation therapy (called brachytherapy) wherein radioactive sources are placed inside or adjacent to the tumour to deliver the radiation dose (Erickson *et al.* 2011, Rosenthal *et al.* 2011, National Cancer Institute 2013). Besides killing cancer cells, radiation therapy can also damage healthy cells adjacent to the tumour. Therefore, treatment plans are carefully designed to minimize the exposure of the healthy tissues to harmful irradiation. Treatment plans are developed for each patient by first taking detailed imaging scans to determine the exact location, shape and size of the tumour and organs at risk. Based on those scans, the treatment team develops a detailed plan describing the total radiation dose that should be delivered to the tumour, the intensity and duration of irradiation, and the safest angles (paths) for external-beam radiation delivery (National Cancer Institute 2013).

With the increasing complexity of modern radiation treatment techniques, sophisticated quality assurance procedures must be developed to ensure that the prescribed radiation dose is delivered to the tumour, while sparing the healthy tissue. As part of quality assurance systems, radiation dosimeters are used by medical physicists to assure that the equipment delivers the intended dose to the correct location. Point-dose

measurements (e.g., ionization chambers) and two-dimensional (e.g. radiochromic film) dosimetry techniques are routinely used in radiation clinics to measure radiation dose (Baldock *et al.* 2010). However, with rapid advancements in treatment techniques, dosimeters that measure entire three-dimensional (3D) dose distributions have become invaluable for full evaluation of delivered radiation doses. A 3D dosimeter that is irradiated instead of a patient as part of a quality assurance program is called a phantom.

3D radiation dosimeters are devices fabricated from radiation-sensitive materials that, upon irradiation, undergo changes that are detectable and quantifiable. These changes are indicative of the amount and spatial distribution of the absorbed radiation dose (Adamovics 2006, Baldock *et al.* 2010). Detectable changes include changes in optical properties (e.g., color, transparency), density and nuclear magnetic resonance (NMR) properties (Hurley *et al.* 2006)

The response of an ideal 3D dosimeter should be measurable, reproducible, and stable (De Deene 2004). Ideally, the response should not be sensitive to environmental conditions that may vary during irradiation and scanning such as humidity, light, temperature, pressure, and atmospheric gases. The response of the 3D dosimeter should depend on the total radiation dose delivered, but should not be influenced by the radiation dose rate or the energy of the radiation beam. Examples of current 3D dosimeters are Fricke gel dosimeters, polymer gel dosimeters, PRESAGE plastic dosimeters, and micelle gel dosimeters (Gore *et al.* 1984, Appleby *et al.* 1987, Maryanski *et al.* 1993, Maryanski *et al.* 1994, Schreiner 2004, Adamovics 2006, Adamovics and Maryanski 2006, Guo *et al.* 2006, Hurley *et al.* 2006, Babic *et al.* 2009, Jordan and Avvakumov 2009, Baldock *et al.* 2010, Vandecasteele *et al.* 2011).

Imaging techniques that are used to extract information from current 3D dosimeters include Magnetic Resonance Imaging (MRI), optical Computed Tomography (CT) and x-ray CT (Maryanski *et al.* 1993, Maryanski *et al.* 1994, Jirasek *et al.* 2010, Olding *et al.* 2011). Fricke gel and polyacrylamide gel (PAG) are examples of dosimeters that are traditionally read out by magnetic resonance imaging (MRI). Use of MRI scanners for read out of clinical phantoms is problematic due to cost, accessibility, and special skills required for quantitative MRI (Vandecasteele *et al.* 2011). Optical CT scanners are a promising alternative to MRI because they are cheaper, easier to use, and more accessible in most clinical environments (Doran 2009, Olding *et al.* 2011, Vandecasteele *et al.* 2011). These advantages of optical CT scanners have stimulated the development of optically clear radiochromic 3D dosimeters such as PRESAGE and radiochromic micelle gel dosimeters (Adamovics 2006, Adamovics and Maryanski 2006, Babic *et al.* 2009, Jordan and Avvakumov 2009, Vandecasteele *et al.* 2011).

1.1.1 Fricke Gel Dosimeters

Fricke or ferrous sulfate solutions, wherein the response to irradiation depends on the dose dependent transformation of ferrous (Fe^{2+}) ions into ferric (Fe^{3+}) ions, have been used to measure radiation doses for many years (Fricke and Morse 1927). The initiation of modern 3D dosimetry is related to two important developments. The first development was the use of MRI to detect and quantify radiation-induced changes in Fricke solutions (Gore *et al.* 1984). The second development was the spatial stabilization of dose information by dispersing Fricke solution throughout a gel matrix (Appleby *et al.* 1987). Unfortunately, the poor spatial stability of Fricke gels due to diffusion of Fe^{3+} ions constrains the permissible time between irradiation and measurements (Schreiner 2004).

A small but beneficial reduction in diffusion rates has been obtained using different gelling agents (gelatin, agarose, sephadex and polyvinyl alcohol) and chelating agents such as xylenol orange, which induces colour changes that permit optical imaging (Baldock *et al.* 2001, Baldock *et al.* 2010).

Fricke gels are attractive for 3D dosimetry as they are easy to prepare and give reproducible results (Schreiner 2004). However, like other popular gels used in dosimetry, Fricke gels are sensitive to conditions during preparation, irradiation and read-out (e.g. impurities and temperature) (Schreiner 2004). Although Fricke gel dosimeters may seem to be simple at first glance, Monte Carlo simulations that predict the fundamental behaviour of Fricke solutions (without a gelling agent) account for more than 60 chemical reactions to simulate interactions between radiation and oxygenated water. Eleven or more additional reactions are required to account for interactions with SO_4^{2-} and Fe^{2+} (Meesungnoen *et al.* 2001, Autsavapromporn *et al.* 2007, Meesat 2012, Meesat *et al.* 2012). Additional reactions would be required to account for interactions with gelatin and a chelating agent. As a result, Fricke gel dosimeters are not really that simple. This inherent level of complexity should be kept in mind when evaluating other potential 3D dosimeters.

1.1.2 Polymer Gel Dosimeters

Polymer gel dosimeters are the most widely used 3D gel dosimeters. They contain water and gelatin, along with monomers and crosslinkers that polymerize in response to free radicals generated by water radiolysis (Baldock *et al.* 2010). The amount of crosslinked polymer that forms and precipitates at each location in the gel depends on the local radiation dose and the local concentration of monomer and crosslinker. Formation

of tightly crosslinked polymer particles (micro-gels) induces changes in the physical properties of the dosimeter that can be detected using several imaging techniques (e.g., MRI, optical CT and x-ray CT scans) (Maryanski *et al.* 1993, Maryanski *et al.* 1994, Jirasek *et al.* 2010, Olding *et al.* 2011). The radiation dose distribution can then be estimated from the resulting 3D images and used to verify the treatment plan that was applied (Baldock *et al.* 2010).

A variety of different monomers and crosslinkers have been tested for use in polymer gel dosimeters (Baldock *et al.* 2010). Polyacrylamide gel (PAG) dosimeters are the most studied because they have fewer problems with dose-rate sensitivity and temperature sensitivity than other polymer gel dosimeters. PAG dosimeters consist of acrylamide (Aam) monomer and N,N'-methylene-bisacrylamide (Bis) crosslinker (see Figure 1.1) dissolved in an aqueous gelatin matrix. The main reactions that occur during free radical copolymerization of acrylamide and bisacrylamide are shown via a cartoon in figure 1.2. Although linear polyacrylamide is water-soluble, crosslinked polyacrylamide precipitates. The precipitated polymer is held in position by the gelatin matrix, preserving spatial information via a more effective means than in Fricke gel dosimeters. Although the precipitated polymer molecules cannot readily diffuse, the unreacted monomers can easily diffuse through the gel during and after irradiation. Consequently, inaccurate dosimetry results can be obtained in situations wherein polymer radicals persist over long periods of time and are able to react with the diffusing monomer and crosslinker (e.g., in oxygen-free (anoxic) PAG gels where radicals can persist for longer than 12 hours (De Deene *et al.* 2006) and in low-dose rate brachytherapy applications where radicals are generated continuously for many weeks (Nasr *et al.* 2012, see chapter 2)). Note that all

current polymer gel dosimeters face this same problem with diffusion of reporter molecules.

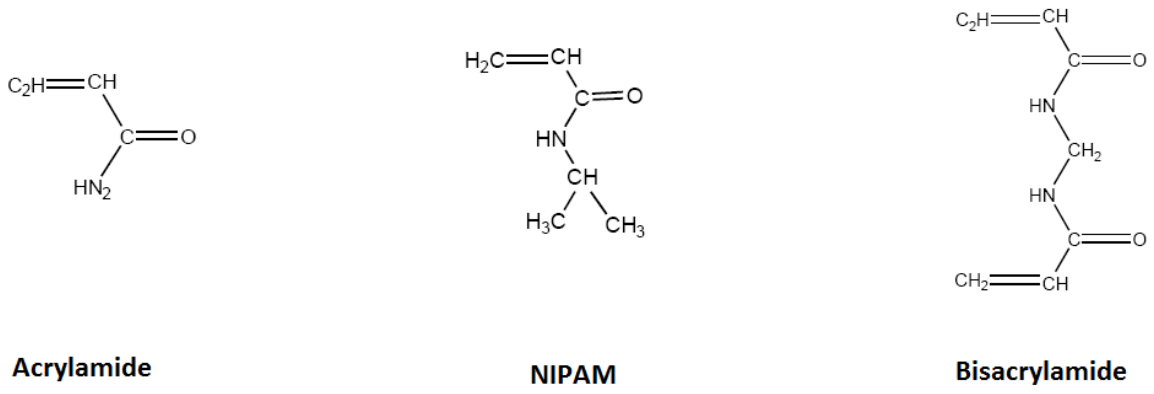

Figure 1.1: Chemical structure of acrylamide and n-isopropyl acrylamide (NIPAM) monomers and bisacrylamide crosslinker used in polymer gel dosimetry. Bisacrylamide is an effective crosslinker because two vinyl groups are available for polymerization.

In some recent dosimetry studies, acrylamide (which is a severe neurotoxin and suspected carcinogen) has been replaced with n-isopropyl acrylamide (NIPAM), shown in Figure 1.1, which has lower toxicity than acrylamide, is less likely to be ingested via inhalation due to its lower volatility, and is less able to pass through human skin (Senden *et al.* 2006, Koeva *et al.* 2009a, Jirasek *et al.* 2010, Chain *et al.* 2011a, Chang KY *et al.* 2011, Chang YJ *et al.* 2011, Hsieh *et al.* 2011, Sedaghat *et al.* 2011a, Jirasek *et al.* 2012, Johnston *et al.* 2012, Pak *et al.* 2012). Note that proper safety precautions (i.e., preparation in a fume hood and use of gloves and goggles) still need to be used when manufacturing these dosimeters. NIPAM-based dosimeters have similar reaction chemistry as the PAG chemistry in Figure 1.2, but seem to be more susceptible to pre-polymerization, which can result in cloudy phantoms prior to irradiation (Senden *et al.* 2006, Koeva *et al.* 2009a, Chain *et al.* 2011a, Sedaghat *et al.* 2011a).

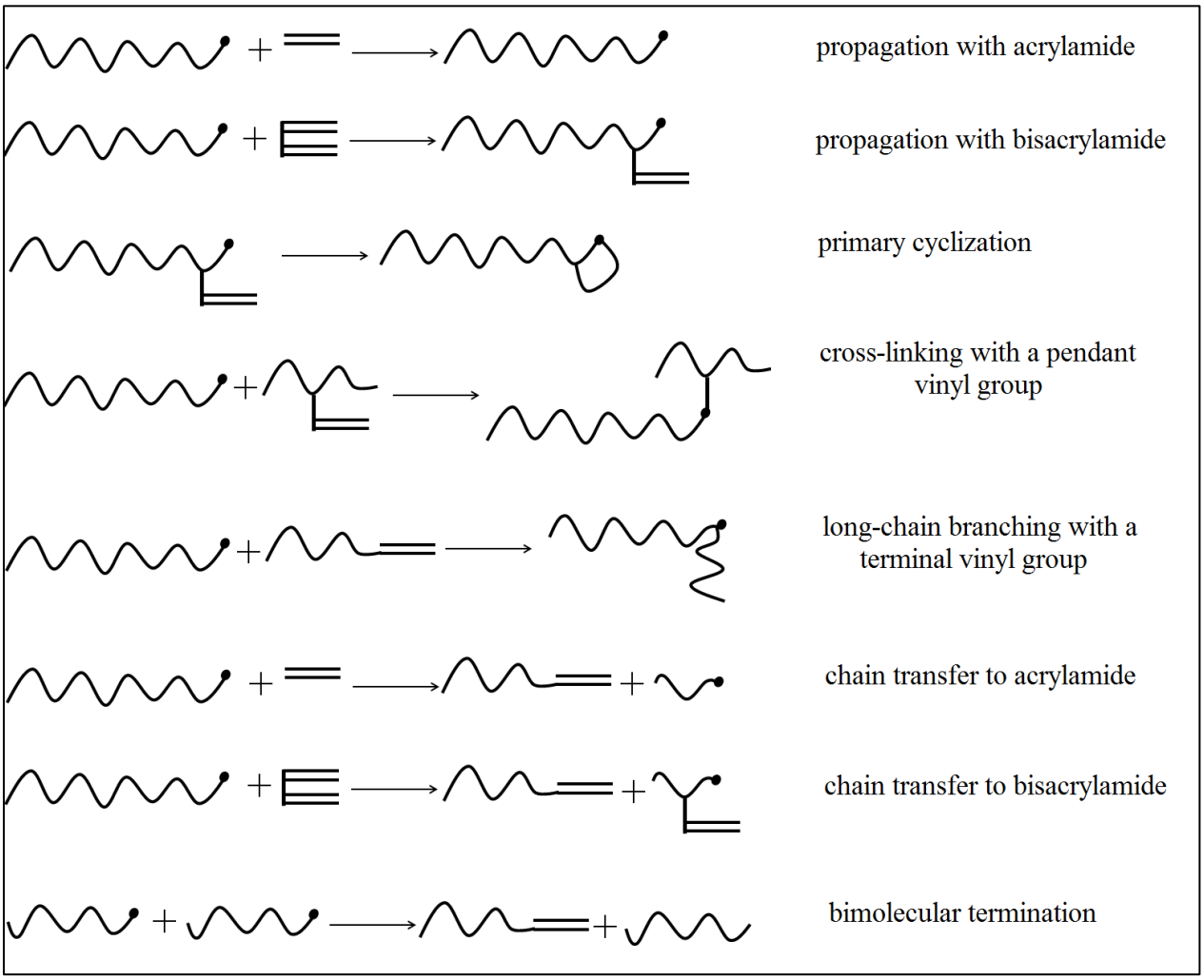

Figure 1.2: Main reactions in free radical copolymerization of acrylamide and bisacrylamide.

The sensitivity of PAG and NIPAM-based polymer gel dosimeters to radiation is directly related to %T, the total weight percent of monomer and crosslinker in the system (Lepage *et al.* 2001a, Hilts *et al.* 2004, De Deene *et al.* 2006), and to %C, the concentration of the crosslinker relative to the total monomer (Maryanski *et al.* 1997, De Deene *et al.* 2006). Increases in both %T and crosslinker concentration tend to produce higher dose sensitivities, as measured by MR and x-ray CT (Maryanski *et al.* 1997, Lepage *et al.* 2001b, Hilts *et al.* 2004, Babic and Schreiner 2006, De Deene *et al.* 2006,

Koeva *et al.* 2009a, Chang KY *et al.* 2011). Measurement accuracy of PAG and NIPAM-based polymer gel dosimeters changes dramatically with %T and %C depending on the read-out technique used. For example, MRI techniques can accurately measure dose distributions in PAG and NIPAM-based gels manufactured using traditional formulations that contains 6%T and 50 %C. However, cone beam optical imaging was complicated by light scattering when used to measure the dose distributions for such gels (Olding *et al.* 2011). Reducing %T from 6 to 4 has improved the accuracy of cone beam optical measurements (Olding *et al.* 2011). When using x-ray CT imaging, increasing %T to as high as 16 % improves dose sensitivity and dose resolution (Jirasek *et al.* 2010). It is clear that different recipes are suitable for use with different read-out techniques.

One of the major difficulties encountered by researchers when making polymer gel dosimeters is oxygen contamination. Oxygen consumes primary free-radicals produced by water radiolysis and inhibits the growth of polymer radicals (Baldock *et al.* 1998, Koeva *et al.* 2009b). Traditionally, PAG dosimeters were manufactured in oxygen-free glove boxes (Baldock *et al.* 1998). More recently, most polymer gel dosimeters are normoxic dosimeters that are manufactured in the presence of air and use an oxygen scavenger such as tetrakis hydroxymethyl phosphonium chloride (THPC) to remove oxygen that is initially dissolved in the gel solution (De Deene *et al.* 2002, Jirasek *et al.* 2006, Senden *et al.* 2006). An additional benefit of using THPC in dosimeter recipes is that it helps to alleviate problems associated with long-lived radicals. Since THPC shortens the time period over which polymerization occurs, problems with edge enhancement (build-up of additional polymer where the dose gradient is high caused by monomer diffusion and subsequent polymerization) are alleviated (i.e., there is a shorter

time period when diffusing monomer and crosslinker can come in contact with polymer radicals). Unfortunately, THPC does not solve problems associated with oxygen that may leak into the phantom between manufacturing and irradiation. Minor oxygen leaks and interactions between this oxygen and THPC can cause severe dose inaccuracy (Sedaghat *et al.* 2011a, Sedaghat *et al.* 2011b, Zehtabian *et al.* 2012). Consequently, internal calibration methods are recommended (e.g., based on depth dose) instead of small calibration vials (Oldham *et al.* 1998, Hilts *et al.* 2000, Jirasek *et al.* 2010, Chain *et al.* 2011b). Unexpected depth-dose behaviour will help to detect when oxygen has leaked into a phantom, so that results from contaminated phantoms can be discarded or used with caution.

Mathematical models have been developed to describe PAG dosimeters under spatially uniform (Fuxman *et al.* 2003, Koeva *et al.* 2009b) and non-uniform (Vergote *et al.* 2004, Fuxman *et al.* 2005, Chain *et al.* 2011b) radiation conditions. These models helped gel dosimetry researchers to better understand the influence of chemical and physical phenomena that occur in PAG and related dosimeters during and after irradiation. The models have been used to simulate edge enhancement, temporal instability problems (Fuxman *et al.* 2005), oxygen inhibition, (Koeva *et al.* 2009b) and the responses of PAG dosimeters to radiation depth-dose profiles (Chain *et al.* 2011b).

1.1.3 PRESAGE Dosimeters

PRESAGE dosimeters are solid polyurethane-based radiochromic 3D dosimeters, developed by Adamovics and coworkers (Adamovics 2006, Adamovics and Maryanski 2006, Guo *et al.* 2006, Hurley *et al.* 2006). These dosimeters contain a leuco-dye (e.g., leuco malachite green (LMG) or leuco crystal violet (LCV) dye), halogenated

hydrocarbons (e.g., carbon tetrachloride or chloroform) along with other components dissolved in a solid polyurethane matrix (Adamovics 2006, Adamovics and Maryanski 2006, Guo *et al.*, 2006). Upon irradiation, the colourless leuco-dye is converted to a coloured dye. Depending on the recipe used, PRESAGE dosimeters may show post-irradiation spatial stability for ~2 days. They are insensitive to oxygen and environmental conditions (Babic *et al.*, 2009, Baldock *et al.*, 2010). Unfortunately, tissue equivalence of PRESAGE has been an issue for this type of dosimeter (Brown *et al.*, 2008). Also, PRESAGE dosimeters cannot easily be manufactured or molded into anthropomorphic phantoms.

1.1.4 Micelle Gel Dosimeters

Jordan and coworkers developed radiochromic micelle gel dosimeters for optical readout. The gel recipes consist of colourless leuco dyes (e.g., LMG or LCV) dissolved in a hydrogel matrix using a surfactant (Babic *et al.* 2009, Jordan and Avvakumov 2009). The leuco-dye molecules react with free radicals generated by water radiolysis, changing from colourless to deeply coloured as the radiation dose increases. Micelles are self-assembled aggregates of surfactant molecules that have both hydrophilic and hydrophobic parts. Above the critical micelle concentration (CMC), surfactant molecules orient themselves so that their hydrophobic parts repel away from surrounding water toward the centres of the micelles, leaving their hydrophilic parts in contact with water. The main purpose of using micelles in radiochromic micelle gel dosimeters is to solubilize the only sparingly water-soluble leuco-dye molecules within the hydrophobic core of the micelles (Babic *et al.* 2009). A second benefit is that micelles are significantly larger than individual leuco-dye molecules. As a result, the micelles, which contain the

majority of the leuco dye, have low diffusivity within the gel matrix. Using leuco-dye molecules solubilized in micelles as reporter molecules results in improved spatial stability of dose information, compared with micelle-free optical dosimeters such as Fricke gel dosimeters and polymer gel dosimeters (Jordan and Avvakumov 2009). Like Fricke gel dosimeters, micelle gel dosimeters can be manufactured and used under "normoxic" conditions (on a bench top, open to the air).

Current micelle gel dosimeters could benefit from further improvements as they are light sensitive and temperature sensitive during irradiation and tend to fade over time (Babic *et al.* 2009). They also have relatively low dose sensitivity and may or may not have significant dose-rate dependence (Babic *et al.* 2009, Vandecasteele *et al.* 2011). One benefit of using micelles in 3D gel dosimeters is that, unlike traditional gel dosimeters, the reporter molecules do not need to be water soluble. In fact, very low or negligible water solubility will help to reduce diffusion and will improve spatial stability. Consequently, a range of new hydrophobic reporter molecules can be considered for use in 3D micelle gels.

1.2 Thesis outlines and objectives

Work in this thesis is divided into two phases: the first phase involved mathematical modeling and simulation of PAG and NIPAM-based polymer gel dosimeters for brachytherapy applications, and the second phase involves developing improved radio-chromic micelle gel dosimeters for optical read out. Objectives of the first phase, as described in Chapter 2, are:

i) To reformulate and extend the dynamic mathematical model developed by Fuxman *et al.* (2005) to simulate the influence of a spherical

radioactive brachytherapy source on polymer formation and crosslinking in PAG and NIPAM-based polymer gel dosimeters

ii) To investigate whether PAG dosimeters will provide accurate dosimetry for different types of brachytherapy sources including High Dose Rate (HDR) sources and Low Dose Rate (LDR) sources.

In the second phase of this thesis, the potential for improving the leuco-dye micelle gel dosimeters developed by Jordan and his co-workers (Jordan and Avvakumov 2009, Babic *et al.* 2009) is investigated, as discussed in Chapter 3 and Chapter 4. In Chapter 3, the use of diacetylenes as reporter molecules (to replace leuco-dyes) in radio-chromic micelle gel dosimeters is evaluated. In Chapter 4, improved recipes for radiochromic LCV micelle gel dosimeters are developed. Conclusions and recommendations are summarized in Chapter 5.

This thesis has been prepared using a manuscript format. Some paragraphs in the current chapter appeared in a review article (McAuley and Nasr 2013). Chapter 2 has been published in *Macromolecular Theory and Simulations* (Nasr *et al.* 2012), and Chapter 3 has been published in *Physics in Medicine and Biology* (Nasr *et al.* 2013). A journal article based on the research in Chapter 4 is in preparation and will be submitted to *Physics in Medicine and Biology*.

1.3 References for chapter 1

Adamovics JA 2006 three dimensional dosimeter for penetrating radiation and method of use *United States Patent # US 7098463B2*.

Adamovics J and Maryanski M 2006 Charaterisation of PRESAGE: a new 3D radio chromic solid polymer dosimeter for ionizing radiation *Radiation Protection Dosimetry.* **120** 107–112

Appleby A, Christman EA and Leghrouz A 1987 Imaging of spatial radiation dose distribution in agarose gels using magnetic resonance. *Med. Phys.* **14** 382-384.

Autsavapromporn N, Meesungnoen J, Plante I and Jay-Gerin JP 2007 Monte Carlo simulation study of the effects of acidity and LET on the primary free-radical and molecular yields of water radiolysis: Application to the Fricke dosimeter *Can. J. Chem.* **85** 214–229.

Babic S and Schreiner L J 2006 An NMR relaxometry and gravimetric study of gelatin-free aqueous polyacrylamide dosimeters *Phys. Med. Biol.* **51** 4171–87.

Babic S, Battista J and Jordan K 2009 Radiochromic leuco dye micelle hydrogels: II. Low diffusion rate leuco crystal violet gel *Phys. Med. Biol.* **54** 6791–6808.

Baldock C, Burford RP, Billingham N, Wagner GS, Patval S, Badawi RD and Keevil SF 1998 Experimental procedure for the manufacture and calibration of polyacrylamide gel (PAG) for magnetic resonance imaging (MRI) radiation dosimetry *Phys. Med. Biol.* **43** 695-702.

Baldock C, Harris PJ, Piercy AR and Healy B 2001 Experimental determination of the diffusion coefficient in two-dimensions in ferrous sulphate gels using the finite element method Australas. *Phys. Eng. Sci. Med.* **24** 19–30.

Baldock C, De Deene Y, Doran S, Ibbott G, Jirasek A, Lepage M, McAuley KB, Oldham M, and Schreiner LJ 2010 Polymer gel dosimetry *Phys. Med. Biol.* **55** 1–63.

Brown S, Venning A, De Deene Y, Vial P, Oliver L, Adamovics J, Baldock C 2008 Radiological properties of the PRESAGE and PAGAT polymer dosimeters. *Applied Radiation and Isotopes* **66** 1970–1974.

Chain JNM, Jirasek A, Schreiner LJ and McAuley KB 2011a Cosolvent-free polymer gel dosimeters with improved dose sensitivity and resolution for x-ray CT dose response *Phys. Med. Biol.* **56** 2091-2102.

Chain JNM, Nasr AT, Schreiner LJ and McAuley KB 2011b Mathematical Modeling of Depth-Dose Response of Polymer-Gel Dosimeters *Macromol. Theory Simul.* **20** 735–751.

Chang KY, Shih TY, Hsieh BT, Chang SJ, Liu YL, Wu TH and Wu J 2011 Investigation of the dose characteristics of an n-NIPAM gel dosimeter with computed tomography *Nuclear Instruments and Methods in Physics Research A* **652** 775–778.

Chang YJ, Hsieh BT and Liang JA 2011 A systematic approach to determine optimal composition of gel used in radiation therapy *Nuclear Instruments and Methods in Physics Research A* **652** 783–785.

De Deene Y, Hurley C, Venning A, Vergote K, Mather M, Healy BJ and Baldock C 2002 A basic study of some normoxic polymer gel dosimeters *Phys. Med. Biol.* **47** 3441–3463.

De Deene Y 2004 Essential characteristics of polymer gel dosimeters *J. Physics. Conference Series* **3**, 34–57.

De Deene Y, Vergote K, Claeys C and DeWagter C 2006 The fundamental radiation properties of normoxic polymer gel dosimeters: a comparison between a methacrylic acid based gel and acrylamide based gels *Phys. Med. Biol.* **51** 653–73.

Doran SJ 2009 The history and principles of optical computed tomography for scanning 3-D radiation dosimeters: 2008 update *Journal of Physics:Conference Series* **164**, 012020.

Erickson BA, Demanes DJ, Ibbott GS, Hayes JK, Hsu CJ, Morris DE, Rabinovitch RA, Tward JD and Rosenthal SA, 2011 American Society for Radiation Oncology (ASTRO) and American College of Radiology (ACR) Practice Guideline for the Performance of High-Dose-Rate Brachytherapy *I. J. Radiation Oncology Biol. Phys.* **79-2** 641-649.

Fricke H and Morse S 1927 The chemical action of Roentgen rays on dilute ferrous sulphate solutions as a measure of radiation dose *Am. J Roent. Radium Ther. Nucl. Med* **18** 430.

Fuxman AM, McAuley KB and Schreiner LJ 2003 Modeling of Free-radical Crosslinking Copolymerization of Acrylamide and N,N'-Methylenebis(acrylamide) for Radiation Dosimetry *Macromol. Theory Simul.* **12** 647-662.

Fuxman AM, McAuley KB and Schreiner LJ 2005 Modeling of polyacrylamide gel dosimeters with spatially non-uniform radiation dose distributions *Chem. Eng. Sci.* **60** 1277-9337.

Gore JC, Kangt YS and Schulz RJ 1984 Measurement of radiation dose distributions by nuclear magnetic resonance (NMR) imaging *Phys. Med. Biol.* **29** 1189-1197.

Guo PY, Adamovics JA and Oldham M 2006 Characterization of a new radiochromic three-dimensional dosimeter *Med. Phys.* **33** 1338-1345.

Hilts M, Audet C, Duzenli C and Jirasek A 2000 Polymer gel dosimetry using x-ray computed tomography: a feasibility study *Phys. Med. Biol.* **45** 2559-2571.

Hilts M, Jirasek A and Duzenli C 2004 Effects of gel composition on the radiation induced density change in PAG polymer gel dosimeters: a model and experimental investigations *Phys. Med. Biol.* **49** 2477–2490.

Hurley C, McLucas C, Pedrazzini G and Baldock C 2006 High-resolution gel dosimetry of a HDR brachytherapy source using normoxic polymer gel dosimeters: Preliminary study *Nuclear Instruments and Methods in Physics Research A* **565** 801–811.

Hsieh BT, Chang YJ, Han RP, Wu J, Hsieh LL and Chang CJ 2011 A study on dose response of NIPAM-based dosimeter used in radiotherapy *J Radioanal Nucl Chem* **290** 141–148.

Jirasek A, Hilts M, Shaw C and Baxter P 2006 Investigation of tetrakis hydroxymethyl phosphonium chloride as an antioxidant for use in x-ray computed tomography polyacrylamide gel dosimetry *Phys. Med. Biol*. **51** 1891–1906.

Jirasek A, Hilts M and McAuley KB 2010 Polymer gel dosimeters with enhanced sensitivity for use in x-ray CT polymer gel dosimetry *Phys. Med. Biol.* **55** 5269-5281.

Jirasek A, Carrick J and Hilts M 2012 An x-ray CT polymer gel dosimetry prototype: I. Remnant artefact removal *Phys. Med. Biol.* **57** 3137–3153.

Johnston H, Hilts M, Carrick J and Jirasek A 2012 An x-ray CT polymer gel dosimetry prototype: II. Gel characterization and clinical application *Phys. Med. Biol.* **57** 3155–3175.

Jordan K and Avvakumov N 2009 Radiochromic leuco dye micelle hydrogels: I. Initial investigation *Phys. Med. Biol.* **54** 6773–6789.

Koeva VI, Olding T, Jirasek A, Schreiner LJ and McAuley KB 2009a Preliminary investigation of the NMR, optical and x-ray CT dose–response of polymer gel dosimeters incorporating cosolvents to improve dose sensitivity *Phys. Med. Biol.* **54** 2779-2790.

Koeva VI, Daneshvar S, Senden RJ, Imam AHM, Schreiner LJ and McAuley KB 2009b Mathematical Modeling of PAG and NIPAM Based Polymer Gel Dosimeters Contaminated by Oxygen and Inhibitor *Macromol. Theory Simul.* **18** 495-510.

Lepage M, Jayasakera PM, Back SAJ and Baldock C 2001a Dose resolution optimization of polymer gel dosimeters using different monomers *Phys. Med. Biol.* **46** 2665–2680.

Lepage M, Whittaker AK, Rintoul L, Back SAJ and Baldock C 2001b The relationship between radiation-induced chemical processes and transverse relaxation times in polymer gel dosimeters *Phys. Med. Biol.* **46** 1061–74.

Maryanski MJ, J. C. Gore JC, Kennan RP and Schulz RJ 1993 NMR relaxation enhancement in gels polymerized and cross-linked by ionizing radiation: a new approach to 3D dosimetry by MRI *Magn. Reson. Imaging.* **11** 253–258.

Maryanski MJ, Schulz RJ, Ibbott GS, Gatenby JC, Xie J, Horton D and Gore JC 1994 Magnetic resonance imaging of radiation dose distributions using a polymer-gel dosimeter *Phys. Med. Biol.* **39** 1437–1455.

Maryanski M J, Audet C and Gore J C 1997 Effects of crosslinking and temperature on the dose response of a BANG polymer gel dosimeter *Phys. Med. Biol.* **42** 303–11.

McAuley KB and Nasr AT 2013 Fundamentals of Gel Dosimeters *Journal of Physics: Conf. Ser.* **444** 012001

Meesat R 2012 Ph.D. Thesis in Radiation Sciences and Biomedical Imaging *Université de Sherbrooke Sherbrooke, Québec, Canada*.

Meesat R, Sanguanmith S, Meesungnoen J, Lepage M, Khalil A and Jay-Gerina JP 2012 Utilization of the Ferrous Sulfate (Fricke) Dosimeter for Evaluating the Radioprotective Potential of Cystamine: Experiment and Monte Carlo Simulation *Radiation Research* **177** 813–826.

Meesungnoen J, Benrahmoune M, Filali-Mouhim A, Mankhetkorn S and Jay-Gerin JP 2001 Monte Carlo calculation of the primary radical and molecular yields of liquid water radiolysis in the linear energy transfer range 0.3–6.5 keV/lm: application to 137Cs gamma rays *Radiation Research* **155** 269–78.

Nasr AT, Schreiner LJ and McAuley KB 2012 Mathematical Modeling of the Response of Polymer Gel Dosimeters to HDR and LDR Brachytherapy Radiation *Macromol. Theory Simul.* **21** 36–51.

Nasr AT, Olding T, Schreiner LJ, and McAuley KB 2013 Evaluation of the potential for diacetylenes as reporter molecules in 3D micelle gel dosimetry *Phys. Med. Biol.* **58** 787–805

National cancer institute, fact sheet: radiation therapy for cancer, http://www.cancer.gov/cancertopics/factsheet/Therapy/radiation (October. 2013)

Oldham M, McJury M, Baustert IB, Webb S and Leach MO 1998 Improving calibration accuracy in gel dosimetry *Phys. Med. Biol.* **43** 2709.

Olding T, Holmes O, DeJean P, McAuley KB, Nkongchu K, Santyr G and Schreiner LJ 2011 Small field dose delivery evaluations using cone beam optical computed tomography-based polymer gel dosimetry *Journal of Medical Physics.* **36** 3-14.

Pak F, Farajollahi A and Miabi Z 2012 SU-E-T-150: The Basic Dosimetric Properties of NIPAM Polymer Gel Dosimeter *Med. Phys.* **39** 3737.

Rosenthal SA, Bittner NHJ, Beyer DC, Demanes DJ, Goldsmith BJ, Horwitz EM, Ibbott GS, Lee WR, Nag S, Suh WW and Potters L 2011 American society for radiation oncology (ASTRO) and American college of radiology (ACR) practice guideline for the transperineal permanent brachytherapy of prostate cancer *I. J. Radiation Oncology Biol. Phys.* **79- 2** 353-341.

Schreiner LJ 2004 Review of Fricke gel dosimeters *Journal of Physics: Conference Series* **3** 9–21.

Schreiner LJ 2006 Dosimetry in modern radiation therapy: limitations and needs *Journal of Physics: Conference Series.* **56** 1–13.

Sedaghat M, Bujold R and Lepage M 2011a Investigating potential physicochemical errors in polymer gel dosimeters *Phys. Med. Biol.* **56** 6083–6107.

Sedaghat M, Bujold R and Lepage M 2011b Severe dose inaccuracies caused by an oxygen-antioxidant imbalance in normoxic polymer gel dosimeters *Phys. Med. Biol.* **56** 601–625.

Senden RJ, De Jean P, McAuley KB and Schreiner LJ 2006 Polymer gel dosimeters with reduced toxicity: a preliminary investigation of the NMR and optical dose–response using different monomers *Phys. Med. Biol.* **51** 3301–3314.

Vandecasteele J, Ghysel S, Baete SH and De Deene Y 2011 Radio-physical properties of micelle leucodye 3D integrating gel dosimeters *Phys. Med. Biol.* **56** 627–651.

Vergote K, De Deene Y, Vanden Bussche E and De Wagter C 2004 On the relation between the spatial dose integrity and the temporal instability of polymer gel dosimeters *Phys. Med. Biol.* **49** 4507-4522.

Zehtabian M, Faghihi R, Zahmatkesh MH, Meigooni AS, Mosleh-Shirazi MA, Mehdizadeh S, Sina S and Bagheri S 2012 Investigation of the dose rate dependency of the PAGAT gel dosimeter at low dose rates *Radiation Measurements* **47** 139-144.

Chapter 2

Mathematical modeling of the response of polymer gel dosimeters to HDR and LDR brachytherapy radiation

2.1 Chapter Overview

In this chapter, an existing dynamic model (Fuxman *et al.* 2003, Fuxman *et al.* 2005) is extended and reformulated to simulate the response of polyacrylamide gel (PAG) dosimeters to a single spherical brachytherapy seed using High Dose Rate (HDR) ^{192}Ir and Low Dose Rate (LDR) ^{125}I. Results show that PAG dosimeters can provide accurate HDR brachytherapy dosimetry but will give poor results for LDR due to monomer diffusion. The complete reaction mechanisms, list of reaction rate expressions and the model parameter values used in this model are provided in appendices B, C, D and E of the MSc thesis by Chain (2010). Note that I contributed to the revised reaction mechanism and rate expressions used in Chain's thesis and I am a co-author of the associated journal article (Chain *et al.* 2011b).

The material presented in Chapter 2 of this thesis has been published in *Macromolecular Theory and Simulation* **2012**, *21*, **36–51**

Mathematical modelling of the response of polymer gel dosimeters to HDR and LDR brachytherapy radiation

A T Nasr[1], L J Schreiner[2,3], K B McAuley[1]

[1]Dept. of Chemical Engineering, Queen's University, Kingston, ON, Canada, K7L 3N6

[2]Cancer Centre of Southeastern Ontario, Kingston, ON, Canada, K7L 5P9

[3]Depts. of Oncology and Physics, Queen's University, Kingston, ON, Canada, K7L 3N6

2.2 Summary

A model is developed to simulate the response of polyacrylamide gel (PAG) dosimeters to single spherical brachytherapy seeds. The model predicts the amount of polymer formed and crosslink density as a function of radial distance and time, using either a High Dose Rate (HDR) ^{192}Ir seed or a Low Dose Rate (LDR) ^{125}I seed. Results indicate that PAG dosimeters should provide accurate dosimetry when used for HDR brachytherapy at distances larger than 4 mm from the centre of the seed and that PAG dosimeters will give poor results for LDR dosimetry because of the long time available for the monomer and crosslinker to diffuse toward the seed during polymerization.

2.3 Introduction

Clinical radiation therapy, which is widely used for cancer treatment, uses ionizing radiation to damage DNA in cancer cells (National Cancer Institute 2013). External-beam radiation therapy techniques deliver radiation doses to tumors using radiation beams from outside the body. Internal radiation therapy techniques (also called brachytherapy) use radioactive sources placed inside or adjacent to the tumor to deliver the radiation dose

(Erickson *et al.* 2011, Rosenthal *et al.* 2011, National Cancer Institute 2013). Brachytherapy can involve either permanent implantation of radioactive seeds that decay over time, or temporary implantation of sources that are removed after the planned radiation dose has been delivered.

In permanent implantation, the radiation source usually has a low activity so that the treatment dose is delivered over an extended period of weeks, while in temporary implantation the dose is delivered over a short period of minutes. To say this in another way, brachytherapy sources can be characterized by the dose rate to the adjacent volume. Brachytherapy source are typically divided into three regimes: Low Dose Rate (LDR) sources deliver doses, at 1 cm distance, at rates of 0.4-2 Gy h^{-1}, Medium Dose Rate (MDR) sources deliver doses at rates of 2-12 Gy h^{-1} and High Dose Rate (HDR) sources deliver doses at rates greater than 12 Gy h^{-1} (Gerbaulet *et al.* 2002).

Besides killing cancer cells, radiation therapy can also damage healthy cells, creating challenges for medical physicists and radiation oncologists who need to ensure accurate and sufficient radiation dose delivery to the tumor while minimizing the exposure of the surrounding healthy tissue. Recent developments in imaging techniques and radiation delivery equipment help in obtaining a closer three-dimensional (3D) conformation of the dose distribution to the tumor volume (Schereiner 2006). Radiation dosimeters are used by medical physicists as part of quality assurance systems to test radiation treatment plans and to make sure that the equipment delivers the intended dose to the correct location.

Point-detection radiation dosimetry techniques (e.g., ionization chambers) and two-dimensional (2D) techniques (e.g., radiographic film) are used to measure and

calibrate radiation doses (Baldock *et al.* 2010). However, for dose delivery to irregularly-shaped tumors it is important to have dosimeters that can detect and measure entire 3D dose distributions delivered by external and internal radiation techniques. An ideal 3D dosimeter should have a response that is stable, measurable, significant, well-defined and reproducible (De Deene 2004). The dose response should not be sensitive to temperature, pressure, light and atmospheric gases, as these factors may vary during irradiation and scanning. Dosimeters should be tissue-equivalent for the kind of radiation used. An ideal dosimeter response depends on the total radiation dose delivered, but is not influenced by the radiation dose delivery rate.

Polymer gel dosimeters are 3D dosimeters made of hydrogels, which contain monomers and crosslinkers that polymerize in response to radiation (Baldock *et al.* 2010). The amount of crosslinked polymer that forms and precipitates at each location depends on the local radiation dose. Formation of tightly crosslinked polymer particles (micro-gels) induces changes in the physical properties of the dosimeter, which can be detected using a variety of imaging techniques (e.g., magnetic resonance imaging (MRI), optical computed tomography (CT) and x-ray CT) (Maryanski *et al.* 1993, Maryanski *et al.* 1994, Jirasek *et al.* 2010, Olding *et al.* 2011). The radiation dose distribution can then be determined from the resulting 3D images and used to verify the treatment plan that was applied (Baldock *et al.* 2010).

Polyacrylamide gel (PAG) dosimeters are the most widely studied polymer gel dosimeters (Baldock *et al.* 2010). These dosimeters consist of acrylamide (Aam or M_1) monomer and N,N'-methylene-bisacrylamide (Bis or M_2) crosslinker (see Figure 2.1) dissolved in an aqueous gelatin matrix. Radiation delivered to the dosimeter causes the

dissociation of water molecules into free radicals that induce polymerization (Maryanski *et al.* 1993). Although linear polyacrylamide is water-soluble, crosslinked polyacrylamide becomes insoluble and precipitates. The precipitated polymer is held in position by the gelatin matrix, preserving information about the location of the radiation dose. In some dosimeters acrylamide, a severe neurotoxin and suspected carcinogen, has been replaced with n-isopropyl acrylamide (NIPAM), shown in Figure 2.1, which is still toxic but has lower toxicity than acrylamide and is easier to handle safely (Senden *et al.* 2006, Koeva *et al.* 2009a, Jirasek *et al.* 2010, Chain *et al.* 2011a).

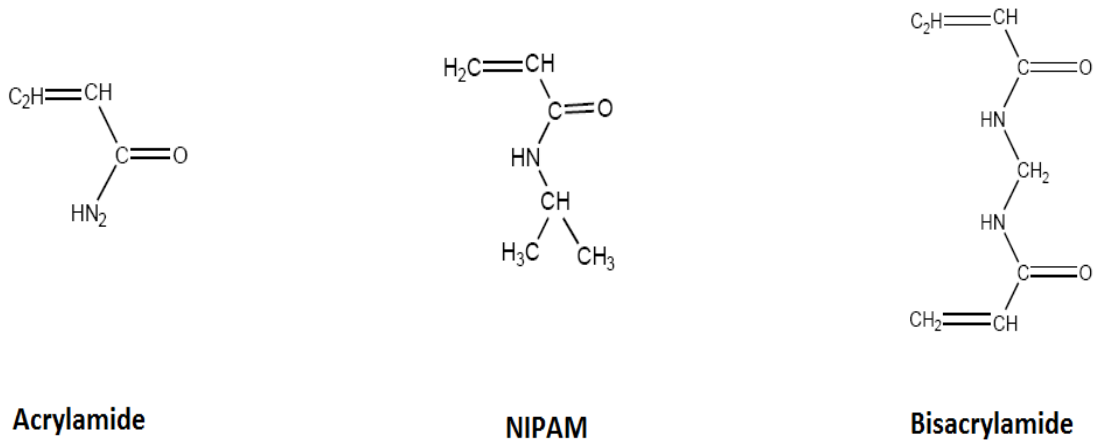

Figure 2.1: Chemical structure of acrylamide and n-isopropyl acrylamide (NIPAM) monomers and bisacrylamide crosslinker used in polymer gel dosimetry. Bisacrylamide is an effective crosslinker because two vinyl groups are available for polymerization.

One of the major difficulties encountered by researchers when making PAG dosimeters is oxygen contamination. Traditionally, PAG dosimeters were manufactured in oxygen-free glove boxes (Baldock *et al.* 1998a). Such dosimeters are called “anoxic” PAG dosimeters. More recently, most polymer gel dosimeters are “normoxic” dosimeters, which are manufactured under normal bench-top conditions and use an

oxygen scavenger such as tetrakis hydroxymethyl phosphonium chloride (THPC) to remove oxygen from the solution (De Deene *et al.* 2002, Jirasek *et al.* 2006, Senden *et al.* 2006). A typical recipe for a normoxic polymer gel is shown in Table 2.1 (Maryanski *et al.* 1994, Baldock *et al.* 1998a). Water, which is the main component in the dosimeter recipe, helps to ensure a tissue-equivalent response to radiation.

Table 2.1: Typical PAG dosimeter recipe (Maryanski *et al.* 1994, Baldock et. al 1998a)

Component	**Quantity (wt%)**
Monomer (Aam or NIPAM)	3
Crosslinker (Bis)	3
Gelatin	5
Water	89

When MRI is used to read out images from irradiated dosimeter phantoms (see, for example, the phantom in Figure 2.2) (Koeva 2008), the spin-spin relaxation rate R_2 is determined at different locations in the gel (Maryanski *et al.* 1993, Maryanski *et al.* 1994). Calibration curves (see Figure 2.3(b)) that give the relationship between the R_2 values and the radiation dose are then used to determine the dose delivered (in units of Gy) at each location. The calibration curve in Figure 2.3(b) (De Deene 2004) was obtained by uniformly irradiating a set of vials containing the polymer gel using different known doses (Figure 2.3(a)) (Koeva *et al.* 2009b). Polymerization in PAG phantoms continues for several hours after irradiation ceases, so the vials are typically scanned one day after irradiation to ensure stable R_2 readings (Baldock *et al.* 2010). Note that the polymer gel phantom in Figure 2.2 received a non-uniform radiation dose that physicists delivered using a series of external radiation beams from different directions (Koeva

2008). For brachytherapy dosimetry, calibration curves are sometimes obtained using externally-irradiated vials (McJury *et al.* 1999, Lin *et al.* 2009), but they can also be obtained by irradiating a phantom with a single brachytherapy seed (De Deene *et al.* 2001, Pantelis *et al.* 2005, Hurley *et al.* 2006, Papagiannis *et al.* 2006). The delivered dose at different distances from the centre of the brachytherapy seed can be accurately calculated using well-known equations (e.g., see equation 2.1 in the next section) and correlated with the measured R_2 response to construct an R_2 vs. dose curve, similar to the one shown in Figure 2.3(b).

Mathematical models have been developed to describe PAG dosimeters under spatially uniform (Fuxman *et al.* 2003, Koeva *et al.* 2009b) and non-uniform (Vergote *et al.* 2004, Fuxman *et al.* 2005) radiation conditions. These models help gel dosimetry researchers to better understand the influence of chemical and physical phenomena that occur in PAG dosimeters during and after irradiation. The models have been used to simulate edge enhancement and temporal instability problems (Fuxman *et al.* 2005), as well as oxygen inhibition (Koeva *et al.* 2009b) and the response of PAG dosimeters to radiation depth-dose profiles (Chain *et al.* 2011b).

Figure 2.2: Photograph of a non-uniformly irradiated polymer gel dosimeter (Koeva 2008), used with permission. The white opaque regions received a higher radiation dose than the surrounding transparent regions in the gel. This dosimeter was irradiated using external Co-60 radiation beams from different directions.

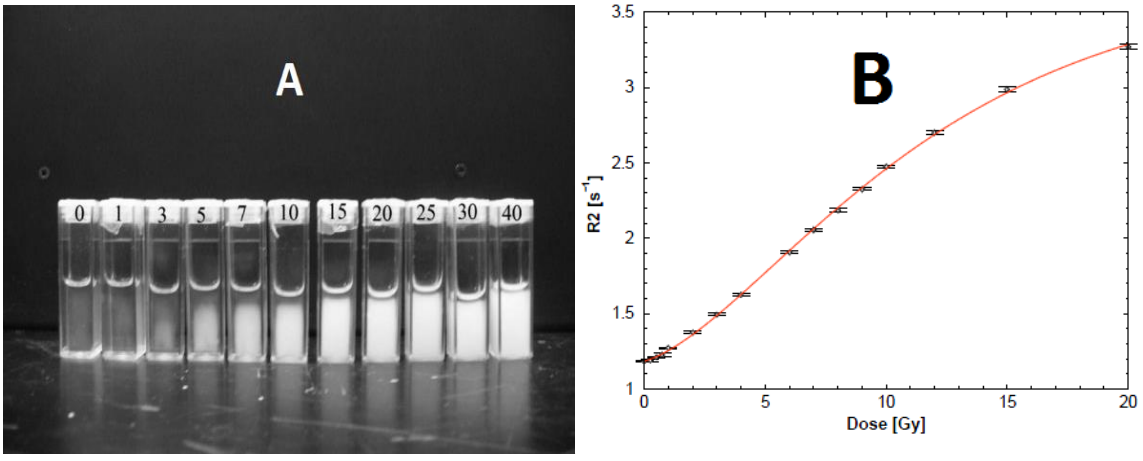

Figure 2.3: Construction of calibration curves for use in polymer gel dosimetry. a) Photograph of PAG calibration vials that were uniformly irradiated using different doses ranging from 0 Gy to 40 Gy (Koeva 2009b) and b) Calibration curve constructed from Magnetic Resonance (MR) analysis of a different series of PAG calibration vials produced using the recipe in Table 2.1 (De Deene 2004), used with permission.

The current article is concerned with mathematical modeling of PAG dosimeters for brachytherapy applications. Brachytherapy involves implanting multiple radioactive seeds in the human body (Erickson *et al.* 2011, Rosenthal *et al.* 2011). Because bones and soft tissues have heterogeneous structures, it is difficult for medical physicists to predict the exact 3D dose distribution that will be delivered within and near the tumour (Maryanski *et al.* 1994, Maryanski *et al.* 1996, Gifford *et al.* 2005, Ibbott and Heard 2010). As a result, they need 3D dosimetry tools to help them plan and achieve better brachytherapy treatments (Baras *et al.* 2002, Kipouros *et al.* 2003, Noda *et al.* 2008, Petrokokkinos *et al.* 2011). Also PAG dosimeters may be useful in characterizing the basic radiation dose properties of new brachytherapy seeds (Maryanski *et al.* 1996, Papagiannis *et al.* 2001, Hurley *et al.* 2006, Pantelis *et al.* 2006, Papagiannis *et al.* 2006), (eg. to determine the seed anisotropy factor for nonspherical seeds (Nath *et al.* 1995), which is included in equation (2.1) below).

As shown in Figure 2.4(a) and (b), radiation doses tend to be highest near the radioactive seeds (also called sources) and become lower as the distance from the seeds increases. Steep changes in radiation dose (dose gradients) occur near the seeds, and a large part of the dose is delivered within a few millimeters or centimeters from the source (Ibbott and Heard 2010).

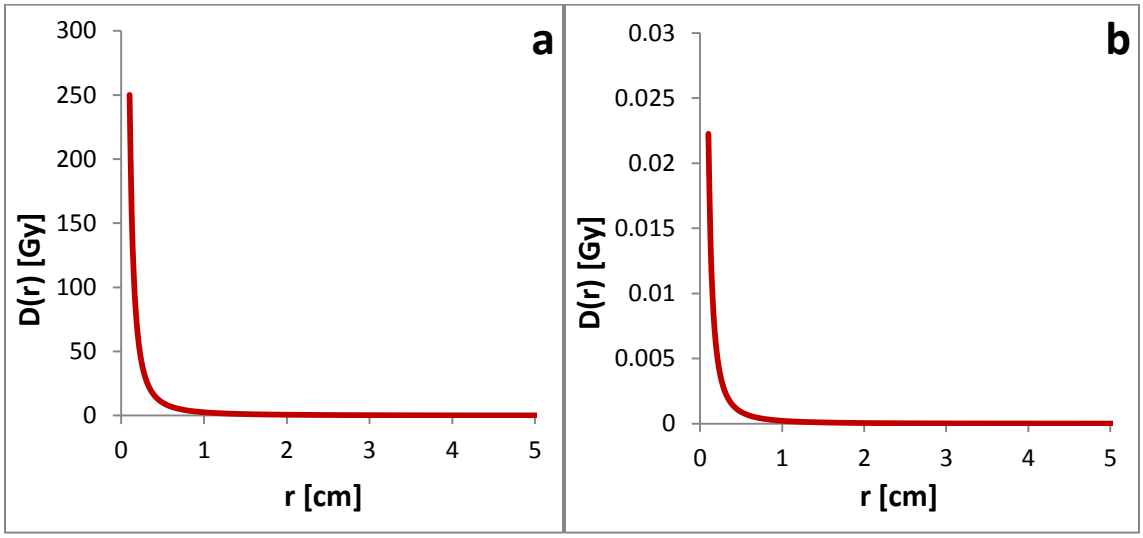

Figure 2.4: Radiation absorbed dose as a function of distance from a spherical 2 mm diameter seed after one minute of irradiation. a) ^{192}Ir HDR seed and b) ^{125}I LDR seed. The vertical axes for plots a) and b) have different scales because of the much higher dose rate of the ^{192}Ir seed.

Several research groups have performed experimental studies that address the issue of the reliability of polymer gel dosimeters for detecting 3D dose distributions near HDR brachytherapy sources (McJury *et al.* 1999, De Deene *et al.* 2001, Papagiannis *et al.* 2001, Kipouros *et al.* 2003, Hurley *et al.* 2006). Other researchers have discussed the applicability and accuracy of polymer gel dosimetry for LDR brachytherapy applications (Farajollahi *et al.* 1999, Fragoso *et al.* 2004, Pantelis *et al.* 2004, Pantelis *et al.* 2005, Massillon *et al.* 2011). Some of these researchers have described problems with obtaining accurate measurements of the radiation dose absorbed near the seeds where dose rates are high and there are steep changes in radiation dose.

Our current research is aimed at modeling the polymerization reactions and monomer diffusion that occur near a single spherical radioactive seed in a PAG dosimeter. The main objectives of this work are i) to simulate the influence of the

radioactive brachytherapy seed on polymer formation and crosslinking and ii) to investigate whether PAG dosimetry will provide accurate dosimetry for different types of brachytherapy sources. The two types of brachytherapy considered are HDR brachytherapy using an ^{192}Ir seed implanted temporarily and LDR brachytherapy using an ^{125}I seed implanted permanently. Model equations are developed and numerical solution of the model equations is described. Simulation results for both ^{192}Ir and ^{125}I brachytherapy seeds are presented. The simulations provide information about the effectiveness of polymer gel dosimeters for HDR brachytherapy applications and about the problems that occur when polymer gel dosimeters are used for LDR brachytherapy dosimetry.

2.4 Model Development

2.4.1 Radial Dose Profiles

Simulations were done assuming a single point-source of radiation at the centre of the radioactive seed, which is in the centre of a spherical phantom as shown in Figure 2.5. The dose rate for a point source at a distance *r* from the centre of the source is given in equation (2.1) as follows (Nath *et al.* 1995):

$$\dot{D}(r) = S_k \Lambda \left(\frac{G(r)}{G(r_0)}\right) T(r) F(r) \qquad (2.1)$$

where:

$\dot{D}(r)$ is the dose rate [Gy min^{-1}]

Λ is the dose rate constant [Gy min^{-1} U^{-1}], which depends on the radioactive source used

$G(r)$ is a geometry factor, which is equal to r^{-2} for a point source in a spherical particle

$G(r_0)$ is the geometry factor at the reference point of r_0 =1 cm.

T(r) is a dimensionless radial dose function, which is different for different radioactive sources, and is influenced by the type and thickness of material used to encapsulate the radioactive source within the seed (Nath *et al.* 1995).

$F(r)$ is an anisotropy function, which has a value of 1 for spherical particles.

S_k is the air kerma strength of the source in units of U, which is used to account for radioactive decay of the seed during irradiation:

$$S_k = S_{k0} exp\left(\frac{t \ln(1/2)}{t_{1/2}}\right) \tag{2.2}$$

t is the time since the measurement of the initial air kerma strength (S_{k0}) is taken and $t_{1/2}$ is the half-life of the source.

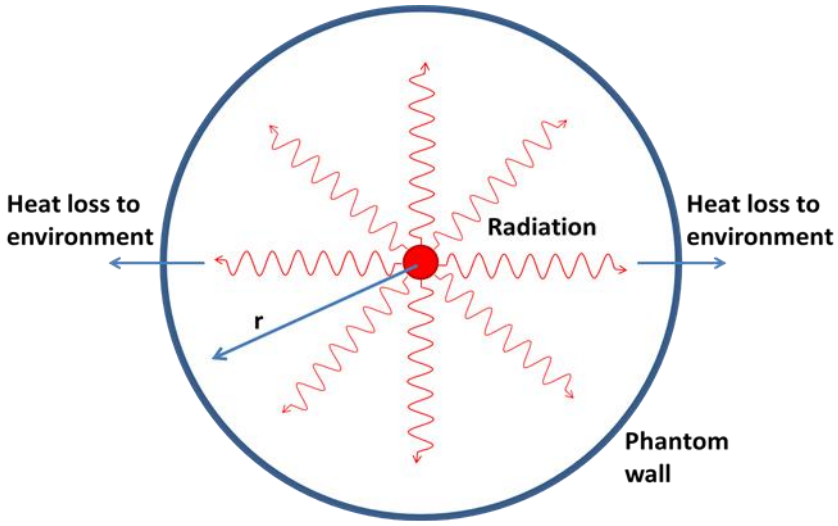

Figure 2.5: Schematic diagram showing irradiation of a simulated spherical phantom. The outer wall of the phantom is 10 cm from the centre of the brachytherapy seed. The seed, in the centre, has a diameter of 2 mm and is not drawn to scale.

In this article the responses of the PAG dosimeter (using the recipe in Table 2.1) to ^{192}Ir (HDR) and ^{125}I (LDR) are simulated. Values of the parameters required in

equation 2.1 and 2.2 for these two types of sources are provided in Table 2.2. The radiation delivery equations presented in Equation 2.1 and 2.2 and Table 2.2 are more accurate than the simpler equation used in our previous simulations (Nasr *et al.* 2010) for an ^{192}Ir seed, which did not account for decay of the radioactive source during radiation delivery. Figure 2.4(a) and (b) show the radial dose profiles from 1 mm-radius seeds of ^{192}Ir and ^{125}I, respectively, after one minute of irradiation. Note the large differences in the scales of the vertical axes for these two sources. The reason for the large differences in dose rate is the higher activity of the ^{192}Ir seed, which is designed to be removed from the body after ~1 minute. The less active ^{125}I seed is designed to remain permanently in the body. Note that we also perform a series of simulations with spatially-uniform radiation throughout the phantom ($\dot{D}(r)$=2.5 Gy min^{-1}) for different amounts of time. The purpose of these simulations is to generate results corresponding to a series of calibration vials like those shown in Figure 2.3.

Table 2.2: Parameters values for ^{192}Ir and ^{125}I brachytherapy radiation (Nath *et al.* 1995).

parameter	**units**	**^{192}Ir**	**^{125}I**
S_{k0}	[U]	13400	1.27
$t_{1/2}$	[min]	106350	85536
Γ	[Gy min^{-1} U^{-1}]	1.8667×10^{-4}	1.55×10^{-4}
$A(r)$	cm^{-2}	1/r^2	1/r^2
$F(r)$	----	1	1
$T(r)$	----	$a_0 + a_1 r + a_2 r^2 + a_3 r^3 + a_4 r^4$	$a_0 + a_1 r + a_2 r^2 + a_3 r^3 + a_4 r^4 + a_5 r^5$
a_0		9.89054×10^{-1}	1.02307
a_1	cm^{-1}	8.81319×10^{-3}	8.63751×10^{-2}
a_2	cm^{-2}	3.51778×10^{-3}	-1.37155×10^{-1}
a_3	cm^{-3}	-1.46637×10^{-3}	3.07795×10^{-2}
a_4	cm^{-4}	9.24370×10^{-5}	-2.86946×10^{-3}
a_5	cm^{-5}	0	9.87558×10^{-5}

2.4.2 Polymerization Model

Previous partial differential equation (PDE) models, developed by Fuxman *et al.* from our research group (Fuxman *et al.* 2003, Fuxman *et al.* 2005, Chain *et al.* 2011b) are extended and reformulated to account for brachytherapy irradiation instead of radiation by an external beam. The original models were expressed in Cartesian coordinates using the spatial variable *x*, whereas the current model uses the radial coordinate *r* to indicate the distance from the centre of the radioactive seed (Fig. 2.5). In addition, the revised model requires modifying Fuxman's original material balance on primary radicals, which is:

$$\frac{\partial[(\dot{P}R)]}{\partial t} = \Gamma(x)R_{(\dot{P}R)}[H_2O]^w M_{w,H_2O} - r_{(\dot{P}R)} - \frac{[(\dot{P}R)]}{\phi}\frac{\partial \phi}{\partial t} \tag{2.3}$$

where $\left[\left(\dot{P}R\right)\right]$ is the concentration of primary radicals generated by water radiolysis, $\Gamma(x)$ identifies zones receiving or not receiving radiation, M_{wH_2O} is molecular weight of water, $[H_2O]^w$ is the water concentration in the aqueous phase, $r_{(\dot{P}R)}$ is the rate of consumption of primary radicals by subsequent reactions, ϕ is the volume fraction occupied by the aqueous phase and $R_{(\dot{P}R)}$ is the rate of generation of primary radicals, which is obtained by multiplying the dose rate by the chemical yield of the free radicals (G=6.27×10^{-7} mol J^{-1}) (Fuxman 2003, Spinks and Woods 1976). Fuxman *et al.* used their model to study edge enhancement at a sharp interface between irradiated and un-irradiated zones. They used $\Gamma(x)$ to distinguish locations that receive radiation ($\Gamma = 1$) from locations that do not ($\Gamma = 0$). When investigating the effects of brachytherapy irradiation on PAG dosimeters Γ is set to one everywhere and the radial dose rate, given by (eq.1), is used to determine the local rate of generation of primary radicals as follow:

$$R_{(\dot{P}R)} = G\,\dot{D}(r) \tag{2.4}$$

All PDEs in Fuxman's model that contain derivatives with respect to the spatial coordinate *x* were reformulated in spherical coordinates to account for variation in the radial direction *r*. For example, the material balance on acrylamide monomer (M_1) was changed from equation (2.5) to equation (2.6) as follow:

$$\frac{\partial[M_1^w]}{\partial t} = D_{M_1^w}\left(\frac{1}{\phi}\frac{\partial\phi}{\partial x}\frac{\partial[M_1^w]}{\partial x} + \frac{\partial^2[M_1^w]}{\partial x^2}\right) + r_{M_1^w} - k_m\left([M_1^w] - \frac{[M_1^p]}{\Phi_{M_1}}\right) - \frac{[M_1^w]}{\phi}\frac{\partial\phi}{\partial t} \quad (2.5)$$

$$\frac{\partial[M_1^w]}{\partial t} = D_{M_1^w}\left(\frac{1}{\phi}\frac{\partial\phi}{\partial r}\frac{\partial[M_1^w]}{\partial r} + \frac{\partial^2[M_1^w]}{\partial r^2} + \frac{2}{r}\frac{\partial[M_1^w]}{\partial r}\right) + r_{M_1^w} - k_m\left([M_1^w] - \frac{[M_1^p]}{\Phi_{M_1}}\right) - \frac{[M_1^w]}{\phi}\frac{\partial\phi}{\partial t} \quad (2.6)$$

All of Fuxman's PDEs that do not contain the variable *x* remain unchanged in the current model (Fuxman *et al.* 2005). Fuxman's boundary conditions were revised (see Table 2.3) to account for the position of the phantom wall at Rmax= 10 cm and to permit heat loss through the phantom wall.

Table 2.3: Transformed Model Equations. The complete model also includes 17 other PDEs, which are provided in Tables 4 and 5 of the article by Fuxman et al (2005).

Species Balance Equations for Aqueous Phase

$$\frac{\partial\left[\left(\dot{P}\dot{R}\right)\right]}{\partial t} = R_{(\dot{P}\dot{R})}M_{wH_2O}[H_2O]^w + r_{(\dot{P}\dot{R})} - \frac{\left[\left(\dot{P}\dot{R}\right)\right]}{\phi}\frac{\partial\phi}{\partial t} \quad (T1)$$

$$\frac{\partial\left[\dot{\mathrm{P}}\mathrm{R}\right]}{\partial t} = D_{\dot{P}R}\left(\frac{2}{\tilde{r}}\frac{\partial\left[\dot{\mathrm{P}}\mathrm{R}\right]}{9.9\partial\tilde{r}} + \frac{1}{\phi}\frac{\partial\phi}{9.9\partial\tilde{r}}\frac{\partial\left[\dot{\mathrm{P}}\mathrm{R}\right]}{9.9\partial\tilde{r}} + \frac{\partial^2\left[\dot{\mathrm{P}}\mathrm{R}\right]}{9.9^2\partial\tilde{r}^2}\right) + r_{\dot{\mathrm{P}}\mathrm{R}} - \frac{\left[\dot{\mathrm{P}}\mathrm{R}\right]}{\phi}\frac{\partial\phi}{\partial t} \quad (T2)$$

$$\frac{\partial[M_1^w]}{\partial t} = D_{M_1^w}\left(\frac{2}{\tilde{r}}\frac{\partial[M_1^w]}{9.9\partial\tilde{r}} + \frac{1}{\phi}\frac{\partial\phi}{9.9\partial\tilde{r}}\frac{\partial[M_1^w]}{9.9\partial\tilde{r}} + \frac{\partial^2[M_1^w]}{9.9^2\partial\tilde{r}^2}\right) + r_{M_1^w} - k_m\left([M_1^w] - \frac{[M_1^p]}{\Phi_{M_1}}\right) - \frac{[M_1^w]}{\phi}\frac{\partial\phi}{\partial t} \quad (T3)$$

$$\frac{\partial[M_2^w]}{\partial t} = D_{M_2^w}\left(\frac{2}{\tilde{r}}\frac{\partial[M_2^w]}{9.9\partial\tilde{r}} + \frac{1}{\phi}\frac{\partial\phi}{9.9\partial\tilde{r}}\frac{\partial[M_2^w]}{9.9\partial\tilde{r}} + \frac{\partial^2[M_2^w]}{9.9^2\partial\tilde{r}^2}\right) + r_{M_2^w} - k_m\left([M_2^w] - \frac{[M_2^p]}{\Phi_{M_2}}\right) - \frac{[M_2^w]}{\phi}\frac{\partial\phi}{\partial t} \quad (T4)$$

$$\frac{\partial[P^w]}{\partial t} = D_{P^w}\left(\frac{2}{\tilde{r}}\frac{\partial[P^w]}{9.9\partial\tilde{r}} + \frac{1}{\phi}\frac{\partial\phi}{9.9\partial\tilde{r}}\frac{\partial[P^w]}{9.9\partial\tilde{r}} + \frac{\partial^2[P^w]}{9.9^2\partial\tilde{r}^2}\right) + r_{P^w} - \frac{[P^w]}{\phi}\frac{\partial\phi}{\partial t} \quad \text{(T5)}$$

$$\frac{\partial[Q^w]}{\partial t} = D_{Q^w}\left(\frac{2}{\tilde{r}}\frac{\partial[Q^w]}{9.9\partial\tilde{r}} + \frac{1}{\phi}\frac{\partial\phi}{9.9\partial\tilde{r}}\frac{\partial[Q^w]}{9.9\partial\tilde{r}} + \frac{\partial^2[Q^w]}{9.9^2\partial\tilde{r}^2}\right) + r_{Q^w} - \frac{[Q^w]}{\phi}\frac{\partial\phi}{\partial t} \quad \text{(T6)}$$

$$\frac{\partial\left[PDB^w_{eff}\right]}{\partial t} = D_{PDB^w_{eff}}\left(\frac{2}{\tilde{r}}\frac{\partial\left[PDB^w_{eff}\right]}{9.9\partial\tilde{r}}\frac{1}{\phi}\frac{\partial\phi}{9.9\partial\tilde{r}}\frac{\partial\left[PDB^w_{eff}\right]}{9.9\partial\tilde{r}} + \frac{\partial^2\left[PDB^w_{eff}\right]}{9.9^2\partial\tilde{r}^2}\right) + r_{PDB^w_{eff}} - \frac{\left[PDB^w_{eff}\right]}{\phi}\frac{\partial\phi}{\partial t} \quad \text{(T7)}$$

$$\frac{\partial[H_2O^w]}{\partial t} = D_{H_2O^w}\left(\frac{2}{\tilde{r}}\frac{\partial[H_2O^w]}{9.9\partial\tilde{r}} + \frac{1}{\phi}\frac{\partial\phi}{9.9\partial\tilde{r}}\frac{\partial[H_2O^w]}{9.9\partial\tilde{r}} + \frac{\partial^2[H_2O^w]}{9.9^2\partial\tilde{r}^2}\right) - k_m\left([H_2O^w] - \frac{[H_2O^p]}{\Phi_{H_2O}}\right) - \frac{[H_2O^w]}{\phi}\frac{\partial\phi}{\partial t} \quad \text{(T8)}$$

$$\frac{\partial[D^w]}{\partial t} = D_{D^w}\left(\frac{2}{r}\frac{\partial[D^w]}{9.9\partial\tilde{r}} + \frac{1}{\phi}\frac{\partial\phi}{9.9\partial\tilde{r}}\frac{\partial[D^w]}{9.9\partial\tilde{r}} + \frac{\partial^2[D^w]}{9.9^2\partial\tilde{r}^2}\right) + r_{D^w} - \frac{[D^w]}{\phi}\frac{\partial\phi}{\partial t} \quad \text{(T9)}$$

Balances on moments of the water soluble growing radical distribution

$$\frac{\partial[\lambda_{11}]}{\partial t} = D_{P^w}\left(\frac{2}{\tilde{r}}\frac{\partial[\lambda_{11}]}{9.9\partial\tilde{r}} + \frac{1}{\phi}\frac{\partial\phi}{9.9\partial\tilde{r}}\frac{\partial[\lambda_{11}]}{9.9\partial\tilde{r}} + \frac{\partial^2[\lambda_{11}]}{9.9^2\partial\tilde{r}^2}\right) + r_{\lambda_{11}} - \frac{[\lambda_{11}]}{\phi}\frac{\partial\phi}{\partial t} \quad \text{(T10)}$$

$$\frac{\partial[\lambda_{12}]}{\partial t} = D_{Q^w}\left(\frac{2}{\tilde{r}}\frac{\partial[\lambda_{12}]}{9.9\partial\tilde{r}} + \frac{1}{\phi}\frac{\partial\phi}{9.9\partial\tilde{r}}\frac{\partial[\lambda_{12}]}{9.9\partial\tilde{r}} + \frac{\partial^2[\lambda_{12}]}{9.9^2\partial\tilde{r}^2}\right) + r_{\lambda_{12}} - \frac{[\lambda_{12}]}{\phi}\frac{\partial\phi}{\partial t} \quad \text{(T11)}$$

$$\frac{\partial[\lambda_{21}]}{\partial t} = D_{P^w}\left(\frac{2}{\tilde{r}}\frac{\partial[\lambda_{21}]}{9.9\partial\tilde{r}} + \frac{1}{\phi}\frac{\partial\phi}{9.9\partial\tilde{r}}\frac{\partial[\lambda_{21}]}{9.9\partial\tilde{r}} + \frac{\partial^2[\lambda_{21}]}{9.9c^2\partial\tilde{r}^2}\right) + r_{\lambda_{21}} - \frac{[\lambda_{21}]}{\phi}\frac{\partial\phi}{\partial t} \quad \text{(T12)}$$

$$\frac{\partial[\lambda_{22}]}{\partial t} = D_{Q^w}\left(\frac{2}{\tilde{r}}\frac{\partial[\lambda_{22}]}{9.9\partial\tilde{r}} + \frac{1}{\phi}\frac{\partial\phi}{9.9\partial\tilde{r}}\frac{\partial[\lambda_{22}]}{9.9\partial\tilde{r}} + \frac{\partial^2[\lambda_{22}]}{9.9^2\partial\tilde{r}^2}\right) + r_{\lambda_{22}} - \frac{[\lambda_{22}]}{\phi}\frac{\partial\phi}{\partial t} \quad \text{(T13)}$$

Energy Balance

$$\frac{\partial T}{\partial t} = \frac{(k)}{\rho C_p}\frac{\partial^2 T}{9.9^2\partial\tilde{r}^2} + \Big(\left(r_{M_1^w} + r_{M_2^w} + (k^w_{x1}[P^w] + k^w_{x2}[Q^w])\left(\left[PDB^w_{eff}\right] + [PDB^w_{acc}]\right) + k^w_c[Q^w]\right)\phi + \left(r_{M_1^p} + r_{M_2^p} + \left(k^p_{x1}\left[R^p_1\right] + k^p_{x2}\left[R^p_2\right]\right)\left[PDB^p_{eff}\right] + k^p_c\left[R^p_2\right]\right)(1-\phi)\Big)\frac{(-\Delta H_r)}{\rho C_p} \quad \text{(T14)}$$

Boundary Conditions

$$\frac{\partial[\dot{\mathrm{P}}\mathrm{R}]}{\partial t}|_{\tilde{r}=0} = \frac{\partial[\dot{\mathrm{P}}\mathrm{R}]}{\partial t}|_{\tilde{r}=R_{max}} = 0 \quad \text{(T15)}$$

$$\frac{\partial[M_1^w]}{\partial t}|_{\tilde{r}=0} = \frac{\partial[M_1^w]}{\partial t}|_{\tilde{r}=R_{max}} = 0 \quad \text{(T16)}$$

$$\frac{\partial[M_2^w]}{\partial t}|_{\tilde{r}=0} = \frac{\partial[M_2^w]}{\partial t}|_{\tilde{r}=R_{max}} = 0 \quad \text{(T17)}$$

$$\frac{\partial[P^w]}{\partial t}|_{\tilde{r}=0} = \frac{\partial[P^w]}{\partial t}|_{\tilde{r}=R_{max}} = 0 \quad \text{(T18)}$$

$$\frac{\partial[Q^w]}{\partial t}|_{\tilde{r}=0} = \frac{\partial[Q^w]}{\partial t}|_{\tilde{r}=R_{max}} = 0 \quad \text{(T19)}$$

$$\frac{\partial[PDB_{eff}^w]}{\partial t}|_{\tilde{r}=0} = \frac{\partial[PDB_{eff}^w]}{\partial t}|_{\tilde{r}=R_{max}} = 0 \quad \text{(T20)}$$

$$\frac{\partial[H_2O^w]}{\partial t}|_{\tilde{r}=0} = \frac{\partial[H_2O^w]}{\partial t}|_{\tilde{r}=R_{max}} = 0 \quad \text{(T21)}$$

$$\frac{\partial[D^w]}{\partial t}|_{\tilde{r}=0} = \frac{\partial[D^w]}{\partial t}|_{\tilde{r}=R_{max}} = 0 \quad \text{(T22)}$$

$$\frac{\partial[\lambda_{11}]}{\partial t}|_{\tilde{r}=0} = \frac{\partial[\lambda_{11}]}{\partial t}|_{\tilde{r}=R_{max}} = 0 \quad \text{(T23)}$$

$$\frac{\partial[\lambda_{12}]}{\partial t}|_{\tilde{r}=0} = \frac{\partial[\lambda_2]}{\partial t}|_{\tilde{r}=R_{max}} = 0 \quad \text{(T24)}$$

$$\frac{\partial[\lambda_{21}]}{\partial t}|_{\tilde{r}=0} = \frac{\partial[\lambda_{21}]}{\partial t}|_{\tilde{r}=R_{max}} = 0 \quad \text{(T25)}$$

$$\frac{\partial[\lambda_{22}]}{\partial t}|_{\tilde{r}=0} = \frac{\partial[\lambda_{22}]}{\partial t}|_{\tilde{r}=R_{max}} = 0 \quad \text{(T26)}$$

$$\frac{\partial T}{\partial t}|_{\tilde{r}=0} = 0, \qquad -k_{cond}\frac{\partial T}{\partial t}|_{\tilde{r}=R_{max}} = h(T - T_s) \quad \text{(T27)}$$

Updated values of model parameters (Koeva *et al.* 2009b) that were fitted using temperature rise and polymer mass data (Salomons *et al.* 2002, Babic and Schreiner 2006) are used in this revised model. Concentration data from the literature were not used for parameter estimation because of the lack of detailed information about storage conditions (such as the temperature and oxygen levels) that influence the monomer

concentrations and polymerization rate (Baldock *et al.* 1998b, Jirasek *et al.* 2001, Jirasek and Duzenli 2001, Lepage *et al.* 2001a, Lepage *et al.* 2001b). A complete list of all model parameters and their values is provided in a recent article by Chain *et al.* (2011b), who verified that the model can predict the qualitative trends in these monomer consumption data using the current parameter values. Note that there is considerable uncertainty in some of these parameter values. It will be important to perform additional experiments that can be used for further parameter estimation if more accurate predictions from the model are required in the future.

2.5 Model Solution

The complete system of 31 PDEs was solved using the VLUGR2 solver in FORTRAN (Blom *et al.* 1996). Note that this PDE model could also be solved using the pdepe subroutine in Matlab™, but simulation times are prohibitively long (Chain *et al.* 2011b). The PDEs were solved to predict the mass and type of polymer formed as well as the temperature distribution as a function of time and radial distance from the brachytherapy seed.

VLUGR2 is a numerical solver that solves initial value problems with boundary conditions for systems of PDEs in either one or two spatial dimensions (Blom *et al.* 1996). The algorithm uses a finite difference method to convert the spatial domains into a set of algebraic equations and uses a second order two-step implicit backward differentiation formula. In the current work, the radial spatial domain was approximated using 400 uniformly-spaced grid points to ensure numerical accuracy. VLUGR2 is designed to solve PDEs on a spatial domain that extends from 0 to 1, but the radial coordinate in our model extends from the edge of the seed at $r = 0.1$ cm to the edge of the

phantom at $r = 10$ cm. Before the PDEs could be solved, the following mathematical transformation was used so that the transformed spatial domain extends from $\tilde{r} = 0$ to $\tilde{r} = 1$:

$$\tilde{r} = (r - 0.1)/9.9 \tag{2.7}$$

Using this transformation, the first derivative with respect to *r* in equation (2.6), for example, becomes:

$$\frac{\partial[\mathrm{M1}]}{\partial r} = \frac{\partial[\mathrm{M1}]}{9.9\,\partial\tilde{r}} \tag{2.8}$$

and the second derivative in the same equation becomes:

$$\frac{\partial^2[\mathrm{M1}]}{\partial r^2} = \frac{\partial^2[\mathrm{M1}]}{9.9^2\,\partial\tilde{r}^2} \tag{2.9}$$

The transformation in equation 2.7 to 2.9 was applied to all of the PDEs in our model that contain spatial derivatives, as shown in Table 2.3. The other 17 PDEs used in the model (without spatial derivatives) are the same as those of Fuxman *et al.* (2005). Note that this approach is an improvement over a simpler transformation and associated assumptions used in our preliminary brachytherapy dosimetry model (Nasr *et al.* 2010) where we neglected the volume occupied by the seed and used a fixed dose rate of of $\dot{\mathrm{D}}(\mathrm{r}) = 770$ [Gy min^{-1}] in the interval $0 < r \leq 0.1$ cm to prevent numerical problems associated with very large dose at small values of *r*.

2.6 Simulation Results and Discussion

Simulations were run to predict the response of a PAG dosimeter (produced using the recipe in Table 2.1) to a 2 mm-diameter brachytherapy seed made from ^{192}Ir. This HDR ^{192}Ir seed was implanted for one minute, at the centre of the spherical phantom, to deliver a total dose of 2.5 Gy at a distance of *r* = 1 cm. Polymerization was simulated up

to a final time of 12 hours to account for the influence of long-lived polymer radicals that continue to polymerize after radiation ceases (McAuley 2004, Fuxman *et al.* 2005). Simulations were also conducted for a similar seed made from ^{125}I, which is a LDR source. This LDR seed remained at the centre of the phantom throughout the simulation time to mimic LDR treatments wherein the radioactive seed is implanted permanently in the patient. Simulations with the ^{125}I seed were attempted for a period of 10 days so that the total delivered dose at r = 1 cm would be 2.5 Gy. Unfortunately, numerical difficulties were encountered after approximately 3.5 days of simulated time. The reasons behind these numerical problems will be discussed below because they have important implications for the accuracy of LDR brachytherapy dosimetry using polymer gels. LDR simulation results are reported at a final time of three days, when the simulation was working without numerical problems.

2.6.1 Results for the HDR ^{192}Ir brachytherapy seed

Figure 2.6(a) shows the amount of polymer formed in response to ^{192}Ir brachytherapy radiation. As expected, polymerization continued after the removal of the seed, and more polymer formed in the highly-irradiated region near the seed than further from the seed where less radiation was received. For example, the polymer concentration at 1 mm from the center of the seed increased from ~40 [gL^{-1}] after one minute of irradiation to ~240 [gL^{-1}] twelve hours after the removal of the seed. The temperature (not shown) increased by about 2 ºC near the seed during the first minute, and then decreased back to room temperature (20 ºC) after the removal of the seed, due to heat transfer through the outer wall of the phantom. Figure 2.6(b) and 2.6(c) show the concentration of acrylamide M_1 and bisacrylamide M_2, respectively, at t = 1 minute

(immediately after the removal of the seed) and at longer times. As expected, a larger drop occurs in $[M_2]$ than in $[M_1]$ due to the higher reactivity of bisacrylamide, which has two vinyl groups. As time proceeds, concentrations of monomers near the seed recover due to diffusion from the low-dose region at larger values of *r*. The total polymeric free-radical concentration at different times is shown in Figure 2.6(d). As expected, the polymeric free-radical concentration is highest at t = 1 min and is higher near the seed than further away because the dose delivered near the seed is higher (see Figure 2.4).

Figure 2.7 (a), (b) and (c) shows the polymer formed, $[M_1]$ and $[M_2]$, respectively, versus time at different radial distances from the centre of the seed. The polymer formation rate, which is the slope of the curves in Figure 2.7(a), begins to decrease after the radiation ceases at t=1 minute due to a decrease in the polymeric free-radical concentration. This decrease is caused by termination reactions. As shown in Figure 2.7(b) and (c), during the first few minutes when the polymerization rate is high, $[M_1]$ and $[M_2]$ fall rapidly near the seed. At times longer than 1 h, $[M_1]$ and $[M_2]$ rise very slowly at r=2 mm because the rate of diffusion toward the seed becomes larger than the rate of consumption by polymerization. Further from the seed, at r = 3 mm and 5 mm, $[M_1]$ and $[M_2]$ continue to fall slowly due to diffusion toward the seed. At very long times (not shown) when all polymerization has ceased and there has been ample time for diffusion, $[M_1]$ and $[M_2]$ become uniform throughout the phantom.

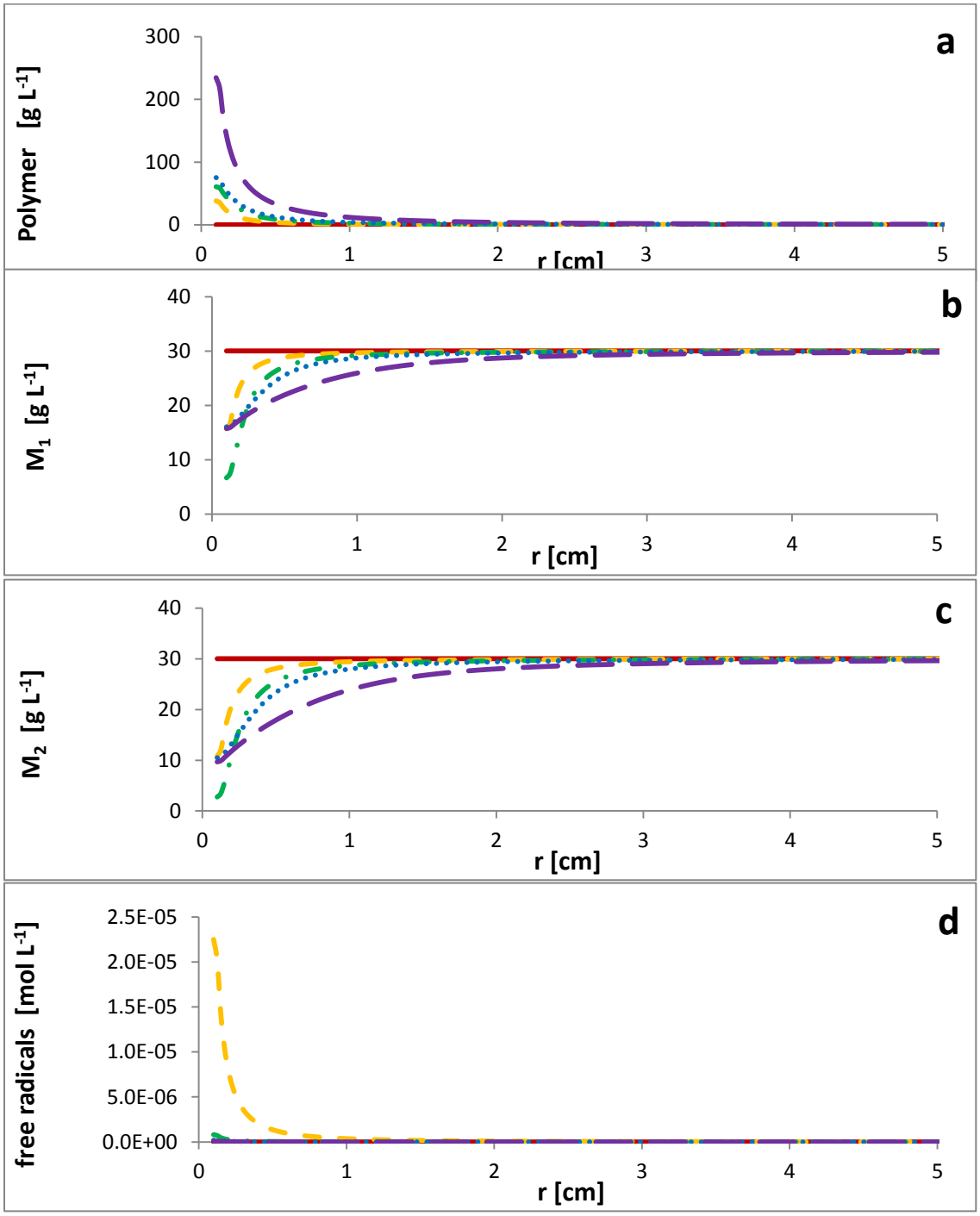

Figure 2.6: Influence of radiation using ^{192}Ir seed on: a) polymer formation, b) acrylamide (M_1) concentration, c) bisacrylamide (M_2) concentration and d) total free radical concentration. Results are reported vs. radial distance from the centre of the seed at the following times: (——) 0 min, (– –) 1 min, (– · – ·) 5 min, (·····) 1 h and (— —) 12 h. The brachytherapy dose shown in (Fig 2.4-a) was delivered for one minute before the seed was removed.

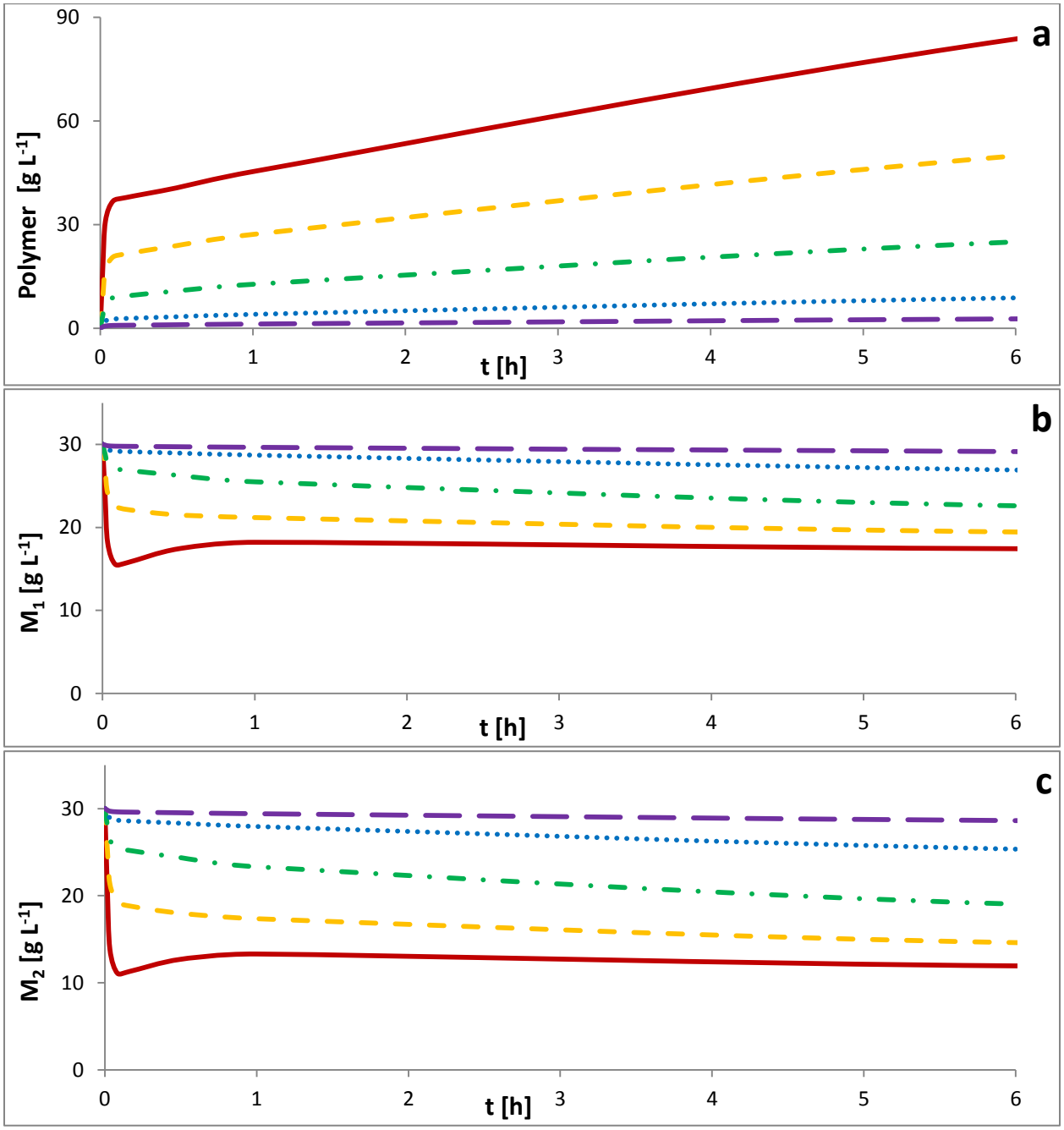

Figure 2.7: Response of PAG dosimeter to ^{192}Ir brachytherapy seed radiation in terms of: a) polymer formation, b) acrylamide (M_1) concentration and c) bisacrylamide (M_2) concentration. Results are reported vs. time at the following radial distances from the centre of the seed: (——) 2 mm, (– – –) 3 mm, (– · – · –) 5 mm, (·····) 10 mm and, (— — —) 20 mm. The brachytherapy dose shown in (Fig 2.4-a) was delivered for one minute before the seed was removed.

Figure 2.8(a) shows that more polymer is produced per Gy of radiation at large values of *r* than at small values near the seed. R_2 (the vertical axis of the calibration curve in Figure 2.3(b)) depends on the mass of polymer that forms and precipitates.[48] An ideal dosimeter would result in a flat profile, with the same amount of polymer produced for every Gy of radiation received, regardless of the distance from the source. The reason for the smaller amount of polymer per Gy near the seed is that radiation is delivered at a higher dose rate at small values of *r*, resulting in a higher local radical concentration near the seed (Figure 2.6(d)). Higher radical concentrations result in a higher rate of termination near the seed than at larger values of *r*, so that less polymer is produced, on average, for each radical generated near the seed.

Figure 2.8(b) shows the moles of crosslinks per mass of polymer formed (i.e., the crosslink density). High crosslink density is associated with high R_2 (McAuley 2004, Babic and Schreiner 2006). An ideal dosimeter would have a flat crosslink density profile. In Figure 2.8(b), crosslink density is higher near the seed than at large values of *r* because bisacrylamide near the seed is consumed more rapidly than acrylamide due to the two vinyl groups on each bisacrylamide molecule. The drop in $[M_2]$ near the seed, shown in Figure 2.6(c) causes bisacrylamide to diffuse toward the seed, where it is consumed, results in the high levels of crosslinking at low values of *r*.

Figure 2.8(c) shows the volume fraction ϕ of the aqueous phase as a function of *r* at different times. As polymer forms near seed, some of the aqueous phase is replaced by precipitated polymer microgels. At the very edge of the seed, the volume fraction occupied by the aqueous phase falls to ~ 25% indicating that ~ 75% of the volume is

occupied by the polymer phase at r = 0.1 at the longest time, t = 12 hours. The relative volume fractions of the aqueous and polymer phases may also influence R_2.

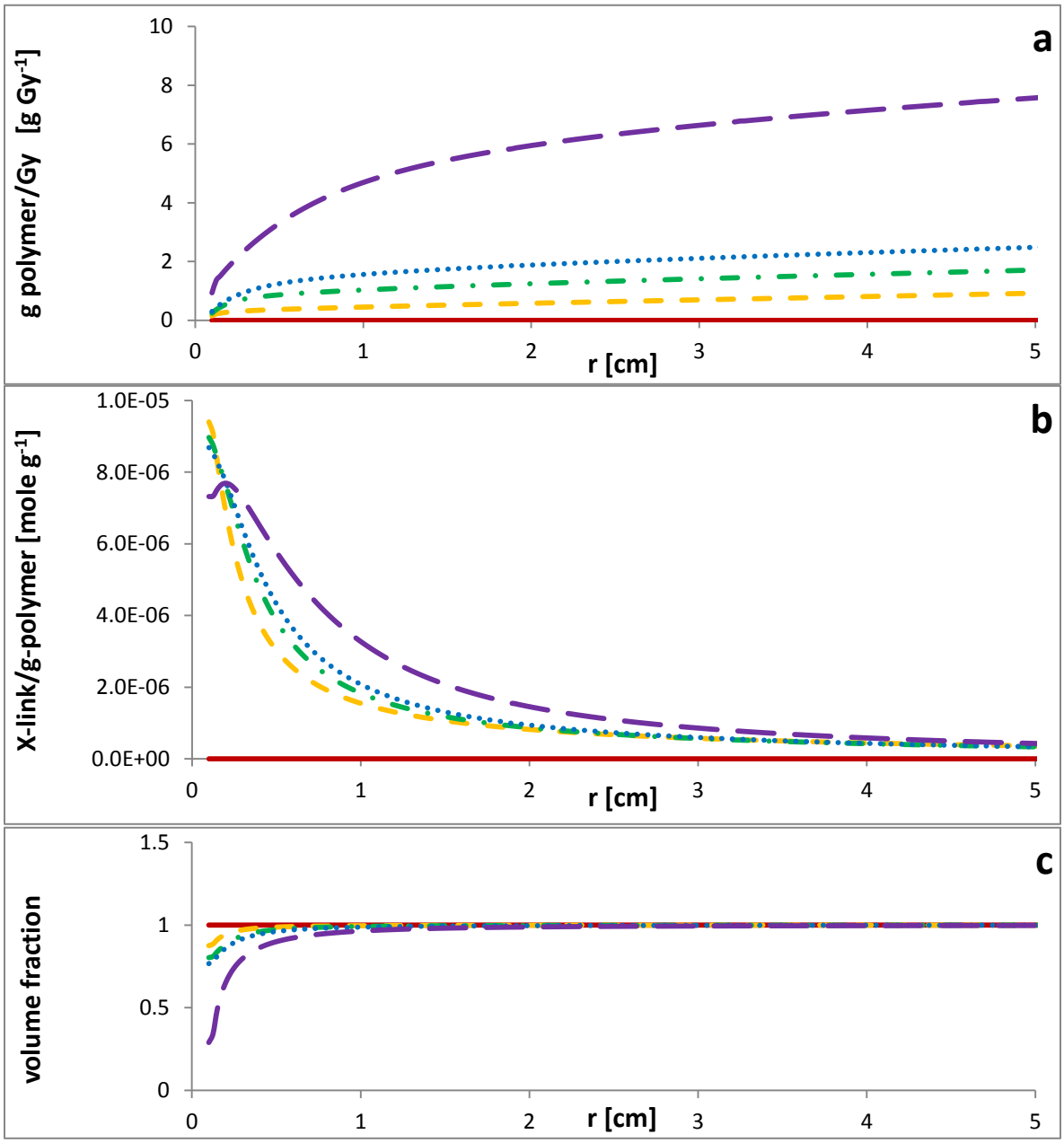

Figure 2.8: Influence of brachytherapy radiation using ^{192}Ir seed on a) polymer formed per Gy, b) crosslink density and c) volume fraction of aqueous phase. Results are reported vs. radial distance from the centre of the seed at the following times: (——) 0 min, (– –) 1 min, (– · –) 5 min, (·····) 1 h and (— —) 12 h. The brachytherapy dose shown in (Fig 2.4-a) was delivered for one minute before the seed was removed.

2.6.2 Results for LDR ^{125}I brachytherapy seed

Simulation results for ^{125}I indicate that temperature (not shown) increases by less than 0.01 ºC near the seed over the course of the three-day simulation. The temperature rise is small because the polymerization rate is low, providing ample time for heat transfer through the phantom wall. Figure 2.9(a) shows the amount of polymer formed, one day, two days and three days after insertion of the radioactive seed. As expected, more polymer forms in the highly-irradiated region near the seed than further from the seed where less radiation is received. Due to decay in radioactivity of the seed over time, more polymer forms during the first day than the amount of incremental polymer that forms in the 2nd and 3rd days.

Figure 2.9(b) and 2.9(c) show that $[M_1]$ and $[M_2]$ are smaller near the edge of the seed than at large values of *r*, as expected. However, these concentration profiles are much flatter than those for the HDR brachytherapy simulations (see Figure 2.6(b) and 2.6(c)). Acrylamide and bisacrylamide have more time to diffuse (relative to the polymerization rate) in LDR brachytherapy dosimetry than in HDR brachytherapy dosimetry where polymerization rates are significantly higher. As expected, the drop in $[M_2]$ near the seed is larger than the drop in $[M_1]$. Figure 2.9(d) shows polymeric free-radical concentrations at different times and positions. The total polymeric free-radical concentration is higher near the seed than further away, as expected. Because of the decay in the radioactivity of ^{125}I with time, the free radical concentration begins to decrease after about one day.

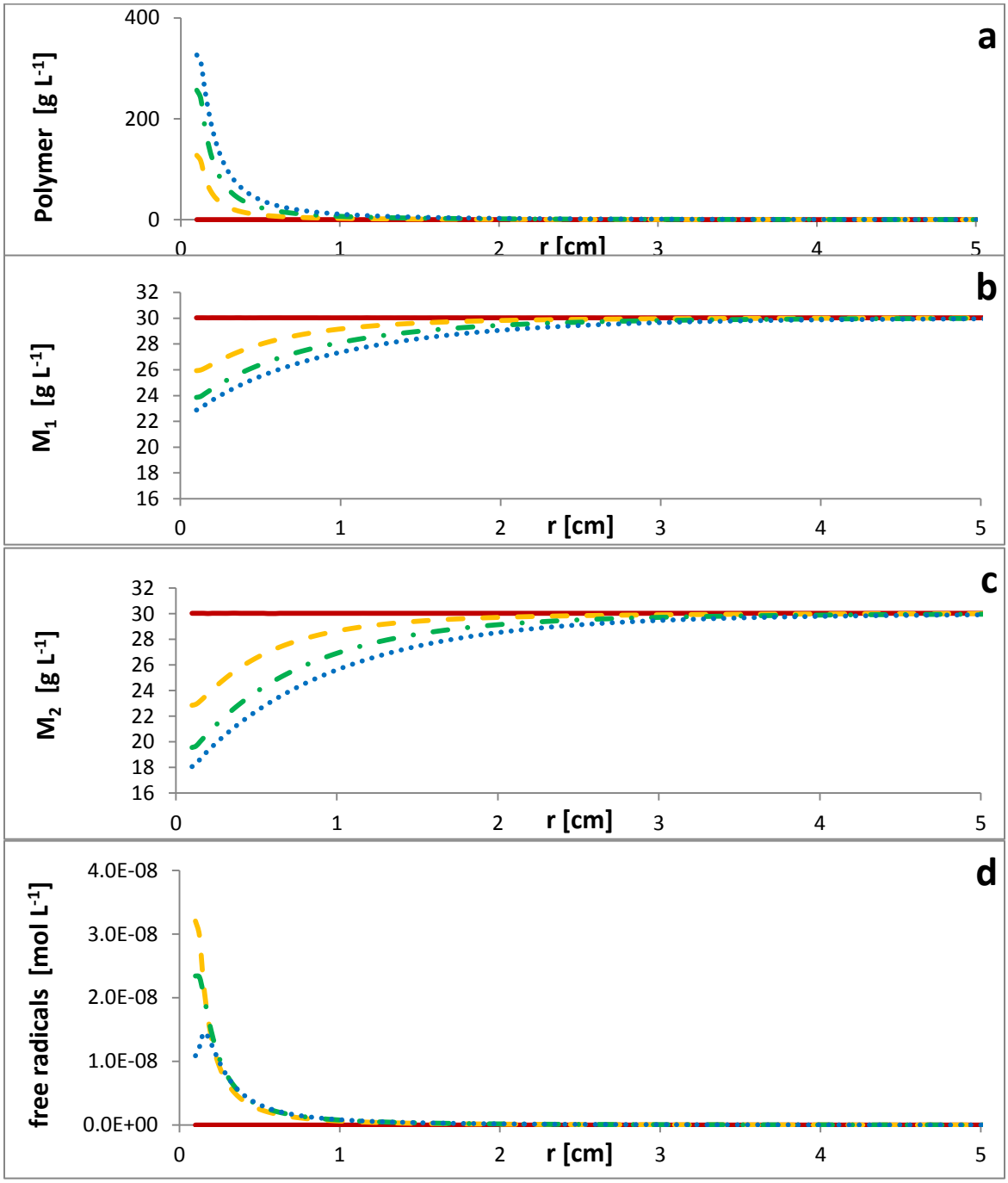

Figure 2.9: Influence of brachytherapy radiation using ^{125}I seed on a) polymer formation, b) acrylamide (M_1) concentration, c) bisacrylamide (M_2) concentration and d) total free radical concentration. Results are reported vs. radial distance from the centre of the seed at the following times: (——) 0 days, (– –) 1 day, (– · –) 2 days and (·····) 3 days. The seed is implanted permanently and the brachytherapy dose delivered is given by [Equation (2.1)] with parameter values for ^{125}I given in [Table (2.2)].

Figure 2.10(a) shows the mass of polymer formed per unit dose of radiation delivered. As in the case of ^{192}Ir, more polymer is produced per Gy of radiation at large values of r than near the seed. Figure 2.10(b) shows the moles of crosslinks per mass of polymer formed. The polymer that forms near the seed has a larger crosslink density than the polymer formed at larger values of r, as was the case for ^{192}Ir. Figure 2.10(c) shows that the volume fraction ϕ of the aqueous phase becomes much lower near the seed than further away, and that ϕ near the seed becomes very small (~ 0) after 3 days, because nearly all of the aqueous phase has been replaced by precipitated polymer microgels. When ϕ becomes even closer to zero (at $t \approx 3.5$ days), severe numerical problems are encountered. The simulation is no longer able to run because ϕ appears in the denominator of many terms in the model (e.g., the final term in equation T1 in Table 2.3) and very small values of ϕ lead to divide-by-zero errors.

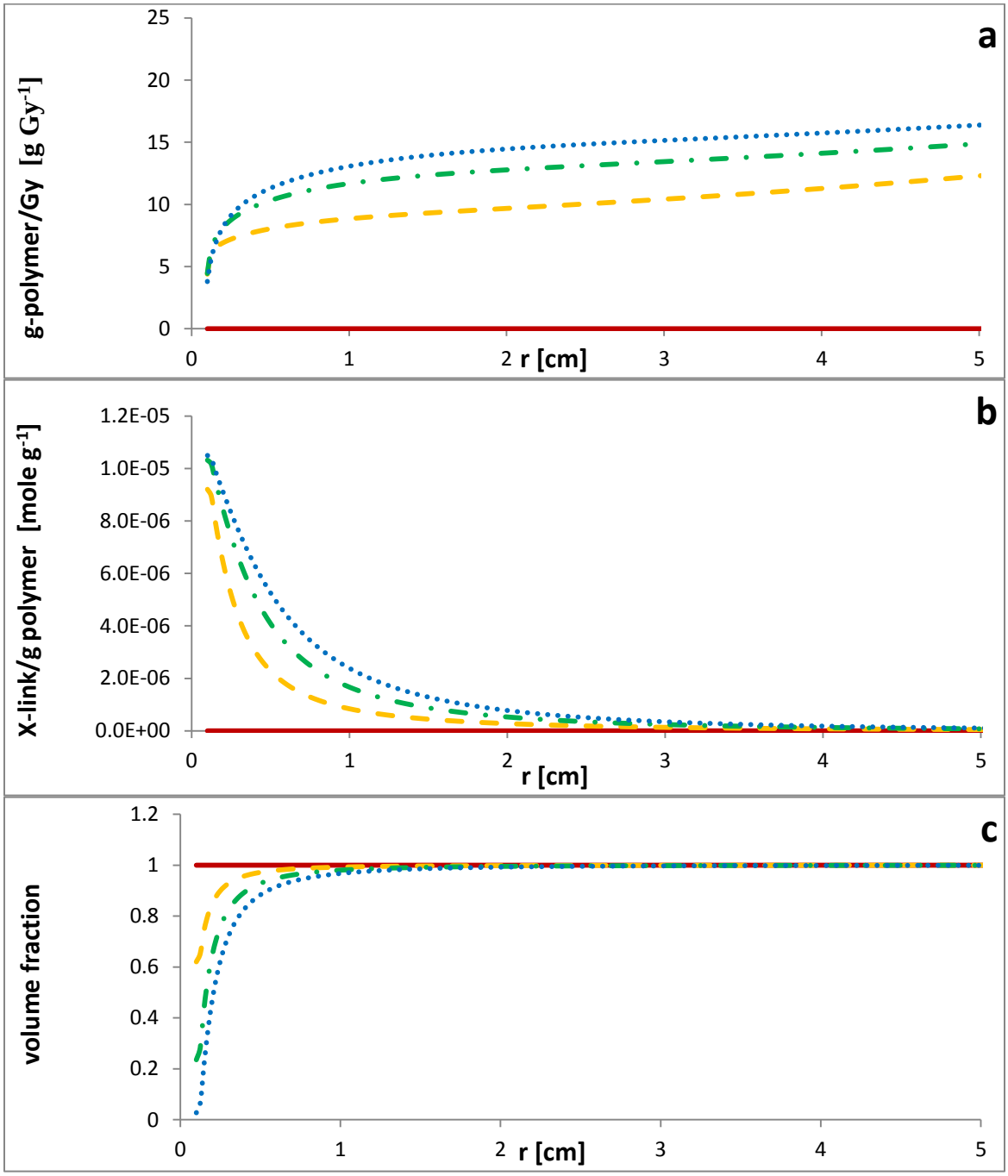

Figure 2.10: Influence of brachytherapy radiation using ^{125}I seed on a) polymer formed per Gy, b) crosslink density and c) local volume fraction of aqueous phase. Results are reported vs. radial distance from the centre of the seed at the following times: (——) 0 days, (– –) 1 day, (– · –) 2 days and (·····) 3 days. The seed is implanted permanently and the brachytherapy dose delivered is given by [Equation (2.1)] with parameter values for ^{125}I given in [Table (2.2)].

We are concerned that the model provides inaccurate results at locations where ϕ becomes small (e.g., $\phi < 0.2$). The model assumes that the only significant pathway for bulk diffusion of acrylamide and bisacrylamide is through the aqueous phase, and it uses a constant value of $D_{M1}= 2.5\times10^{-4}$ cm^2 min^{-1} for the bulk diffusivity of acrylamide and $D_{M2} = 0.75D_{M1}$ for bisacrylamide. This assumption was valid in previous modeling studies from our research group (Fuxman *et al.* 2005, Chain *et al.* 2011b), where ϕ remained relatively high at all locations in the simulated gel phantoms. Because the current model involves low values of ϕ at longer reaction times, the rate of diffusion of acrylamide and bisacrylamide calculated by the model is too high near the seed. As the aqueous phase disappears, a secondary route for monomer diffusion toward the seed becomes important (i.e., diffusion through the precipitated polymer phase). The diffusivity of monomer through the polymer phase, which is swollen with water and unreacted monomers, is only ~6×10^{-6} cm^2 min^{-1} (Fuxman *et al.* 2005). As a result, the rate of polymer formation near the seed will be over-predicted after about two days because our model assumes a bulk diffusivity of $D_{M1}= 2.5\times10^{-4}$ cm^2 min^{-1}, even when ϕ approaches zero. Note, however, that the trend of excess polymer formation near the seed and disappearance of the aqueous phase, as predicted by the model, is correct and has important implications for LDR polymer gel dosimetry.

The model could be improved to account for reduced diffusion rates at low values of ϕ by adjusting the diffusion coefficients so that they decrease as ϕ decreases. For example, Figure 2.11 shows several different sigmoidal functions that could be used to account for changes in bulk diffusivity resulting from an increase in polymer-phase and decrease in aqueous-phase volume fractions. We decided not to revise our model to

include this type of dependency because we have little information about exactly how D_{M1} changes with ϕ, and selection of any one of the sigmoidal functions in Figure 2.11 would be arbitrary. The very fact that the model predicts that ϕ becomes small near the seed for LDR brachytherapy after about two days of radiation delivery causes us to worry about the accuracy of PAG dosimetry for LDR brachytherapy. We are concerned that the relative amounts of the polymer and aqueous phases could have an important influence on R_2 (and optical and x-ray CT responses), which would lead to inaccurate dose determination from traditional calibration curves developed from uniformly irradiated vials.

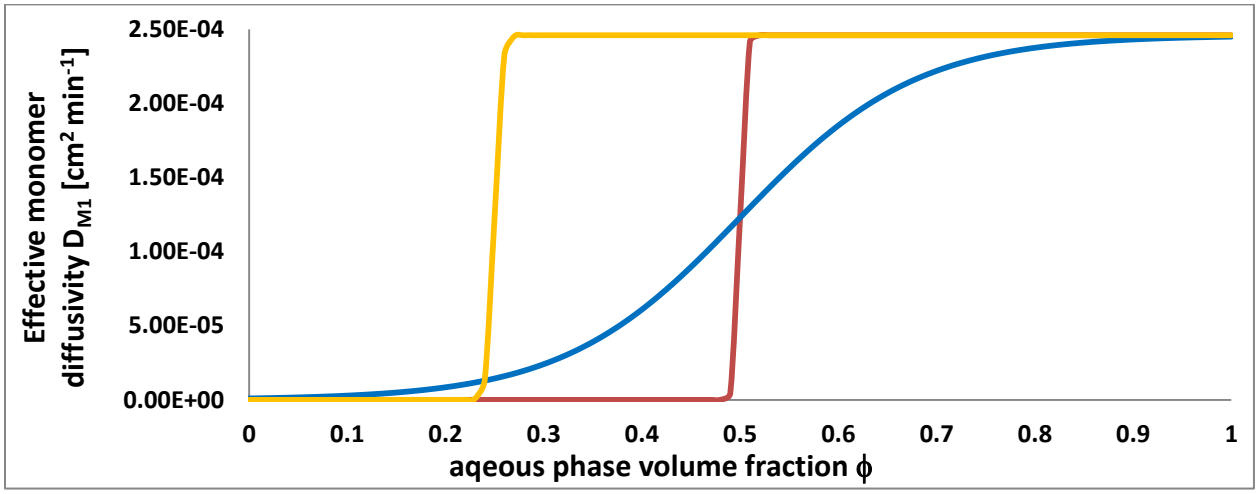

Figure 2.11: Possible functions that could be used to account for the effect of aqueous phase volume fraction on the effective diffusivity of acrylamide and bisacrylamide in the phantom. Diffusion is impeded when the aqueous phase is replaced by polymer

2.6.3 Prospects for accurate HDR and LDR brachytherapy dosimetry

Our model does not predict R_2 or other convenient gel read-out variables but it does predict: i) the amount of polymer formed per unit volume of gel, ii) the crosslink density in moles of crosslinks per gram of polymer formed and iii) the volume fraction ϕ occupied by the aqueous phase. These response variables are important because they influence R_2 and, presumably, common optical and x-ray CT readout variables (Salomons *et al.* 2002). Figure 2.12 shows these three responses obtained from our HDR and LDR simulations as a function of the absorbed radiation dose. Also shown in Figure 2.12 are corresponding curves obtained by simulating a series of uniformly-irradiated calibration vials (vials like those in Figure 2.3).

For the uniformly-irradiated vials, concentration gradients are zero and no diffusion occurs. The amount and type of polymer formed in the vials during each experiment will depend on the monomer and bisacrylamide concentrations, the total radiation dose and, to some extent, the dose rate. As a result, use of calibration vials will account for variation in key response variables (i.e., polymer formed per Gy, crosslink density and ϕ) with the delivered dose, but calibration vials cannot compensate for the variation of these variables in the brachytherapy phantom due to monomer and crosslinker diffusion over time.

To construct Figure 2.12, a series of vial simulations was conducted using a uniform radiation profile ($\dot{D}(r)$ = 2.5 Gy min^{-1}) with the radiation delivered for different periods of time to achieve final absorbed doses of 0.5, 1.0, 2.0, 5.0, 10, 20, 50 and 250 Gy. Polymerization in the calibration vials was simulated for 12 h after the beginning of the irradiation to account for the influence of long-lived radicals. After 250 Gy was delivered

(not shown in Figure 2.12) all of the monomer and bisacrylamide were consumed, resulting in a final value of ϕ=0.8, indicating that the maximum volume fraction of the polymer phase that could be obtained in the vials is approximately 20 %, using the recipe in Table 2.1. Note that the final value of ϕ is higher than the initial volume fraction of the monomer and bisacrylamide because our model accounts for water absorbed in the polymer phase (Fuxman *et al.* 2003, Fuxman *et al.* 2005).

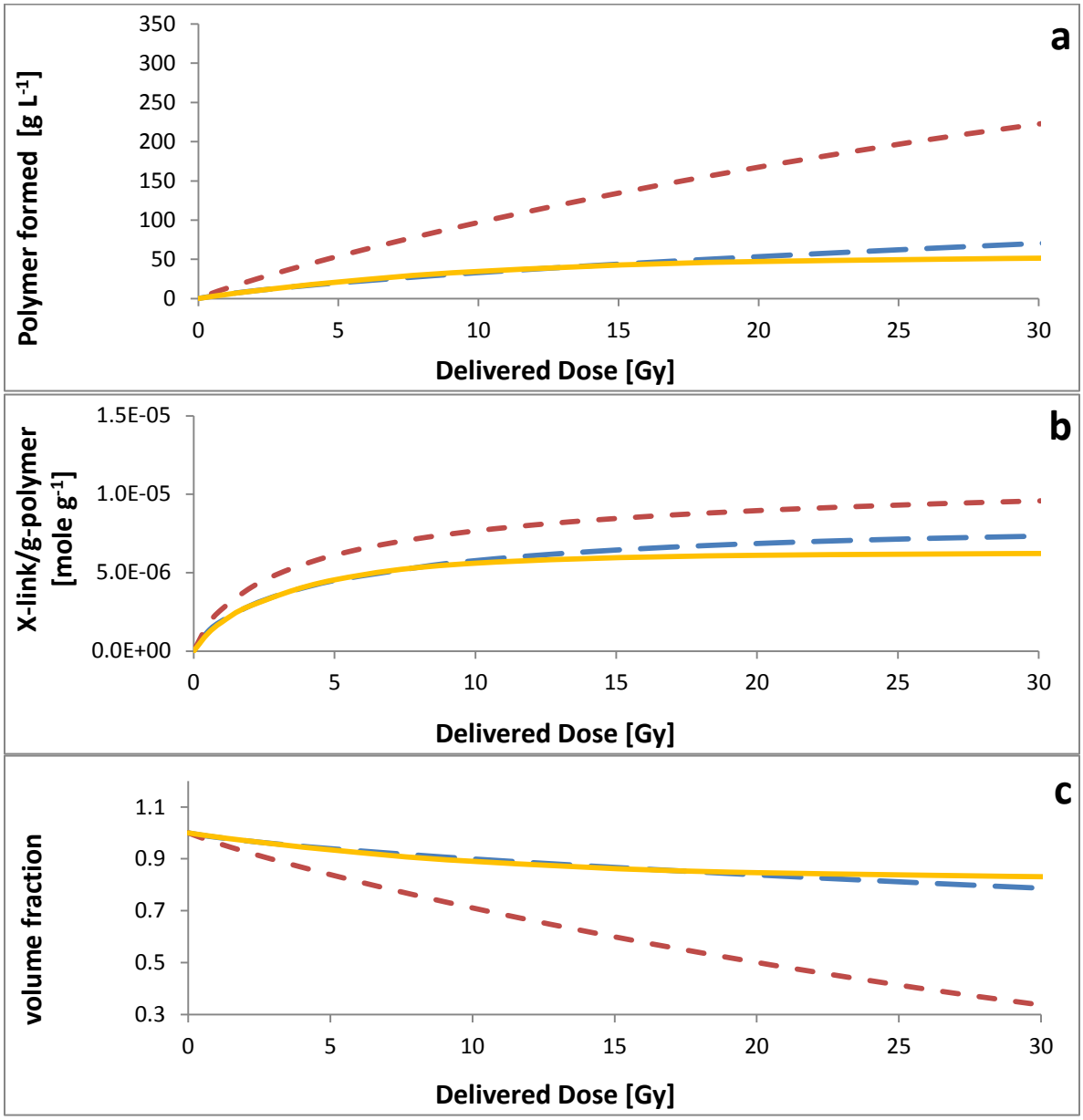

Figure 2.12: Comparison of dosimeter responses in calibration vials (——) with dosimeter responses to ^{192}Ir (— — —) and ^{125}I (- - - -) brachytherapy seeds. Simulation results are shown 12 hours after the start of irradiation for the vials and the ^{192}Ir phantom. For ^{125}I, results are shown after three days. At the same dose levels, the external beam radiation delivered to the calibration vials and ^{192}Ir brachytherapy radiation result in similar a) amount of polymer formed per Gy, b) x-link density and c) volume fraction of aqueous phase. Responses to ^{125}I are significantly different.

Diffusion of monomer and crosslinker during polymerization is the main reason that much lower values of ϕ (and higher polymer-phase fraction) are obtained in LDR brachytherapy dosimetry than in uniformly irradiated calibration vials or in HDR brachytherapy. In HDR brachytherapy, only a few hours elapse before polymerization rates become negligibly small. In LDR brachytherapy, irradiation and the associated polymerization occur over many days, providing a long time where monomer and crosslinker can diffuse and become incorporated into the growing polymer molecules.

Figure 2.12 shows that PAG dosimeters will result in poor accuracy for LDR brachytherapy dosimetry. There are large deviations in the amount of polymer formed, the crosslink density and the aqueous-phase volume fraction when comparing the LDR phantom and the calibrations vials. Because polymerization occurs over an extended period of time during LDR brachytherapy, there is ample time for excess monomer and crosslinker to diffuse toward the seed, resulting in large differences in the amount and type of polymer formed at each dose, when compared with the calibration vials. Similar problems are expected when single LDR brachytherapy seeds are used to construct calibration curves for multi-seed brachytherapy dosimetry experiments. In this situation, there may be significantly different concentration gradients and rates of diffusion in the vicinity of the multiple seeds than near the single calibration seed, which could lead to inaccurate dosimetry. As a result, we do not recommend PAG dosimeters and other polymer gel dosimeters for application to LDR brachytherapy. Alternative dosimetry systems are required wherein the chemical agent that interacts with the free radicals generated by radiation is not able to diffuse at any appreciable rate within the phantom.

Figure 2.12 also shows that PAG dosimeters can provide accurate HDR brachytherapy dosimetry. The amount of polymer (Figure 2.12 (a)) formed at each dose is in good agreement with the amount of polymer formed in the corresponding uniformly-irradiated calibration vials. Similar good agreement is obtained for the crosslink density and the aqueous-phase volume fraction (Figure 2.12(b) and (c), respectively). Deviations can be noticed for doses larger than about 15 Gy, which are encountered at values of $r <$ 0.4 cm. The reasons for discrepancies near the seed are the high dose rates (see Figure 2.4(a)), which are much higher than the 2.5 Gy min^{-1} used for the calibration vials and the high dose gradients that result in monomer diffusion near the seed. Even better results are expected when single HDR brachytherapy seeds are used to construct calibration curves for complex HDR brachytherapy dosimetry involving complex geometry and multiple seeds. The limited amount of time available for diffusion during polymerization ensures that similar dosimeter properties will be obtained using similar total radiation doses. In addition, the high dose rates near the seeds will be similar in single-seed and multi-seed situations, which will help to improve dosimeter accuracy.

Note that our model does not account for the effects of oxygen-scavenging agents, such as THPC, which are added to normoxic PAG dosimeters. These effects have not yet been included in mathematical models due to our limited understanding of the complex side reactions that occur (Jirasek *et al.* 2006, Koeva *et al.* 2009b). However, we anticipate that discrepancies between vials and HDR PAG dosimetry will be even smaller for dosimeters that contain THPC. PAG dosimeter recipes that include THPC result in less dose-rate dependence and shorter polymerization times due to fewer long-lived polymer radicals (McAuley 2004, De Deene *et al.* 2006). In dosimeters with THPC, monomer

consumption will cease within a few hours after the removal of the radioactive seed, providing less time for diffusing acrylamide and bisacrylamide to polymerize. HDR results are expected to be similar or slightly better for NIPAM-based polymer gel dosimeters than polyacrylamide gel dosimeters because NIPAM has a slightly lower diffusivity than acrylamide, due to its larger size. Unfortunately, addition of THPC will not tend to make LDR brachytherapy dosimetry more accurate using polymer gels. In LDR brachytherapy, continuous generation of radicals over a period of many days provides ample time for diffusing monomer and crosslinker to be consumed by polymerization, leading to inaccurate results, regardless of whether THPC is present or not.

2.7 Conclusions

A mathematical model is developed and used to simulate the influence of a spherical radioactive brachytherapy source on polymer formation and crosslinking in a polyacrylamide gel dosimeter. The model is used to investigate the accuracy of PAG dosimetry for HDR brachytherapy using an ^{192}Ir seed implanted for one minute and for LDR brachytherapy using an ^{125}I seed implanted permanently. Simulations of the response of PAG to both ^{192}Ir and ^{125}I seeds show that monomer and crosslinker concentration profiles are much flatter in the LDR simulations than in the HDR simulations because acrylamide and bisacrylamide are consumed more slowly in LDR brachytherapy dosimetry and have more time to diffuse. The temperature rise due to polymerization near the seed is small for the HDR (~2 °C) and LDR (0.01 °C) simulations that were conducted.

The proposed model cannot predict R_2 or other commonly measured responses for 3D dosimetry (e.g., optical and x-ray CT read-out variables) but it does predict important properties that are related to these common measurements, including the mass of polymer per unit volume, crosslink density and the volume fraction of the aqueous phase. Simulations results show large deviations between the phantom irradiated by the LDR brachytherapy seed and simulated calibration vials for all three of these properties. As a result, we do not recommend PAG dosimeters or any other polymer gel dosimeters with diffusing monomers for application to LDR brachytherapy. Effective dosimetry for LDR brachytherapy applications will require negligible diffusion of the chemical agent that records the radiation dose, both prior to and after irradiation.

On the other hand, our model shows a very good match between simulation results for the HDR-irradiated phantom and uniformly-irradiated vials in terms of the mass of polymer per unit volume, the crosslink density and volume fraction of aqueous phase for all distances larger than 4 mm from the centre of the seed. For example, at a distance of 1 cm from centre of seed, the deviation between the HDR phantom and the vials was less than 2.3% for all three simulated properties. Closer to the seed, discrepancies between the simulated HDR phantom and the vials increase due to the large dose rate near seed and the diffusion that occurs.

2.8 Acknowledgments

This work was funded by Canadian Institutes for Health Research (CIHR), Mathematics of Information Technology and Complex Systems (MITACS) and the Natural Sciences and Engineering Research Council of Canada (NSERC). The authors would like to thank Mr. Jonathan Chain, Dr. Chandra Joshi and Dr. Timothy Olding for technical advice.

2.9 Nomenclature

Symbols	
a_i	Constants used in the radial dose function, with i = 0, 1 ... 5
C_p	Heat capacity of the PAG gel system [J kg^{-1} K^{-1}]
R_{max}	Maximum radius of the phantom [cm]
$\dot{D}(r)$	Delivered dose rate [Gy min^{-1}]
D^i	Dead polymer chain in the i^{th} phase, where I = aq for the aqueous phase and p for the polymer phase
D_j	Diffusivity of the j^{th} species [cm^2 min^{-1}], where j=D, H_2O, M_1, M_2, P, $\dot{PR}$, PDB_{eff} and Q as defined in the subscripts section
$F(r)$	Anisotropy function for radiation delivery
G	Chemical yield of free radicals [mol J^{-1}]
$G(r)$	Geometry factor for radiation delivery
h	Heat transfer coefficient for heat transfer from the PAG to the surrounding environment [J cm^{-2} K^{-1} min^{-1}]
H_2O	Water
ΔH_R	Energy released per mole of double bonds consumed [J mol^{-1}]

k_{cond}	Thermal conductivity in the PAG dosimeter [J cm^{-1} K^{-1} min^{-1}]
k^{i}_{c}	Rate constant for intermolecular cyclization reactions in the *i*th phase [mol^{-1} min^{-1}]
k_m	Mass transfer coefficient for fast transfer of monomer, bisacrylamide and water between aqueous and polymer phases [min^{-1}]
$k_{x\,j}^{\,i}$	Rate constant for crosslinking in the i^{th} phase between an unreacted pendant double bond and a polymer radical with terminal species j. For acrylamide j=1 and for bisacrylamide j=2 [mol^{-1} min^{-1}]
M_1	Acrylamide monomer
M_2	Bisacrylamide crosslinker
$M_{w,H2O}$	Molecular weight of water [kg mol^{-1}]
P	Polymer radical with terminal acrylamide unit
$(\dot{PR})$	Initial primary radical (in the "cage")
$\dot{PR}$	Primary radical that has diffused away from its counterpart radical
Q	Polymer radical with terminal bisacrylamide unit
r	Radial distance from the centre of the seed [cm]
r_o	Reference radius (1 cm from the centre of the seed).
$\tilde{r}$	Transformed radial coordinate calculated from r using equation (2.7)
r_i	Net rate of generation of species i by chemical reactions [mol L^{-1} min^{-1}]
R_2	Transverse spin-spin relaxation rate [s^{-1}]
$R_{(\dot{PR})}$	Rate of generation of primary radicals [mol kg^{-1} min^{-1}]
S_k	The air kerma (Kinetic Energy Released per unit Mass) strength of the radiation source [U, where 1 U = 1 cGy cm^2 h^{-1}]
S_{k0}	Initial air kerma strength [U]
$T(r)$	Dimensionless radial dose function in equation (2.1) and Table 2.2

T	Temperature inside the PAG phantom [°C]
T_S	Temperature of the surrounding environment [°C]
t	Time [min]
$t_{1/2}$	The half-life of the source [min]
x	Horizontal coordinate [cm]

Subscripts

1	Acrylamide
2	Bisacrylamide
D	Dead polymer
H_2O	Water
M_1	Acrylamide monomer
M_2	Bisacrylamide crosslinker
P	Polymer radical with terminal acrylamide unit
PDB_{acc}	pendant double bond belonging to the polymer phase and available for cross-linking with growing radicals in the aqueous phase
PDB_{eff}	Pendant double bond available for crosslinking
$\dot{PR}$	Primary radical that has diffused away from its counterpart radical
Q	Polymer radical with terminal bisacrylamide unit

Superscripts

●	Radical species
w	Aqueous phase
p	Polymer phase

Greek Symbols	
Λ	The dose rate constant [Gy min^{-1} U^{-1}]
Γ	Dose delivery parameter used to indicate regions receiving radiation
$\lambda_{i,j}$	i^{th} moment of chain-length distribution for radicals in aqueous phase with terminal monomer j
ρ	Density of the PAG gel system [kg L^{-1}]
ϕ	Volume fraction occupied by aqueous phase
Φ_i	Ratio of the concentration of species i in the polymer-phase over the concentration of the same species in the aqueous phase

Acronyms	
2D	Two dimensional
3D	Three dimensional
Aam	Acrylamide monomer
Bis	N,N'-methylene-bisacrylamide crosslinker
CT	Computed Tomography
Gy	Gray, unit for radiation dose [J kg^{-1}]
HDR	High Dose Rate
LDR	Low Dose Rate
MR	Magnetic Resonance
MRI	Magnetic Resonance Imaging
NIPAM	N-isopropylacrylamide monomer
PAG	Polyacrylamide gel
PDB_{acc}	pendant double bond belonging to the polymer phase and available for cross-linking with growing radicals in the aqueous phase

PDB_{eff}	Pendant double bond available for crosslinking
PDE	Partial differential equation
THPC	Tetrakis (hydroxymethyl) phosphonium chloride
U	Unit of air kerma strength [cGy cm^2 h^{-1}]

2.10 References for chapter 2

Babic S and Schreiner L J 2006 An NMR relaxometry and gravimetric study of gelatin-free aqueous polyacrylamide dosimeters *Phys. Med. Biol.* **51** 4171–87.

Baldock C, Burford RP, Billingham N, Wagner GS, Patval S, Badawi RD and Keevil SF 1998a Experimental prpcedure for the manufacture and calibration of polyacrylamide gel (PAG) for magnetic resonance imaging (MRI) radiation dosimetry *Phys. Med. Biol.* **43** 695-702.

Baldock C, Rintoul L, Keevil SF, Pope JM, and George GA 1998b Fourier transform Raman spectroscopy of polyacrylamide gels (PAGs) for radiation dosimetry *Phys. Med. Biol.* **43**, 3617.

Baldock C, De Deene Y, Doran S, Ibbott G, Jirasek A, Lepage M, McAuley KB, Oldham M, and Schreiner LJ 2010 Polymer gel dosimetry *Phys. Med. Biol.* **55** 1–63Y. De Deene, Journal of Physics. 2004, Conference Series 3, 34–57.

Baras P, Seimenis I, Kipouros P, Papagiannis P, Angelopoulos A, Sakelliou L, Pappas E, Baltas D, Karaiskos P, Sandilos P and Vlachos L 2002 Polymer gel dosimetry using a three-dimensional MRI acquisition technique, *Med. Phys.* 2002, **29 (11)** 2506-2516.

Blom JG, Trompert RA, and Verwer JD 1996 Algorithm 758: VLUGR2: A Vectorizable Adaptive-Grid Solver for PDEs in 2D ACM *Transactions on Mathematical Software.* **22 (3)** 302-328.

Chain JNM (December 2010) Recip Improvement and Mathematical Modelling of Polymer Gel Dosimeters *MSc. (Eng.) University, Kingston, ON, Canada*.

Chain JNM, Jirasek A, Schreiner LJ and McAuley KB 2011a Cosolvent-free polymer gel dosimeters with improved dose sensitivity and resolution for x-ray CT dose response *Phys. Med. Biol.* **56** 2091-2102.

Chain JNM, Nasr AT, Schreiner LJ and McAuley KB 2011b Mathematical Modeling of Depth-Dose Response of Polymer-Gel Dosimeters *Macromol. Theory Simul.* **20** 735–751.

De Deene Y, Reynaert N and DeWagter C 2001 On the accuracy of monomer/polymer gel dosimetry in the proximity of a high-dose-rate ^{192}Ir source *Phys. Med. Biol.* **46** 2801–2825.

De Deene Y, Hurley C, Venning A, Vergote K, Mather M, Healy BJ and Baldock C 2002 A basic study of some normoxic polymer gel dosimeters *Phys. Med. Biol.* **47** 3441–3463.

De Deene Y 2004 Essential characteristics of polymer gel dosimeters *J. Physics. Conference Series* **3**, 34–57

De Deene Y, Vergote K, Claeys C and DeWagter C 2006 The fundamental radiation properties of normoxic polymer gel dosimeters: a comparison between a methacrylic acid based gel and acrylamide based gels *Phys. Med. Biol.* **51** 653–73.

Erickson BA, Demanes DJ, Ibbott GS, Hayes JK, Hsu CJ, Morris DE, Rabinovitch RA, Tward JD and Rosenthal SA, 2011 American Society for Radiation Oncology (ASTRO) and American College of Radiology (ACR) Practice Guideline for the Performance of High-Dose-Rate Brachytherapy *I. J. Radiation Oncology Biol. Phys.* **79-2** 641-649.

Farajollahi AR, Bonnett DE, Ratcliffe AJ, Aukett RJ and Mills JA 1999 Dosimetry of Interstitial Brachytherapy Sources *The British Journal of Radiology*, **72** 1085-1092.

Fragoso M, Love PA, Verhaegen F, Nalder C, Bidmead AM, Leach M and Webb S 2004 The dose distribution of low dose rate Cs-137 in intracavitary brachytherapy: comparison of Monte Carlo simulation, treatment planning calculation and polymer gel measurement *Phys. Med. Biol.* **49** 5459–5474.

Fuxman AM (July 2003) Modelling Chemical and Physical Phenomena in Polyacrylamide Gel for Radiation Dosimetry *M.Sc. (Eng.), Queen's University, Kingston, ON, Canada*.

Fuxman AM, McAuley KB and Schreiner LJ 2003 Modeling of Free-radical Crosslinking Copolymerization of Acrylamide and N,N'-Methylenebis(acrylamide) for Radiation Dosimetry *Macromol. Theory Simul.* **12** 647-662.

Fuxman AM, McAuley KB and Schreiner LJ 2005 Modeling of polyacrylamide gel dosimeters with spatially non-uniform radiation dose distributions *Chem. Eng. Sci.* **60** 1277-9337.

Gerbaulet A, Pötter R, Mazeron JJ, Meertens H and Van Limbergen E The GEC ESTRO Handbook of Brachytherapy *ACCO, Leuven, Belgium* 2002.

Gifford KA, Horton JL, Jackson EF, Steger TR, Heard MP, Mourtada F, Lawyer AA and Ibbott GS 2005 Comparison of Monte Carlo calculations around a Fletcher Suit Delclos ovoid with radiochromic film and normoxic polymer gel dosimetry *Med. Phys.* **32 (7)** 2288-2294.

Hurley C, McLucas C, Pedrazzini G and Baldock C 2006 High-resolution gel dosimetry of a HDR brachytherapy source using normoxic polymer gel dosimeters: Preliminary study *Nuclear Instruments and Methods in Physics Research A* **565** 801–811.

Ibbott GS and Heard MP 2010 3D dosimetry for brachytherapy and heterogeneities *Journal of Physics. Conference Series* **250** 436-441.

Jirasek AI, and Duzenli C 2001 Effects of crosslinker fraction in polymer gel dosimeters using FT Raman spectroscopy *Phys. Med. Biol.* **46** 1949–1961.

Jirasek AI, Duzenli C, Audet C, and Eldridge J 2001 Characterization of monomer/crosslinker consumption and polymer formation observed in FT-Raman spectra of irradiated polyacrylamide gels *Phys. Med. Biol.* **46** 151-165

Jirasek A, Hilts M, Shaw C and Baxter P 2006 Investigation of tetrakis hydroxymethyl phosphonium chloride as an antioxidant for use in x-ray computed tomography polyacrylamide gel dosimetry *Phys. Med. Biol*. **51** 1891–1906.

Jirasek A, Hilts M and McAuley KB 2010 Polymer gel dosimeters with enhanced sensitivity for use in x-ray CT polymer gel dosimetry *Phys. Med. Biol.* **55** 5269-5281.

Kipouros P, Papagiannis P, Sakelliou L, Karaiskos P, Sandilos P, Baras P, Seimenis I, Kozicki M, Anagnostopoulos G and Baltas D 2003 3D dose verification in ^{192}Ir

HDR prostate monotherapy using polymer gels and MRI *Med. Phys.* **30 (8)** 2031-2039.

Koeva VI (December 2008) Improved Recipes for Polymer Gel Dosimeters Containing N-IsoPropyl Acrylamide *MSc. (Eng.) Queen's University, Kingston, ON, Canada*.

Koeva VI, Olding T, Jirasek A, Schreiner LJ and McAuley KB 2009a Preliminary investigation of the NMR, optical and x-ray CT dose–response of polymer gel dosimeters incorporating cosolvents to improve dose sensitivity *Phys. Med. Biol.* **54** 2779-2790.

Koeva VI, Daneshvar S, Senden RJ, Imam AHM, Schreiner LJ and McAuley KB 2009b Mathematical Modeling of PAG and NIPAM Based Polymer Gel Dosimeters Contaminated by Oxygen and Inhibitor *Macromol. Theory Simul.* **18** 495-510.

Lepage M, Whittaker AK, Rintoul L, Back SAJ, and Baldock C 2001a Modelling of post-irradiation events in polymer gel dosimeters *Phys. Med. Biol.* **46** 2827–2839

Lepage M, Whittaker AK, Rintoul L, and Baldock C 2001b ^{13}C-NMR, ^{1}H-NMR, and FT-Raman Study of Radiation- Induced Modifications in Radiation Dosimetry Polymer Gels *J. Appl. Polym. Sci.* **79** 1572

Lin MH, Huang TC, Kao MJ, Wu J, Chen CL and Wu TH 2009 Three-dimensional dosimetry in brachytherapy: A MAGAT study *Applied Radiation and Isotopes* **67** 1432–1437.

Maryanski MJ, J. C. Gore JC, Kennan RP and Schulz RJ 1993 NMR relaxation enhancement in gels polymerized and cross-linked by ionizing radiation: a new approach to 3D dosimetry by MRI *Magn. Reson. Imaging.* **11** 253–258.

Maryanski MJ, Schulz RJ, Ibbott GS, Gatenby JC, Xie J, Horton D and Gore JC 1994 Magnetic resonance imaging of radiation dose distributions using a polymer-gel dosimeter *Phys. Med. Biol.* **39** 1437–1455.

Maryanski MJ, Ibbott GS, Eastman P, Schulz RJ and Gore JC 1996 Radiation therapy dosimetry using resonance imaging of polymer gels *Med. Phus.* **23 (5)** 699-706.

Massillon-JL G, Minniti R, Mitch MG, Soares CG and Hearn RA 2011 High-resolution 3D dose distribution measured for two low-energy x-ray brachytherapy seeds: ^{125}I and ^{103}Pd *Radiation Measurements* **46** 238-243.

McAuley KB 2004 The chemistry and physics of polyacrylamide gel dosimeters: why they do and don't work *Journal of Physics: Conference Series.* **3** 29–33.

McJury M, Tapper PD, Cosgrove VP, Murphy PS, Griffin S, Leachk MO, Webb S and Oldham M 1999 Radiation dosimetry using polymer gels: methods and applications *Phys. Med. Biol.* **44** 2431–2444.

Nasr AT, Chain JNM, Schreiner LJ and McAuley KB 2010 Mathematical modelling of response of polymer gel dosimeters to brachytherapy radiation *journal of physics: Conference series* **250** 321-323.

National cancer institute, fact sheet: radiation therapy for cancer, http://www.cancer.gov/cancertopics/factsheet/Therapy/radiation (October 2013)

Nath R, Anderson LL, Luxton G, Weaver KA, Williamson JF and Meigooni AS 1995 Dosimetry of Interstitial Brachytherapy Sources *Med. Phys.* **22** 209-234.

Noda S, Suzuki Y, Hoshino Y, Furukawa S, Katoh H, Kurotaki K and Nakano T 2008 Clinical application of the Fricke-glucomannan gel dosimeter for high-dose-rate ^{192}Ir brachytherapy *Phys. Med. Biol.* **53** 3985–3993.

Olding T, Holmes O, DeJean P, McAuley KB, Nkongchu K, Santyr G and Schreiner LJ 2011 Small field dose delivery evaluations using cone beam optical computed tomography-based polymer gel dosimetry *Journal of Medical Physics.* **36** 3-14.

Pantelis E, Karlis AK, Kozicki M, Papagiannis P, Sakelliou L and Rosiak JM 2004 Polymer gel water equivalence and relative energy response with emphasis on low photon energy dosimetry in brachytherapy *Phys. Med. Biol.* **49** 3495–3514.

Pantelis P, Lymperopoulou G, Papagiannis P, Sakelliou L, Stiliaris E, Sandilos P, Seimenis I, Kozicki M and Rosiak JM 2005 Polymer gel dosimetry close to an ^{125}I interstitial brachytherapy seed *Phys. Med. Biol.* **50** 4371–4384.

Pantelis E, Baltas D, Georgiou E, Karaiskos P, Lymperopoulou G, Papagiannis P, Sakelliou L, Seimenis I and Stilliaris E 2006 Dose characterization of the new Bebig IsoSeeds I25.S17 using polymer gel and MRI, *Nuclear Instruments and Methods in Physics Research A* **569** 529–532.

Papagiannis P, Pappas E, Kipouros P, Angelopoulos A, Sakelliou L, Baras P, Karaiskos P, Seimenis I, Sandilos P and Baltas D 2001 Dosimetry close to an ^{192}Ir HDR source using N-vinylpyrrolidone based polymer gels and magnetic resonance imaging *Med. Phys.* **28 (7)** 1416-1426.

Papagiannis P, Pantelis E, Georgiou E, Karaiskos P, Angelopoulos A, Sakelliou L, Stiliaris S, Baltas D and Seimenis I 2006 Polymer gel dosimetry for the TG-43 dosimetric characterization of a new ^{125}I interstitial brachytherapy seed *Phys. Med. Biol.* **51** 2101–2111.

Petrokokkinos L, Zourari K, Pantelis E, Moutsatsos A, Karaiskos P, Sakelliou L, Seimenis I, Georgiou E and Papagiannis P 2011 Dosimetric accuracy of a

deterministic radiation transport based ^{192}Ir brachytherapy treatment planning system. Part II: Monte Carlo and experimental verification of a multiple source dwell position plan employing a shielded applicator *Med. Phys.* **38 (4)** 1981-1992.

Rosenthal SA, Bittner NHJ, Beyer DC, Demanes DJ, Goldsmith BJ, Horwitz EM, Ibbott GS, Lee WR, Nag S, Suh WW and Potters L 2011 American society for radiation oncology (ASTRO) and American college of radiology (ACR) practice guideline for the transperineal permanent brachytherapy of prostate cancer *I. J. Radiation Oncology Biol. Phys.* **79- 2** 353-341.

Salomons G, Park Y, McAuley KB and Schreiner LJ 2002 Temperature increases associated with polymerization of irradiated PAG dosimeters *Phys. Med. Biol.* **47** 1435–1448.

Schreiner LJ 2006 Dosimetry in modern radiation therapy: limitations and needs *Journal of Physics: Conference Series.* **56** 1–13.

Senden RJ, De Jean P, McAuley KB and Schreiner LJ 2006 Polymer gel dosimeters with reduced toxicity: a preliminary investigation of the NMR and optical dose–response using different monomers *Phys. Med. Biol.* **51** 3301–3314.

Spinks JWT and Woods R 1976 An introduction to radiation chemistry, *second edition, John Wiley & Sons* New York.

Vergote K, De Deene Y, Vanden Bussche E and De Wagter C 2004 On the relation between the spatial dose integrity and the temporal instability of polymer gel dosimeters *Phys. Med. Biol.* **49** 4507-4522.

Chapter 3

Evaluation of the potential for diacetylenes as reporter molecules in 3D micelle gel dosimetry

3.1 Chapter Overview

Results from the previous chapter suggest that PAG gels will give poor dosimetry results when they are used with LDR brachytherapy sources because of the long time when un-reacted monomers can diffuse. As a result, developing gel dosimeters with low diffusion will be beneficial for obtaining accurate dosimetry results. Radiochromic leuco-dye micelle gel dosimeters introduced by Jordan and his co-workers (Jordan and Avvakumov 2009, Babic *et al.* 2009) are promising because they show superior spatial stability compared to polymer and Fricke gel dosimeters and they can be read out by optical CT scanners. In an effort to develop improved radiochromic micelle gel dosimeters, the use of pentacosa-10,12-diynoic acid (PCDA) (which is the radio-sensitive material used in GafChromic® films for two dimensional dosimetry) as reporter molecules to replace leuco-dyes in radiochromic micelle gel dosimeter is evaluated in this chapter.

The material presented in this chapter has been published in *Physics in Medicine and Biology* **2013**, *58*, **787–805**.

Evaluation of the potential for diacetylenes as reporter molecules in 3D micelle gel dosimetry

AT Nasr[1], T Olding[2], LJ Schreiner[2,3] and KB McAuley[1]

[1] Dept. Chemical Engineering, Queen's University, Kingston, Canada, K7L 3N6

[2] Cancer Centre of Southeastern Ontario, Kingston, Canada, K7L 5P9

[3] Depts. of Oncology and Physics, Queen's University, Kingston, Canada, K7L 3N6

3.2 Summary

Radiochromic micelle gel dosimeters are promising for three-dimensional (3D) radiation dosimetry because they can be read out by optical CT techniques and they have superior spatial stability compared to polymer and Fricke gel dosimeters. This study evaluates the use of diacetylenes as reporter molecules in micelle gel dosimeters. Several gels containing pentacosa-10,12-diynoic acid (PCDA) solubilized using sodium dodecyl sulfate (SDS) changed from colourless to blue upon irradiation. Unfortunately, all phantoms that experienced a colour change were turbid and would be unsuitable for 3D dosimetry. Two techniques (use of organic solvent and aqueous-phase additives) were successful in increasing colloidal stability to prevent the turbidity problem, but none of the resulting transparent gels changed colour in response to radiation. Transparent PCDA solutions were prepared using NaOH with no SDS or other surfactants, but these transparent solutions also did not change colour. Only turbid gels and surfactant solutions with precipitated PCDA particles responded to radiation. These results indicate that the colour change was due to the oligomerization within precipitated PCDA crystals, and that

liquid-phase PCDA solubilized in micelles did not undergo oligomerization. As a result, PCDA is not suitable for use in micelle gel dosimeters, and other radiochromic reporter molecules will need to be identified.

3.3 Introduction

Developments in radiation delivery equipment and imaging techniques have helped to obtain closer three-dimensional (3D) conformation of dose distribution to tumor volume (Schreiner 2006). Various radiation dosimeters are used in quality assurance systems to assure that radiation equipment delivers the intended dose to the correct location while minimizing the exposure of healthy tissues to radiation. Radiation dosimeters are devices fabricated from radiation-sensitive materials that, upon irradiation, undergo changes that are detectable and quantifiable. These changes are indicative of the amount and spatial distribution of the absorbed radiation dose (Adamovics 2006, Baldock *et al.* 2010). Detectable changes include changes in optical properties (e.g., color, transparency), changes in density and changes in nuclear magnetic resonance properties (Hurley *et al.* 2006).

Point-detection radiation dosimetry techniques (e.g., ionization chambers) and two-dimensional (2D) techniques (e.g., radiographic film) are routinely used to measure and calibrate radiation doses (Baldock *et al.* 2010). However, for full evaluation of complex dose deliveries, it is important to have dosimeters that can verify entire three-dimensional (3D) dose distributions delivered by external beam and internal brachytherapy radiation techniques. An ideal 3D dosimeter should have a response that is stable, measurable, significant, well-defined and reproducible (De Deene 2004). The dose response should not be sensitive to temperature, pressure, light and atmospheric gases, as

these factors may vary during irradiation and scanning. Dosimeters should be tissue-equivalent for the type of radiation used. The response of an ideal dosimeter depends on the total radiation dose delivered, but should not be influenced by the energy or dose rate. Examples of current 3D dosimeters are Fricke gel dosimeters, polymer gel dosimeters, the PRESAGE plastic dosimeter and, recently, micelle gel dosimeters. 3D dosimeters have been developed for readout using a variety of imaging techniques including Magnetic Resonance Imaging (MRI), optical Computed Tomography (CT) and x-ray CT (Maryanski *et al.* 1993, Maryanski *et al.* 1994, Maryanski *et al.* 1996, Jirasek *et al.* 2010 and Olding *et al.* 2011,).

Unfortunately implementation of 3D gel dosimeters in radiation clinics is not widespread because of limitations and difficulties associated with the different 3D phantoms and associated readout techniques (Baldock *et al.* 2010, Vandecasteele *et al.* 2011). Fricke gel dosimeters (typically read out by MRI or optical CT) do not retain spatial stability beyond a few hours due to rapid diffusion of iron ions (Gore *et al.* 1984, Appleby *et al.* 1987, Schreiner 2004, Hurley *et al.* 2006, Baldock *et al.* 2010). Polymer gel dosimeters, especially polyacrylamide gels (PAG) and NIPAM-based gels, show relatively better post irradiation stability (Maryanski *et al.* 1993, Maryanski *et al.* 1994, Maryanski *et al.* 1996, De Deene *et al.* 2002a, Senden *et al.* 2006, Koeva *et al.* 2009a, Baldock *et al.* 2010, Jirasek *et al.* 2010, Chain *et al.* 2011a, Olding *et al.* 2011), but they experience problems due to oxygen contamination and diffusion of unreacted monomers (De Deene *et al.* 2002b, McAuley 2004, Vergote *et al.* 2004, Jirasek *et al.* 2006, Senden *et al.* 2006, Koeva *et al.* 2009b, Baldock *et al.* 2010, Chain *et al.* 2011b, Sedaghat *et al.* 2011, Nasr *et al.* 2012).

Fricke gel and PAG are examples of dosimeters that are traditionally read out by MRI. The main issues using MRI scanning techniques in clinics are related to cost, availability, and lack of special skills required for quantitative MRI (Vandecasteele *et al.* 2011). Among the different alternative readout techniques, optical CT scanners seem to be the most promising because they are low in cost, portable and could be readily accessible in most clinical environments (Doran 2009, Olding *et al.* 2011, Vandecasteele *et al.* 2011). These advantages of optical CT scanners have stimulated the development of optically clear radiochromic 3D dosimeters such as PRESAGE and micelle gel dosimeters (Adamovics 2006, Adamovics and Maryanski 2006, Babic *et al.* 2009, Jordan and Avvakumov 2009, Vandecasteele *et al.* 2011).

PRESAGE dosimeters are solid polyurethane-based radiochromic 3D dosimeters, developed by Adamovics and coworkers (Adamovics 2006, Adamovics and Maryanski 2006, Guo *et al.* 2006, Hurley *et al.* 2006). These dosimeters contain free radical initiators and a leuco-dye dissolved in the solid polyurethane. Upon irradiation, the colourless leuco-dye is converted to a coloured dye. Unfortunately, tissue equivalence of PRESAGE is an issue for this type of dosimeter (Brown *et al.* 2008).

Jordan and coworkers recently developed new radiochromic micelle gel dosimeters for optical readout. In these phantoms, a colourless leuco-dye (e.g., leuco malachytegreen or leuco crystal violet) is solubilized in a hydrogel matrix using a surfactant (Babic *et al.* 2009, Jordan and Avvakumov 2009, Vandecasteele *et al.* 2011). The leuco-dye molecules react with free radicals generated by water radiolysis, changing from colourless to deeply coloured as the radiation dose increases. Since the main

component of micelle gel dosimeters is water, these dosimeters should be more tissue equivalent than PRESAGE.

Micelles are self-assembled aggregates of surfactant molecules that have both hydrophilic and hydrophobic parts. Above the critical micelle concentration (CMC), surfactant molecules orient themselves so that their hydrophobic parts repel away from surrounding water toward the centres of the micelles, leaving their hydrophilic parts in contact with water. The main purpose of using micelles in gel dosimeters is to solubilize the mostly water-insoluble leuco-dye molecules, thereby distributing the leuco-dye throughout the 3D gel volume (Babic *et al.* 2009). A second benefit is that micelles are significantly larger than individual molecules so that the leuco-dye molecules solubilized in micelles have low diffusivity compared to reporter molecules in micelle-free gel dosimeters. As a result, current micelle gel dosimeters have improved spatial stability of dose information, compared with traditional optical dosimeters such as Fricke gel dosimeters (Jordan and Avvakumov 2009). Current micelle gel dosimeters could benefit from further improvements as they are light-sensitive and temperature-sensitive during irradiation and tend to fade over time (Babic *et al.* 2009). They also have relatively low dose sensitivity and may have significant dose-rate dependence (Vandecasteele *et al.* 2011).

In an attempt to develop improved micelle gel dosimeters, the use of diacetylenes solubilized in micelles, as reporter molecules is investigated in this work. Diacetylenes are organic molecules that contain two conjugated acetylene groups (i.e., two carbon-carbon triple bonds separated by a single bond) (Rink *et al.* 2008). Note that the diacetylene pentacosa-10,12-diynoic acid (PCDA) is the reporter molecule in commercial

GafChromic® film, which is used for 2D dosimetry (Rad *et al*. 1998, Rink *et al.* 2008). Other diacetylenes have also been used as reporter molecules in self-developing films (Patel 2005, Watanabe *et al.* 2006). Upon irradiation, diacetylene molecules can react to form oligomers that have conjugated double and triple bonds. These oligomer molecules exhibit intense colour, leading to a response that is approximately proportional to absorbed dose (Ogawa 1989, Rink *et al.* 2008). Figure 3.1 shows the three diacetylenes considered in this study, along with their melting points. Note that these diacetylenes are solids at room temperature. It has been reported that the acetylene groups in adjacent diacetylene monomers should be within 0.4 nm of each other to oligomerize (Rink *et al.* 2008). In a closely packed state, such as Langmuir-Blodgett films, vesicles, and micelles some diacetylenes undergo a 1,4 oligomerization reaction as shown in figure 3.2 for PCDA (Mino *et al.* 1992, Ogawa 1992, Rad *et al.* 1998, Kim *et al.* 2005, Su *et al.* 2005, Ma *et al.* 2007, Choi *et al.* 2008, Rink *et al.* 2008, Araghi *et al.* 2011, Perino *et al.* 2011).

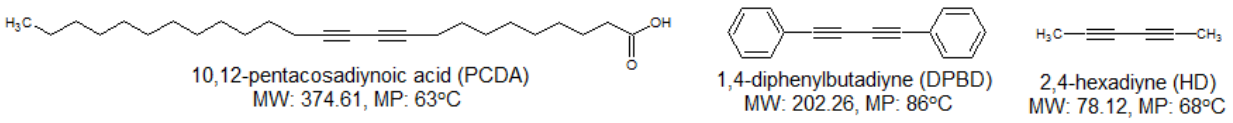

Figure 3.1: Chemical structure of three commercially available diacetylenes with their molecular weights and melting points.

An essential component in micelle gel dosimeters is the surfactant. The solubilizing ability of surfactants can be roughly estimated by an empirical factor known as the Hydrophilic-Lipophilic Balance (HLB) (Davies 1957, Davies and Rideal 1963). HLB can be calculated from the chemical structure of the surfactant, based on its functional groups (Davies 1957, Davies and Rideal 1963). Using the Davies method, any

surfactant with a HLB value between 13 and 15 will be a good detergent that forms micelles in water.

Surfactants are classically divided into anionic, cationic, and nonionic surfactants. In many surfactants, especially ionic surfactants, when temperature decreases surfactant molecules can precipitate out of the solution as hydrated crystals (Evans and Wennerstrom 1999). The temperature at which this phenomenon occurs is called the Krafft temperature (T_k) (Shinoda and Fontell 1995, Evans and Wennerstrom 1999, Qian *et al.* 2005). A surfactant is effective as an emulsifier or a solubilizer at temperatures above T_k (Shinoda and Fontell 1995). Other factors that can affect stability of surfactant solutions include pH and salt concentration (ionic strength) (Binks 1998).

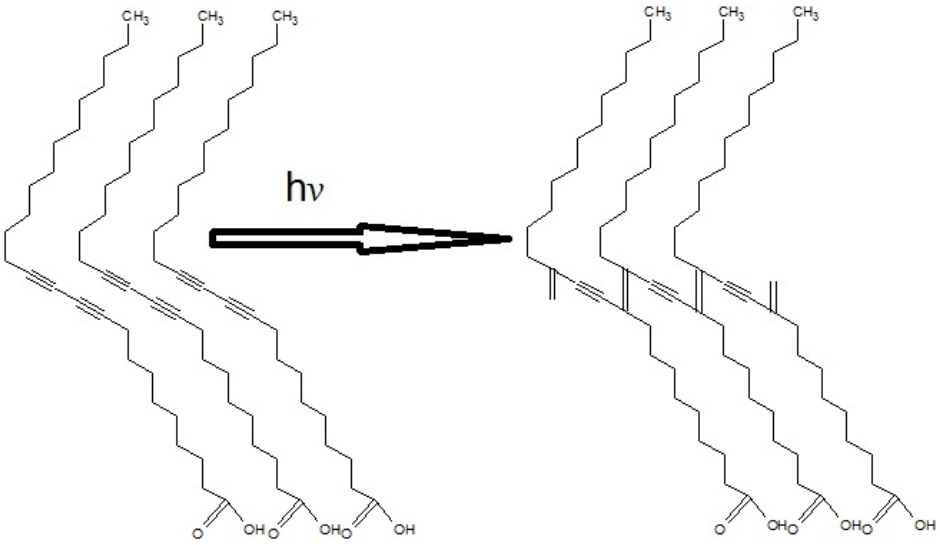

Figure 3.2: Schematic representation of radiation induced oligomerization of three PCDA molecules (Ogawa 1992, Kim *et al.* 2005). Note the conjugated triple and double bonds in the product molecule, which produce colour.

In this article, the use of diacetylenes solubilized in micelles as reporter molecules in gel dosimeters is studied. The radiation response of PCDA, solubilized using three common surfactants (sodium dodecyl sulfate (SDS), Triton x-100 and cetyl trimethyl ammonium bromide (CTAB)), is investigated and the performance of two additional diacetylenes (DPBD and HD) is compared with that of PCDA, using SDS as the surfactant. Problems with stability of surfactant solutions of PCDA, lack of response (colour change) and poor reproducibility are investigated via additional experiments. Finally, conclusions are drawn concerning the relationship between PCDA phase change (i.e., precipitation) and response to radiation dose.

3.4 Materials and methods

3.4.1 Preparation procedure of PCDA surfactant solutions and gels

All solutions were manufactured by first preparing stock solutions of surfactants at the required concentration. The diacetylene was then added to the surfactant solutions and the resulting mixtures were stirred at 58 ºC for 15 minutes, prior to heating to slightly above the melting point of the diacetylene (see figure 3.1) and stirring for at least 15 minutes until the mixtures became clear, indicating that the diacetylene was solubilized. Mixtures were then cooled to room temperature. Bovine gelatin (300 Bloom bovine bones, Eastman Gelatin Corp., MA, USA) was then added to the cooled diacetylene surfactant solutions and left to swell for 30 minutes. Bovine gelatin was selected because it may lead to better optical properties than porcine gelatin (Olding *et al.* 2010). Mixtures were then heated and stirred at 45 ºC until the gelatin dissolved. Samples of the gel mixture were poured into polystyrene cuvettes (10 mm light path, 4.5 ml capacity, Fisher

scientific), which were then sealed using a cap and parafilm and refrigerated at 4 ºC until irradiation.

3.4.2 Irradiation procedure

Irradiation was performed using a Varian Clinac 6EX linear accelerator (Varian Medical Systems, Palo Alto, CA, USA) to different doses at a dose rate of 400 cGy/min. The cuvettes were irradiated using an isocentric setup, with a source-to axis distance (SAD) of 100 cm, 2 cm of plastic water buildup, 10 cm of plastic water backscatter, and 10×10 cm^2 field size. The long dimension (height) of the cuvettes was perpendicular to the beam axis.

3.4.3 Optical transmission spectrometer measurements

Absorption spectra were measured for cuvettes irradiated to different doses between 15 and 25 minutes after irradiation. All samples were at room temperature (20-23 ºC) at the time when the spectra were measured, using a SpectroVis Plus spectrophotometer (Vernier Software & Technology, OR, USA) over the wavelength region λ = 380-900 nm. All the measurements were calibrated to the 0 Gy cuvette of each diacetylene surfactant solution or gel.

3.4.4 Preliminary experiments

Preliminary experiments focused on solubilizing PCDA (GFS chemicals, Ohio, USA) using three different common surfactants at different concentrations. The three surfactants (Fisher Scientific, Ottawa, Canada) are the anionic surfactant SDS, the nonionic surfactant Triton x-100, and the cationic surfactant CTAB. All were dissolved in deionized water. A variety of concentrations for both the PCDA and surfactants were tested and only the recipes that resulted in transparent solutions are shown in table 3.1.

Bovine gelatin was added in some cases to make gels. Samples of prepared PCDA surfactant solutions and gels were refrigerated at 4 ºC for 48 h after manufacturing and were then irradiated to 100 Gy. Irradiated and un-irradiated samples of the prepared PCDA surfactant solutions and gels were also kept at 4 ºC for 40 days.

3.4.5 Comparing PCDA radiation response with that of other diacetylenes

Gels of PCDA, DPBD (Aldrich) and HD (Aldrich) were prepared using reporter molecule concentrations of 3 mM, with 51 mM SDS and 5 wt% gelatin. Samples of the gels were irradiated 24 h after manufacturing to 0, 5, 10, 20 and 40 Gy. Spectra of irradiated gel samples were measured approximately 20 minutes after irradiation. Samples of PCDA in its pure solid state were also irradiated to 20 Gy to check if they would change colour in response to irradiation.

3.4.6 Effect of PCDA concentration on dose response

The effect of PCDA concentration on the dose response was studied. Solutions of PCDA using a SDS concentration of 51 mM and 5 wt% gelatin were prepared at monomer concentrations of 1.5, 3, 6, 9, and 21 mM. Gel samples were irradiated 24 h after manufacturing to 0, 2, 5, 10, 15 and 20 Gy. Spectra of irradiated gel samples were measured approximately 20 minutes after irradiation.

Table 3.1: Transparent solutions and gels manufactured for preliminary testing.

Vial #	PCDA Conc. mM	Surfactant Type	Surfactant Conc. mM	Gelatin Added wt%	Irradiated
1	3	SDS	51	0	Y
2	3	SDS	51	0	N
3	3	SDS	51	5	Y
4	3	SDS	51	5	N
5	16	SDS	327	0	Y
6	16	SDS	327	0	N
7	16	SDS	327	5	Y
8	16	SDS	327	5	N
9	8	Tx-100	60	0	Y
10	8	Tx-100	60	0	N
11	8	Tx-100	60	5	Y
12	8	Tx-100	60	5	N
13	5	CTAB	54	0	Y
14	5	CTAB	54	0	N
15	5	CTAB	54	5	Y
16	5	CTAB	54	5	N

3.4.7 Influence of PCDA surfactant solution and gel phase stability on radiation response

The purpose of these experiments was to check if colour change is related to turbidity, caused by either PCDA precipitation from the micelles or precipitation of SDS surfactant below its Krafft temperature of 18 ºC. In the experiments in sections 3.4.4 to 3.4.6, gels that became turbid during refrigeration tended to change colour in response to irradiation, whereas transparent gels did not.

3.4.7.1. Gelatin effect on SDS phase behavior.

Experiments were performed to check whether gelatin influenced precipitation behavior of SDS solutions that did not contain any reporter molecules. A gel with 51 mM SDS and 5 wt% gelatin was prepared, along with a similar gelatin-free solution. Samples

with and without gelatin were refrigerated at 4 ºC for 10 days and were then examined visually.

3.4.7.2. Effect of adding solvent on gels phase stability.

A solvent was added to the recipe to determine whether it would improve the phase stability of gels. Xylene was selected because it is a good solvent for PCDA and its melting point is -34 ºC which will ensure that it will not precipitate when the gel samples are refrigerated. A stock solution of 51 mM SDS solution was prepared using 3 mM PCDA and 5 wt% gelatin, which was then cooled to room temperature. Xylene was added to different samples using the following concentrations: 1.5, 3, 6 and 15 mM and clear gels were obtained. Samples with and without xylene were refrigerated at 4 ºC and irradiated 24 h after manufacturing to 20 Gy. Spectra of irradiated gel samples were measured. Un-irradiated samples of the prepared gels, with and without xylene, were also kept at 4 ºC for two weeks and were observed visually.

3.4.7.3. Effect of salt, acid and base additives on phase stability of gels.

A mixture containing 51 mM SDS, 3mM PCDA and 5 wt% gelatin was prepared and stirred at 45 ºC. The following additives were added to samples of the mixture: tetrakis hydroxymethyl phosphonium chloride (THPC) (Sigma Aldrich, Oakville, Canada), NaCl, NaOH and HCl (all from Fisher, Ottawa, Canada) at a concentration of 6 mM. Samples of the resulting gels with and without additives were refrigerated at 4 ºC and irradiated 24 h after manufacturing to 20 Gy. Spectra of irradiated gel samples were measured. Un-irradiated samples of the prepared gels, with and without additives, were also kept at 4 ºC for two weeks.

3.4.7.4. Gel ageing and phase behaviour.

This experiment was performed to observe the phase behavior of refrigerated PCDA gels over time, and to verify whether transparent gels respond to irradiation or whether only turbid gels change colour. 3 mM and 9 mM PCDA gels were prepared using 51 mM SDS and 5 wt% gelatin. Refrigerated samples were observed visually 0.5, 1.5, 2.5, 3.5 and 7.5 days after manufacturing. At each time period, vials were removed from the refrigerator and irradiated to 10 Gy. Spectra were measured approximately 20 minutes after irradiation.

3.4.8 Response of surfactant-free PCDA micelle gels

As shown in figure 3.1, PCDA has a hydrophilic carboxyl head group and a hydrophobic tail, making it a potential surfactant. Note that SDS may have interfered with the molecular arrangement of diacetylene groups in micelles in previous experiments, thereby inhibiting oligomerization and colour change. To avoid this problem, the creation and irradiation of PCDA micelles with no gelatin and SDS or other added surfactants was investigated, using the recipes shown in table 3.2, wherein NaOH was added to adjust the HLB of the PCDA molecules so that stable solutions would form. PCDA was added to NaOH solutions and the resulting mixtures were heated to 65 ºC and stirred for about 20 minutes until the mixtures became clear, indicating that a solution had formed. Some samples were cooled to room temperature (22 ºC) and are referred to as cold samples and some were kept at 65 ºC and are referred to as hot samples. Samples were irradiated 24 h after manufacturing. The hot samples were irradiated immediately after removal from the container that was kept at 65 ºC, so that the temperature decrease during irradiation was

minor. Particle sizes were measured by dynamic light scattering, for samples C15 and C16 using Zetasizer Nano ZS particle sizer (Malvern Instruments Ltd., Worcestershire, UK)

3.5 Results

3.5.1 Results of preliminary evaluation

Figure 3.3 shows a photograph of non-irradiated and irradiated vials (0 and 40 days after irradiation) from the experiments in table 3.1. Vials containing CTAB did not show any noticeable colour change. SDS and Triton x-100 vials, with and without gelatin, turned blue in response to radiation. Irradiated vials containing SDS showed deeper blue colour compared to those containing Triton x-100 (figure 3.3(a)). Note that the samples that showed colour change are cloudy. Figure 3.3(b) shows that the coloured vials remained coloured after 40 days, but that the colour intensity may have changed for some samples. Based on these preliminary experiments, the next set of experiments focused on solutions containing various diacetylenes using SDS as the surfactant or the solubilizer.

Table 3.2: Cold and hot samples prepared to study the effect of packing on the response of PCDA solutions

Cold sample # (T=22 ºC)	Hot sample # (T=65 ºC)	PCDA Conc. mM	NaOH Conc. mM	pH	Irradiated
C1	H1	0.36	1	11.55	N
C2	H2	0.36	1	11.55	Y
C3	H3	0.36	3	12.06	N
C4	H4	0.36	3	12.06	Y
C5	H5	0.36	9	12.58	N
C6	H6	0.36	9	12.58	Y
C7	H7	1	1	11.18	N
C8	H8	1	1	11.18	Y
C9	H9	1	3	11.91	N
C10	H10	1	3	11.91	Y
C11	H11	1	9	12.44	N
C12	H12	1	9	12.44	Y
C13	H13	3	1	10.38	N
C14	H14	3	1	10.38	Y
C15	H15	3	3	11.58	N
C16	H16	3	3	11.58	Y
C17	H17	3	9	12.32	N
C18	H18	3	9	12.32	Y

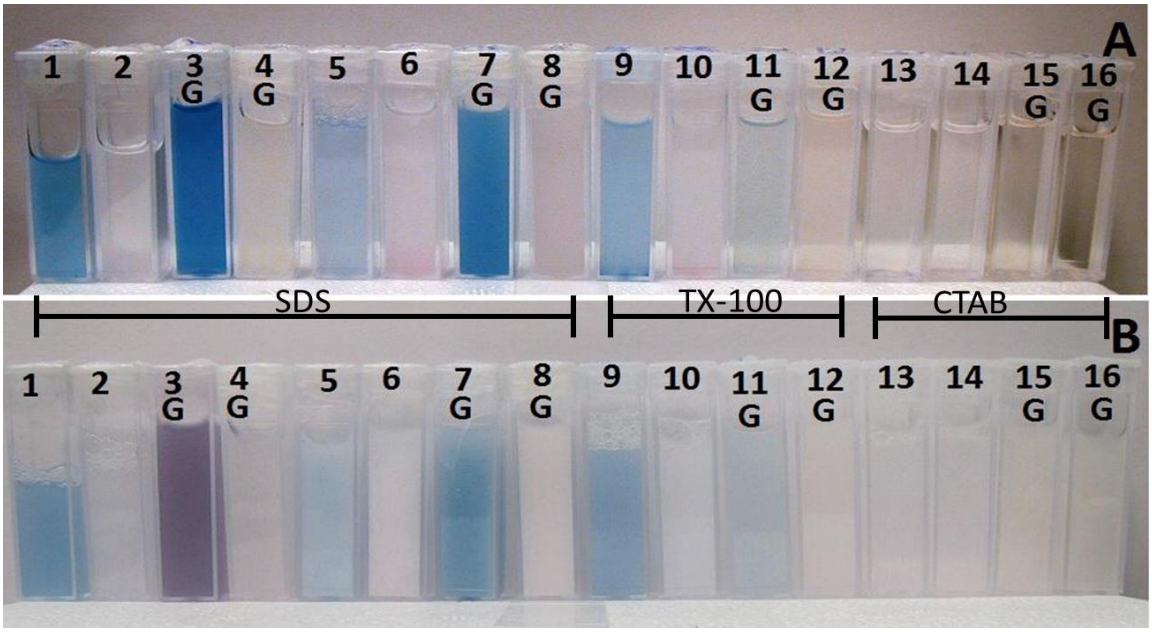

Figure 3.3: Irradiated (odd-numbered) and un-irradiated (even-numbered) vials containing PCDA surfactant solutions and gels manufactured for preliminary evaluation of PCDA in 3D micelle gel dosimeters. The odd-numbered vials were irradiated to 100 Gy and are shown at: A) 0-days and B) 40-days after irradiation. Vial numbers correspond to the sample numbers in table 3.1. The symbol G indicates that the vial contained gelatin.

3.5.2 Radiation response of PCDA and the other diacetylenes

In this set of experiments, vials (not shown) containing DPBD and HD did not change colour in response to irradiation. Vials containing PCDA (figure 3.4) responded to irradiation by changing from colourless to deeply coloured as the radiation dose increased. The spectra of the irradiated vials containing PCDA are shown in figure 3.4(b). Figure 3.4(c) shows that the radiation response of the PCDA gel increased smoothly with increasing dose, with no apparent threshold that would indicate oxygen inhibition. This type of response was observed for three experiments conducted using PCDA gels containing 3 mM PCDA, 51 mM SDS and 5 wt% gelatin that were manufactured and irradiated at various times over the course of this study using doses ranging from 2 to 20

Gy. However, for seven gels with this same recipe, no colour change was observed. All gels that exhibited a colour change were turbid, and gels that remained clear during the 24 h period between manufacturing and irradiation did not have a noticeable response to irradiation.

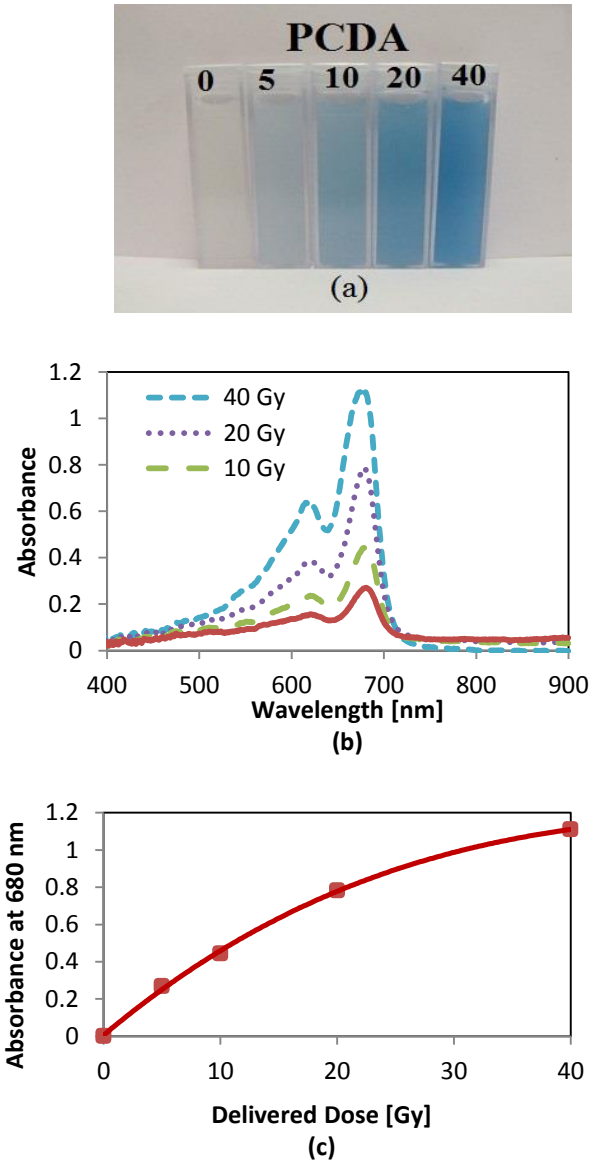

Figure 3.4: Response of PCDA (3 mM) gel with SDS (51 mM) to 0, 5, 10, 20, and 40 Gy doses, irradiated 24 h after manufacturing. The figure shows a) a photograph of the vials immediately after irradiation, b) measured spectra for these vials and c) absorbance at 680 nm for the irradiated vials.

After producing several sets of gels that did not change colour, solid PCDA powder samples were irradiated to 20 Gy to check whether the PCDA had degraded. As shown in figure 3.5, the irradiated PCDA crystals turned blue, indicating that the PCDA had not degraded and that solid PCDA changes colour upon irradiation.

Figure 3.5: Un-irradiated PCDA powder and PCDA powder irradiated to 20 Gy.

3.5.3 Effect of PCDA concentration on dose response

The effect of PCDA concentration on the gel response to irradiation was studied. Colour changed in response to irradiation, with greater colour change observed as the absorbed dose increased. Figure 3.6 shows a photograph of the irradiated vials for gels with different PCDA concentrations and figure 3.7 shows the absorbance of the irradiated gels at 680 nm. The responses of the gels increases smoothly with increasing dose, with no apparent threshold that would indicate oxygen inhibition (figure 3.7). Note that all gels that showed a noticeable colour change upon irradiation were turbid before irradiation.

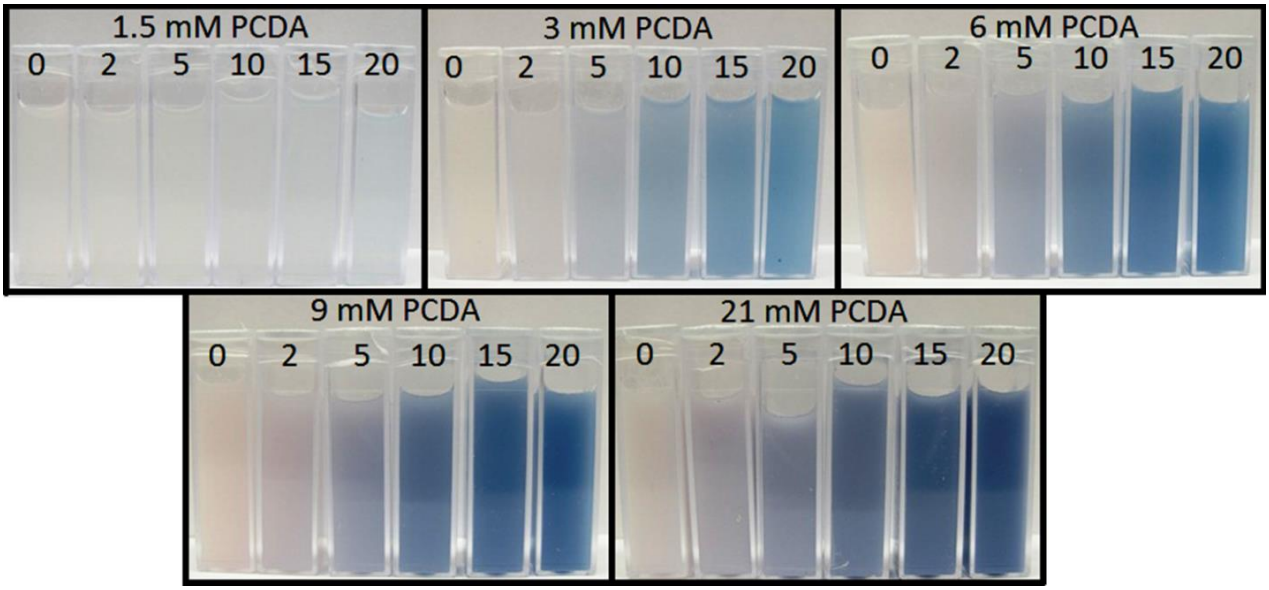

Figure 3.6: photograph of irradiated PCDA micelle gels containing 51 mM SDS, 5 wt% gelatin and PCDA at the following concentrations: 1.5, 3, 6, 9 and 21 mM. Gels were irradiated to 0, 2, 5, 10, 15 and 20 Gy, 24 h after manufacturing. The photo was taken about 24 h after irradiation.

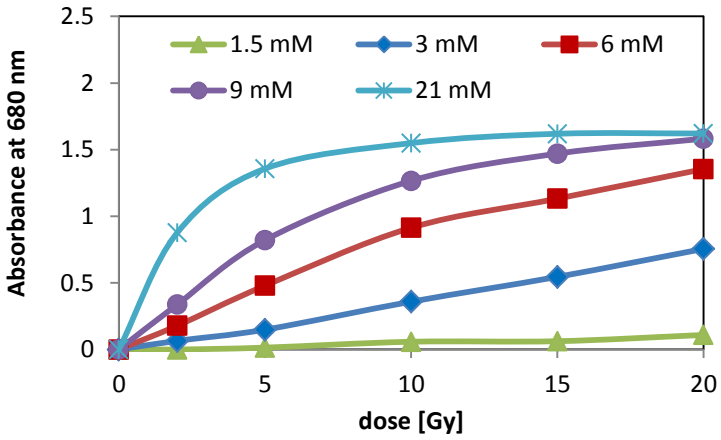

Figure 3.7: Absorbance spectra of the irradiated PCDA micelle gels containing 51 mM SDS, 5 wt% gelatin and PCDA at the following concentrations: 1.5, 3, 6, 9 and 21 mM. Gels were irradiated to 0, 2, 5, 10, 15 and 20 Gy, 24 h after manufacturing. The spectra were measured 20 minutes after irradiation.

3.5.4 Influence of phase stability of surfactant solution and gel on radiation response

The objectives of these experiments were to investigate if colour change in response to irradiation is related to initial turbidity. Turbidity could be caused by either the precipitation of PCDA solubilized in micelles or the precipitation of SDS surfactant below its Krafft temperature of 18 ºC.

3.5.4.1. Gelatin effect on SDS phase behaviour.

The effect of gelatin on SDS precipitation below its Krafft temperature was studied. Surfactant solutions of 51 mM SDS with 0 and 5 wt% gelatin were prepared and refrigerated at 4 ºC for 10 days. The vials containing SDS solutions with no gelatin became turbid in less than 12 h after manufacturing, while the vials containing SDS and gelatin at 5 wt% stayed transparent for more than 10 days as shown in figure 3.8.

3.5.4.2. Effect of adding solvent on gel phase stability.

Adding the organic solvent, xylene, to the PCDA gels improved phase stability. All gels containing xylene remained transparent for at least three days, indicating that no PCDA had precipitated. Gels with higher xylene concentrations (i.e. 6 and 15 mM) stayed transparent for longer times than gels with lower xylene concentrations (1.5 and 3mM). None of the PCDA gels containing xylene (not shown) changed colour when irradiated to 20 Gy 24 h after manufacturing, when all of these gels were transparent.

3.5.4.3. Effect of salt, acid and base additives on phase stability of PCDA gels.

The addition of THPC, NaCl, NaOH and HCl to the PCDA gel recipe had various effects on the phase stability of the prepared gels. All of the phantoms remained transparent prior to irradiation (i.e., 24 h after manufacturing) and did not change colour when irradiated. Phantoms containing 6 mM NaCl and NaOH became turbid in the refrigerator about two days after manufacturing while phantoms containing THPC and HCl stayed clear for

more than 10 days. All of the phantoms were irradiated again two weeks after manufacturing, when all had become turbid, and changed colour in response to irradiation (not shown).

Figure 3.8: Photograph showing vials containing 51 mM SDS with 0 wt% (left) and 5 wt% (right) gelatin, refrigerated at 4 °C for 10 days. Adding 5 wt% gelatin appears to have stopped or postponed SDS precipitation for more than 10 days, maintaining gel transparency.

3.5.4.4. Gel ageing and phase behaviour.

Gel ageing experiments were designed to further investigate whether the colour change is related to turbidity. The goal was to track gel clarity over time and to check whether colour change occurs only in gels with precipitated PCDA (turbid gels), or whether it can also occur sometimes in gels containing PCDA solubilized in SDS micelles (transparent gels). The two PCDA gels (3 mM and 9 mM) remained clear during the first 24 h after manufacturing, and the 9 mM PCDA gel showed some cloudiness after 1.5 d. The 3 mM PCDA gel started to become cloudy about 2.5 days after manufacturing. Turbidity increased with time for both gels. Figure 3.9 shows absorbance (at 670 nm where

maximum absorbance occurred) for the two PCDA gel recipes irradiated to 10 Gy at different times. As expected, gels that were transparent showed no colour change. Turbid gels turned blue during irradiation and the colour intensity was higher for older gels that were more turbid. Also, colour intensity was higher for 9 mM gel samples than for 3 mM samples, presumably due to a larger amount of precipitated PCDA in the 9 mM gels.

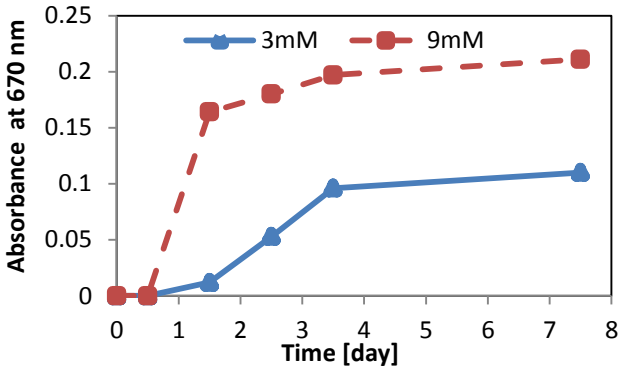

Figure 3.9: Absorbance at 670 nm of PCDA gels (3 mM and 9 mM) solubilized using SDS at 51 mM with 5 wt% gelatin, irradiated to 10 Gy. The absorbance of the 9 mM PCDA gel is higher than that for the 3 mM gel.

3.5.5 Response of surfactant-free PCDA micelle gels

PCDA solutions with no SDS or other added surfactant were prepared in a final effort to produce transparent PCDA micelle gels that would be effective for 3D dosimetry. PCDA molecules have a structure that makes them a potential surfactant (i.e., a hydrophilic carboxyl head group and a hydrophobic tail). As a result, PCDA molecules are expected to position themselves in SDS micelles so that their hydrophilic heads are in contact with the aqueous phase and their hydrophobic tales are repelled toward the hydrophobic core of the micelle. The tails of the SDS surfactant molecules in this configuration will be near the tails of the PCDA molecules and may affect the packing of diacetylene groups (see

figure 3.2) thereby preventing oligomerization. Therefore, PCDA solutions with no SDS or other added surfactant were prepared and irradiated in this set of experiments to avoid this potential problem, in a final effort to produce transparent PCDA micelle gels that would be effective for 3D dosimetry.

When PCDA powder is mixed with additive-free deionized water, the powder floats as a thin layer on top of the water surface. However, when PCDA was added to the NaOH solutions shown in table 3.2 at room temperature, the powder distributed throughout the volume of the container, producing turbid mixtures. Heating these mixtures to 65 ºC resulted in the formation of transparent solutions of PCDA in the basic medium. These transparent basic solutions became turbid soon after cooling to room temperature. As a result, we decided to keep some samples hot (at 65 ºC) and to keep others at room temperature (22 ºC) prior to and during irradiation. No gelatin was used in these experiments because it may affect the pH value of the solutions.

Figure 3.10 shows the un-irradiated and irradiated cold samples (figure 3.10(a)) and hot samples (figure 3.10(b)). All cold samples were cloudy prior to irradiation and changed colour in response to radiation. Note that irradiated samples C6, C12 and C18 were initially blue after irradiation, but subsequently experienced a colour transition from blue to red. Samples C13 and C14 were blue prior to irradiation indicating that some PCDA particles may have oligomerized before irradiation, possibly due to the exposure to UV light. However, the irradiated sample C14 became darker blue in response to the 10 Gy radiation dose. Hot samples were transparent prior to irradiation and none of them showed any noticeable colour change upon irradiation. Particle sizes for samples C15 and C16 were measured and the results are shown in table 3.3. The particle sizes in both

samples are large relative to the size of SDS micelles, which have an average radius of 1.84 nm (Duplatre *et al.* 1996).

Table 3.3: Particle sizes of samples C15 and C16 from table 3.2. C15 was not irradiated and C16 was tested after irradiating to 10 Gy. The particle size distribution has three main peaks.

Sample #	PCDA Conc. mM	NaOH Conc. mM	pH	Peak #1: size (nm) (Intensity %)	Peak #2: size (nm) (Intensity %)	Peak #3: size (nm) (Intensity %)
C15	3	3	11.58	502.3 (50%)	1980 (25%)	985.3 (25%)
C16	3	3	11.58	979.4 (37.3%)	705.1 (31.3%)	1749 (31.3%)

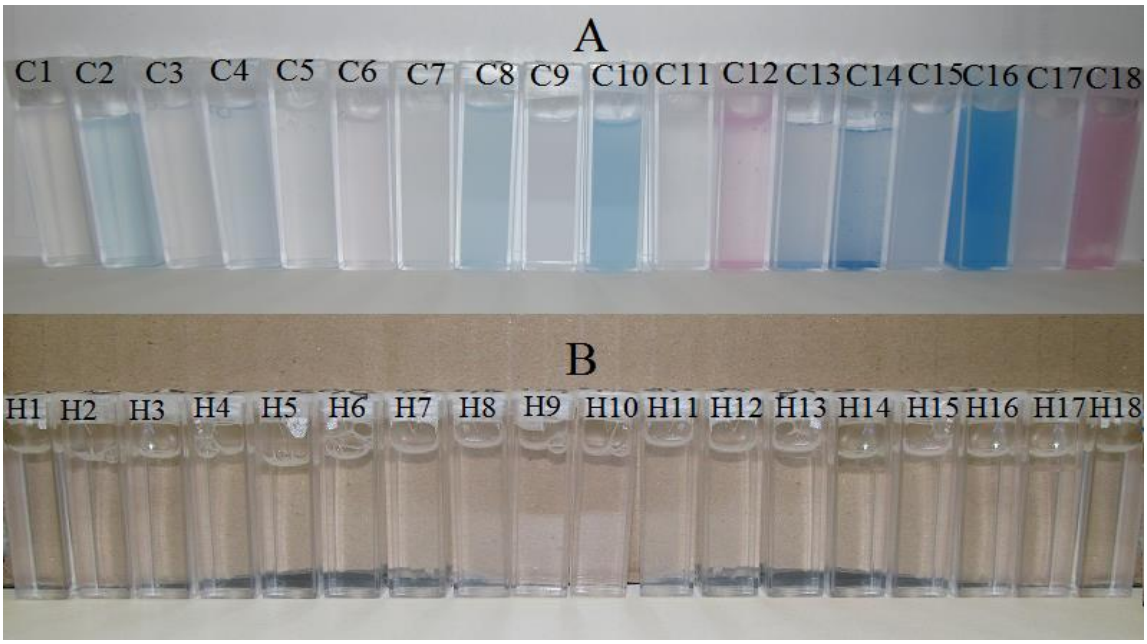

Figure 3.10: Un-irradiated (odd-numbered) and irradiated (even-numbered) cold and hot samples containing solutions of PCDA in NaOH solutions prepared using the recipes in table 3.2. The cold samples (A) stored and irradiated at room temperature became turbid prior to irradiation and turned blue immediately after irradiation. Some samples subsequently turned red. The hot samples (B) that were stored and irradiated at 65 ºC remained transparent and did not change colour. All vials were irradiated 24 h after manufacturing to 10 Gy. Vial numbers correspond to the sample numbers in table 3.2.

3.6 Discussions

For a gel dosimeter to be effective for optical CT readout, it should undergo a measureable, stable and reproducible response to radiation. In addition, diffusion of the reporter molecules through the gel should be slow compared with the time scale for irradiation and subsequent read out. As a result, micelle gel dosimeters, first developed by Jordan and coworkers, are particularly promising. They are transparent gels with no opaque particles that scatter light and have low diffusion rates because water-insoluble reporter molecules remain in the micelles, which are relatively large and are slow to diffuse. Unfortunately, current micelle gel dosimeters with leuco malachite green (LMG) and leuco crystal violet (LCV) as reporter molecules are light-sensitive and temperature-sensitive during irradiation and tend to fade over time. They also have relatively low dose sensitivity and may have significant dose-rate dependence.

In an attempt to develop improved micelle gel dosimeters, the use of diacetylenes solubilized in micelles as reporter molecules was studied in the current work. Radiochromic diacetylenes are used as reporter molecules in the commercial GafChromic® films and may have more desirable chemical behavior (e.g., with respect to fading over time, light sensitivity, temperature dependence and dose-rate dependence) than the leuco-dyes used by Jordan *et al.* In response to radiation, diacetylene molecules can react to form oligomers that exhibit intense colour change that is approximately proportional to absorbed dose (Ogawa 1989, Rink *et al.* 2008).

Preliminary investigations focused on solubilizing PCDA molecules in micelles using the three different surfactants SDS, Triton x-100 and CTAB. When heated to its melting temperature, PCDA crystals disappeared, producing transparent gels and

solutions. The initial gels, containing 5 wt% gelatin, stayed clear at 4 ºC for the first 12 h after manufacturing. Samples of these gels were irradiated to 100 Gy, 48 h after manufacturing when some of the samples had become turbid. Samples containing SDS surfactant showed the deepest colour change in response to irradiation and SDS was selected for use in additional experiments.

The response of PCDA micelle gels to radiation was compared to that of gels made using two other diacetylenes (DPBD and HD), with SDS as the surfactant. The gels containing DPBD and HD did not show any noticeable response to irradiation, presumably because no oligomerization occurred. Gels containing PCDA showed an absorbance response at 680 nm that increased with increasing dose, with no apparent threshold that would indicate oxygen inhibition. This same type of response was also observed in gels prepared using different PCDA concentrations (figures 3.6 and 3.7). As expected, larger PCDA concentrations led to a larger dose response. Unfortunately, all of the gels that showed this type of response were turbid prior to and after irradiation, which would make them unsuitable for optical CT readout. In addition, problems with reproducibility were noted. Over the course of this study, PCDA gels from different batches were replicated (manufactured and irradiated) 10 times using a recipe with 3 mM PCDA, 51 mM SDS and 5 wt% gelatin, and were irradiated to doses ranging from 2 to 20 Gy. Of the 10 batches, the type of response shown in figures 3.3, 3.4, 3.6 and 3.7 was observed for only three replicates. In the other seven trials, no colour change was observed. All vials that exhibited a colour change were turbid before irradiation. Vials that remained clear at the time of irradiation did not change colour. No error bars are shown on Figures 3.4c and 3.7 due to these reproducibility problems.

The lack of response to irradiation for a portion of the gels raised questions about the relationship between turbidity and response to irradiation. Also, gels that were produced early in the course of the experiments tended to change colour in response to radiation, and gels that were produced later stayed clear and did not change colour, even though the same recipe, procedure and batch of PCDA were used. As a result, samples of solid PCDA crystals were irradiated to determine whether the lack of response was due to degradation of PCDA. These samples turned blue indicating that the PCDA had not degraded and was still responsive to radiation.

Since gels that contain PCDA crystals would not be ideal for 3D dosimetry with optical readout, due to light scattering and reproducibility problems, additional experiments were conducted to search for transparent gels that change colour in response to radiation. Two techniques were tried. The first technique involved using xylene as a solvent (section 3.4.7.2) to keep the PCDA dissolved inside the micelles, thereby preventing PCDA crystallization. The second technique (section 3.4.7.3) involved aqueous-phase additives (acid, base and salt) that affect pH and ionic strength in an effort to influence colloidal stability. Both techniques were successful in enhancing the phase stability of the gels, so that the gels remained transparent for more than 10 days using some of the recipes, indicating that the PCDA remained solubilized and did not crystallize. Using higher concentrations of xylene resulted in gels that remained transparent for longer times. Gels containing NaCl and NaOH at the concentrations used in the study became turbid about two days after manufacturing, while those containing THPC and HCl stayed clear for more than 10 days. Note that THPC is acidic and produces a chloride ion when it dissociates, so that both the THPC and HCl may have

influenced the surface of the micelles in a similar way, leading to improved colloidal stability. Unfortunately none of the transparent gels prepared using xylene or the aqueous-phase additives changed colour when irradiated. Phantoms containing the aqueous-phase additives were irradiated again, two weeks after manufacturing when they had become turbid. These gels changed colour in response to irradiation, confirming prior observations that PCDA gels produced using SDS only respond when the PCDA has precipitated.

Turbidity could be caused either by precipitation of PCDA solubilized in micelles or precipitation of SDS surfactant below its Krafft temperature. To check whether SDS precipitation contributed to turbidity, an experiment was conducted to study SDS precipitation in the presence of gelatin as described in section 3.4.7.1. SDS is known to form stable solutions in water at room temperature and to precipitate below its Krafft temperature of 18 ºC. Addition of 5 wt % gelatin helped to keep the gels containing only gelatin and SDS transparent after refrigeration for more than 10 days, whereas SDS solutions with no gelatin became turbid within 12 hours of manufacturing. These results indicate that the gelatin stopped or postponed the SDS precipitation.

Gel aging experiments were designed to track gel clarity over time and to check once more whether colour change would occur only in gels with precipitated PCDA (turbid gels), or whether it could also occur in gels containing PCDA solubilized in SDS micelles (transparent gels). Results of this experiment confirmed that transparent gels do not change colour in response to irradiation and that only the gels containing precipitated PCDA responded to radiation by changing colour, suggesting that PCDA molecules inside SDS micelles do not undergo the oligomerization reaction that leads to colour

change. The fact that colour intensity appears to increase with increased turbidity and with PCDA concentration in the recipe, as shown in figure 3.9, confirms this conclusion.

PCDA solutions with no SDS or other added surfactant were prepared in a final effort to produce transparent PCDA micelle gels that could be effective for 3D dosimetry. Because both PCDA and SDS molecules contain hydrophilic and hydrophobic parts, the arrangement of the hydrophobic tails inside the SDS micelles may disturb the packing of diacetylene groups on adjacent PCDA molecules, thereby inhibiting oligomerization. To avoid this problem, new recipes were designed wherein PCDA molecules were solubilized in NaOH solution, with no added surfactants. PCDA molecules have a very low HLB value (i.e., -2.3 according to Davies's method) due to the weak tendency of the hydrogen ion (H+) to dissociate from the carboxylic acid end of the PCDA molecule in deionized water. This dissociation tendency can be affected by changing the pH of the aqueous phase (Davies 1957, Davies and Rideal 1963). Increasing pH by adding a strong base (e.g., NaOH) induces dissociation of the carboxyl end of PCDA molecules, thereby adjusting the HLB value of molecules like PCDA, so that they can form transparent solutions (Perino *et al.* 2011).

PCDA molecules were successfully solubilized in the NaOH solutions at different concentrations as described in table 3.2. These solutions were not stable at room temperature, but were stable at higher temperatures. Solutions that were stored and irradiated at 65 ºC were transparent and did not change colour upon irradiation. All of the turbid room-temperature samples changed colour in response to radiation, confirming that the colour change is caused by oligomerization of the crystallized PCDA particles. Note that some samples (particularly samples C6, C12 and C18) were blue immediately

after irradiation and subsequently changed to red. Oligomerized PCDA particles are known to experience a colour transition from blue to red at high temperature and at high pH values (Mino *et al.* 1991, Mino *et al.* 1992).

Particle sizes of samples C15 and C16 were measured. These samples were selected because sample C16 experienced the most intense colour change in response to radiation. Particle sizes in both samples were found to be large compared to the size of SDS micelles, which is consistent with the precipitation of relatively large PCDA crystals. The large particles lead to light scattering, making the phantoms turbid and unsuitable for 3D radiation dosimetry. Note that the size and position of the peaks in the particle size distributions for samples C15 and C16 are somewhat different, but it is difficult to tell whether the particle size distribution was influenced by the radiation dose, or was due to slightly different conditions in the sample vials during crystal nucleation and growth. In experiments aimed at synthesizing micelles for uses as biosensors and carriers for drug delivery, Choi *et al.* (2008) reported that micelles made from two PCDA molecules attached to a single polyethylene amine head group showed deep colour change in response to irradiation. However, it is unlikely that the diacetylene molecules solubilized in micelles were responsible for the colour change, because the samples that changed colour contained particles with average diameters ranging from 160 of 850 nm. Samples containing the largest particles experienced the deepest colour change. These large particle sizes are consistent with precipitation and crystallization of the diacetylene molecules prior to oligomerization.

In summary, we do not recommend diacetylene-based micelle-gel dosimeters for 3D readout using optical methods. In all of the samples that were tested, colour change

occurred only in turbid phantoms. Experimental results suggest that these turbid phantoms contained solid PCDA crystals that scatter light, leading to turbidity. Many samples were made wherein the PCDA remained solubilized, producing transparent phantoms that would be suitable for optical readout, except that no colour change occurred, presumably because the PCDA did not oligomerize. Furthermore, we do not recommend any 3D dosimeters that rely on precipitation of reporter molecules prior to irradiation, because crystal nucleation and growth phenomena tend to be irreproducible and difficult to control (Mullen 2001). It will be important to find alternative reporter molecules that respond to radiation in the liquid state, like the leuco-dye micelle dosimeters introduced by Jordan *et al.* (Babic *et al.* 2009, Jordan and Avvakumov 2009). One benefit of using micelles in 3D gel dosimeters is that, unlike traditional gel dosimeters, the reporter molecules do not need to be water soluble. In fact, very low or negligible water solubility will help to reduce diffusion and improve spatial stability. Consequently, a range of new hydrophobic reporter molecules may well be available for use in 3D micelle gels.

3.7 Conclusions

3D micelle gel dosimeters introduced by Jordan *et al.* (Babic *et al.* 2009, Jordan and Avvakumov 2009) showed promise because of their suitability for optical readout and their superior spatial stability. Unfortunately, these first micelle gel dosimeters are sensitive to light and temperature during irradiation, tend to fade over time, have relatively low dose sensitivity and may have significant dose-rate dependence. In the current work, three diacetylenes were evaluated as potential reporter molecules for

micelle gel dosimeters, with the hope that the shortcomings of leucodye-based micelle gels could be overcome.

Micelle gels containing pentacosa-10,12-diynoic acid (PCDA) as reporter molecule and sodium dodecyl sulfate (SDS) as a surfactant changed from colourless to blue in response to irradiation. Similar gels containing two other diacetylenes (DPBD and HD) did not show any colour change. The response of gels containing PCDA to irradiation was monotonic, with no apparent dose threshold that would indicate oxygen inhibition. Gels with larger PCDA concentrations experienced a larger dose response. Unfortunately, all gels that changed colour in response to radiation were turbid prior to and after irradiation, making them unsuitable for optical CT readout. Moreover, problems with reproducibility were noted. Experiments involving SDS and gelatin without any diacetylene suggest that turbidity is caused by PCDA precipitation, rather than precipitation of SDS below its Kraft temperature. Precipitation of PCDA was successfully prevented by adding xylene as an organic solvent, and by adding acids to the aqueous phase to enhance the colloidal stability of the gels. Transparent solutions were also prepared successfully without added surfactant, using only PCDA, deionized water and NaOH, so that disturbances to the position of diacetylene groups that might be caused by SDS could be avoided. Although transparent gels were prepared successfully using these three different methods, none of the resulting gels changed colour in response to irradiation. Gel ageing experiments using the original recipe (3 mM PCDA, 51 mM SDS, 5 wt% gelatin) confirmed that gels that remained transparent did not respond to radiation, whereas gels that became turbid prior to irradiation responded by changing colour. These results indicate that the colour change observed in PCDA micelle

dosimeters is due to oligomerization within solid PCDA particles, rather than oligomerization of PCDA solubilized in micelles.

Since turbid gels are undesirable for optical CT readout, the use of PCDA as the reporter molecule in micelle gels is not promising. However, we recommend that other radiochromic reporter molecules should be evaluated for use in micelle gel dosimeters. If a suitable reporter molecule is identified, micelle gels have the potential to produce accurate 3D dosimetry results with excellent spatial stability.

3.8 Acknowledgments

This work was funded by the Canadian Institutes for Health Research (CIHR).

3.9 References for chapter 3

Adamovics JA 2006 three dimensional dosimeter for penetrating radiation and method of use *United States Patent # US 7098463B2*.

Adamovics J and Maryanski M 2006 Charaterisation of PRESAGE: a new 3D radio chromic solid polymer dosimeter for ionizing radiation *Radiation Protection Dosimetry.* **120** 107–112

Appleby A, Christman EA and Leghrouz A 1987 Imaging of spatial radiation dose distribution in agarose gels using magnetic resonance. *Med. Phys.* **14** 382-384.

Araghi HY and Paige MF 2011 Deposition and photopolymerization of phase-separated perfluorotetradecanoic acid-10,12-pentacosadiynoic acid Langmuir-Blodgett monolayer films *Langmuir.* **27** 10657-10665.

Babic S, Battista J and Jordan K 2009 Radiochromic leuco dye micelle hydrogels: II. Low diffusion rate leuco crystal violet gel *Phys. Med. Biol.* **54** 6791–6808.

Baldock C, De Deene Y, Doran S, Ibbott G, Jirasek A, Lepage M, McAuley KB, Oldham M, and Schreiner LJ 2010 Polymer gel dosimetry *Phys. Med. Biol.* **55** 1–63.

Binks BP 1998 Modern aspects of emulsion science. *The royal society of chemistry*.

Brown S, Venning A, De Deene Y, Vial P, Oliver L, Adamovics J, Baldock C 2008 Radiological properties of the PRESAGE and PAGAT polymer dosimeters. *Applied Radiation and Isotopes* **66** 1970–1974.

Chain JNM, Jirasek A, Schreiner LJ and McAuley KB 2011a Cosolvent-free polymer gel dosimeters with improved dose sensitivity and resolution for x-ray CT dose response *Phys. Med. Biol.* **56** 2091-2102.

Chain JNM, Nasr AT, Schreiner LJ and McAuley KB 2011b Mathematical Modeling of Depth-Dose Response of Polymer-Gel Dosimeters *Macromol. Theory Simul.* **20** 735–751.

Choi H, Bae YM, Yu GS, Huh KM and Choi JS 2008 Synthesis of Poly(ethylene glycol)-Polydiacetylene Conjugates and Their Micellar and Chromic Characteristics *J. Nanoscience and Nanotechnology*. **8** 5104-5108.

Davies JT 1957 A quantitative kinetic theory of emulsion type: I. physical chemistry of the emulsifying agent *Gas/Liquid and Liquid/Liquid Interface. Proceedings of the International Congress of Surface Activity.* 426-438.

Davies JT and Rideal EK 1963 Interfacial phenomena, 2nd edition *Academic press.*

De Deene Y, Venning A, Hurley C, Healy BJ and Baldock C 2002a Dose–response stability and integrity of the dose distribution of various polymer gel dosimeters *Phys. Med. Biol.* **47** 2459–2470

De Deene Y, Hurley C, Venning A, Vergote K, Mather M, Healy BJ and Baldock C 2002b A basic study of some normoxic polymer gel dosimeters *Phys. Med. Biol.* **47** 3441–3463.

De Deene Y 2004 Essential characteristics of polymer gel dosimeters *J. Physics. Conference Series* **3**, 34–57.

Doran SJ 2009 The history and principles of optical computed tomography for scanning 3-D radiation dosimeters:2008 update *Journal of Physics:Conference Series* **164**, 012020.

Duplatre G, Marques MF and da Graca Miguel M 1996 Size of Sodium Dodecyl Sulfate Micelles in Aqueous Solutions as Studied by Positron Annihilation Lifetime Spectroscopy *J. Phys. Chem.* **100** 16608-16612

Evans DF and Wennerstrom H 1999 The Colloidal Domain, 2nd edition, *Wiley-VCH, NY, USA.*

Gore JC, Kangt YS and Schulz RJ 1984 Measurement of radiation dose distributions by nuclear magnetic resonance (NMR) imaging *Phys. Med. Biol.* **29** 1189-1197.

Guo PY, Adamovics JA and Oldham M 2006 Characterization of a new radiochromic three-dimensional dosimeter *Med. Phys.* **33** 1338-1345.

Hurley C, McLucas C, Pedrazzini G and Baldock C 2006 High-resolution gel dosimetry of a HDR brachytherapy source using normoxic polymer gel dosimeters: Preliminary study *Nuclear Instruments and Methods in Physics Research A* **565** 801–811.

Jirasek A, Hilts M, Shaw C and Baxter P 2006 Investigation of tetrakis hydroxymethyl phosphonium chloride as an antioxidant for use in x-ray computed tomography polyacrylamide gel dosimetry *Phys. Med. Biol.* **51** 1891–1906.

Jirasek A, Hilts M and McAuley KB 2010 Polymer gel dosimeters with enhanced sensitivity for use in x-ray CT polymer gel dosimetry *Phys. Med. Biol.* **55** 5269-5281.

Jordan K and Avvakumov N 2009 Radiochromic leuco dye micelle hydrogels: I. Initial investigation *Phys. Med. Biol.* **54** 6773–6789.

Kim JM, Lee JS, Choi H, Sohn D and Ahn DJ 2005 Rational Design and in-Situ FTIR Analyses of Colorimetrically Reversibe Polydiacetylene Supramolecules *Macromolecules.* **28** 9366-9376.

Koeva VI, Olding T, Jirasek A, Schreiner LJ and McAuley KB 2009a Preliminary investigation of the NMR, optical and x-ray CT dose–response of polymer gel dosimeters incorporating cosolvents to improve dose sensitivity *Phys. Med. Biol.* **54** 2779-2790.

Koeva VI, Daneshvar S, Senden RJ, Imam AHM, Schreiner LJ and McAuley KB 2009b Mathematical Modeling of PAG- and NIPAM Based Polymer Gel Dosimeters Contaminated by Oxygen and Inhibitor *Macromol. Theory Simul.* **18** 495-510.

Ma Z, and Ren J 2007 Fabrication of stable polydiacetylene vesicles with 2,4-akyl-diacetylenic acid *Colloids and surfaces A: Physicochem. Eng. Aspects.* **303** 179-183.

Maryanski MJ, J. C. Gore JC, Kennan RP and Schulz RJ 1993 NMR relaxation enhancement in gels polymerized and cross-linked by ionizing radiation: a new approach to 3D dosimetry by MRI *Magn. Reson. Imaging.* **11** 253–258.

Maryanski MJ, Schulz RJ, Ibbott GS, Gatenby JC, Xie J, Horton D and Gore JC 1994 Magnetic resonance imaging of radiation dose distributions using a polymer-gel dosimeter *Phys. Med. Biol.* **39** 1437–1455.

Maryanski MJ, Ibbott GS, Eastman P, Schulz RJ and Gore JC 1996 Radiation therapy dosimetry using magnetic resonance imaging of polymer gels. *Med. Phys.* **23** 699-706.

McAuley KB 2004 The chemistry and physics of polyacrylamide gel dosimeters: why they do and don't work *Journal of Physics:Conference Series* **3** 29–33.

Mino N, Tamura H, and Ogawa K 1991 Analysis of Color Transitions and Changes on Langmuir-Blodgett Films of a Polydiacetylene Derivative *Langmuir*. **7** 2336-2341.

Mino N, Tamura H and Ogawa K 1992 Photoreactivity of 10,12-Pentacosadiynoic Acid Monolayers and Color Transitions of the Polymerized Monolayers on an Aqueous Sub-phase *Langmuir*. **8** 594-598.

Mullin JW 2001 Crystallization, 4th edition *Butterworth-Heinemann.*

Nasr AT, Schreiner LJ and McAuley KB 2012 Mathematical Modeling of the Response of Polymer Gel Dosimeters to HDR and LDR Brachytherapy Radiation *Macromol. Theory Simul.* **21** 36–51.

Ogawa K. 1989 Study on Polymerization Mechanism of Pentacosadiynoic Acid Langmuir-Blodgett Films Using High Energy Beam Irradiations *J. Phys. Chem.* **93** 5305-5310.

Ogawa K 1992 Control of Polymerization Processes of 10,12-Pentacosadiynoic Acid LB Films *polymer international*. **28** 25-33.

Olding T, Darko J and Schreiner LJ 2010 Effective Management of FXG Gel Dosimetry *Journal of Physics: Conference Series* **250** 012028.

Olding T, Holmes O, DeJean P, McAuley KB, Nkongchu K, Santyr G and Schreiner LJ 2011 Small field dose delivery evaluations using cone beam optical computed tomography-based polymer gel dosimetry *Journal of Medical Physics.* **36** 3-14.

Patel GN 2005 thick radiation sensitive devices *United States Patent # US 0208290A1*

Perino A, Klymchenko A, Morere A, Contal E, Rameau A, Guenet JM, Mely Y and Wagner A, 2011 Structure and Behavior of Polydiacetylene-Based Micelles Macromol. *Chem. phys.* **212** 111-117.

Qian JH, Zhu LW and Guo R 2005 Effect of Sodium Barbital on the Physico-chemical Properties of Surfactants with Different Charges *Journal of the Chinese Chemical Society* **52** 1245-1252.

Rad AN, Blackwell CR, Coursey BM, Gall KP, Galvin JM, McLaughlin WL, Meigooni AS, Nath R, Rodgers JE and Soares CG 1998 Radiochromic film dosimetry: recommendations of AAPM Radiation Therapy Committee Task Group 55. *Med. Phys.* **25** 2093-2115.

Rink A, Lewis DF, Varma S, Vitkin IA and Jaffray DA 2008 Temperature and hydration effects on absorbance spectra and radiation sensitivity of a radiochromic medium *Med. Phys.* **35** 4545-4555.

Schreiner LJ 2004 Review of Fricke gel dosimeters *J. Physics. Conference Series* **3**, 9-21.

Schreiner LJ 2006 Dosimetry in modern radiation therapy: limitations and needs *Journal of Physics: Conference Series*. **56** 1–13.

Sedaghat M, Bujold R and Lepage M 2011 Severe dose inaccuracies caused by an oxygen-antioxidant imbalance in normoxic polymer gel dosimeters *Phys. Med. Biol.* **56** 601–625

Senden RJ, De Jean P, McAuley KB and Schreiner LJ 2006 Polymer gel dosimeters with reduced toxicity: a preliminary investigation of the NMR and optical dose–response using different monomers *Phys. Med. Biol.* **51**, 3301–3314.

Shinoda K and Fontell K 1995 ionic surfactants capable of being used in hard water *Advances in Colloid and interface science* **54** 55-72.

Su YL, Li JR and Jiang L 2005 A study on the interactions of surfactants with phospholipid/polydiacetylene vesicles in aqueous solutions *Colloids and surfaces A: Physicochem. Eng. Aspects* **257** 25-30.

Vandecasteele J, Ghysel S, Baete SH and De Deene Y 2011 Radio-physical properties of micelle leucodye 3D integrating gel dosimeters *Phys. Med. Biol.* **56** 627–651.

Vergote K, De Deene Y, Vanden Bussche E and De Wagter C 2004 On the relation between the spatial dose integrity and the temporal instability of polymer gel dosimeters *Phys. Med. Biol.* **49** 4507-4522.

Watanabe Y, Patel GN and Patel P 2006 Evaluation of a new self-developing instant film for imaging and dosimetry *Radiation Protection Dosimetry* **120** 121-124.

Chapter 4

Improving the performance of Leuco crystal violet micelle gel dosimeters

4.1 Chapter Overview

In this chapter, a new radiochromic micelle gel dosimeter recipe is developed for optical readout. The recipe contains leuco crystal violet (LCV), trichloro acetic acid (TCAA), Cetyl Trimethyl Ammonium Bromide (CTAB), 2,2,2-Trichloroethanol (TCE), and gelatin. The dose sensitivity of this gel is 1.5 times higher than the standard LCV gel suggested by Babic *et al.* (2009). Experiments were conducted to gain a deeper understanding of the different interactions between the various LCV micelle gel components. Finally, designed experiments were used to build a statistical model to optimize the LCV micelle gel recipe.

The material presented in this chapter will be submitted to *Physics in Medicine and Biology* in the future.

Improving the performance of leuco crystal violet micelle gel dosimeters

AT Nasr[1], K Alexander[2], LJ Schreiner[2, 3, 4] and KB McAuley[1]

[1] Dept. Chemical Engineering, Queen's University, Kingston, Canada, K7L 3N6

[2] Dept. of Physics, Queen's University, Kingston, Ontario, Canada, K7L3N6

[3] Dept. of Oncology, Queen's University, Kingston, Ontario, Canada, K7L3N6

[4] Cancer Centre of Southeastern Ontario, Kingston, Canada, K7L 5P9

4.2 Summary

Radiochromic Leuco Crystal Violet (LCV) micelle gel dosimeters are promising for three-dimensional (3D) radiation dosimetry because of their spatial stability and suitability for optical readout. Effects of surfactant type and concentration on dose sensitivity of LCV micelle gels were tested, demonstrating that dose sensitivity and initial colour of the gel increases with increasing Triton x-100 (Tx100) concentration. Using Cetyl Trimethyl Ammonium Bromide (CTAB) in place of Tx100 reduces the dose sensitivity and produces gels that are nearly colourless prior to irradiation. Experiments with different concentrations of Tri-chloro acetic acid (TCAA) revealed that the highest dose sensitivity is obtained at a pH of 3.6. The sensitizing effect of chlorinated species on dose sensitivity was tested using 2,2,2-trichloroethanol (TCE), chloroform, and 1,1,1-trichloro-2-methyl-2-propanol hemihydrate (TCMPH). TCE gave the largest improvement in dose sensitivity. Factorial experiments and empirical models were used to optimize the gel recipe. Dose sensitivity of the optimized gel is 1.5 times higher than Jordan's standard LCV gel. Dose distribution information is maintained for more than

two weeks when the gel is subjected to spatially non-uniform radiation. Additional testing in large phantoms will be required to assess the effectiveness of the optimized gel.

4.3 Introduction

Radiation therapy is a localized treatment that aims to deliver ionizing radiation to the body to control tumour growth (Schreiner 2009). With the increasing complexity of modern radiation treatment techniques, sophisticated quality assurance procedures must be developed to ensure that the prescribed radiation dose is delivered to the tumour, while sparing dose to healthy tissue. Point-dose measurements (e.g., ionization chambers) and two-dimensional (e.g. radiochromic film) dosimetry techniques are routinely used in the clinic to measure radiation dose (Baldock *et al.* 2010). However, with rapid advancements in treatment techniques and increasing use of highly modulated beams, dosimeters that measure entire three-dimensional (3D) dose distributions have proven invaluable for full evaluation of conformal dose deliveries. Some of the dosimetry tools, such as detector arrays and electronic portal imaging devices (Neilson *et al.* 2013, Mans *et al.* 2010) provide only surrogate validation of the 3D dose delivery (Mijnheer *et al.* 2010, Schreiner 2011). Therefore, specific problems in small field characterization (Pappas 2009), commissioning of new conformal or intensity modulated radiation therapy techniques (Olding *et al.* 2013, Ceberg *et al.* 2010) or radiation therapy process validation in adaptive techniques (Schreiner *et al.* 2011) would still benefit from the development of stable, reproducible fully 3D gel dosimeters.

3D radiation dosimeters are fabricated from radiation-sensitive materials. Upon irradiation, dosimeters undergo detectable and quantifiable changes that are related to the amount and spatial distribution of the absorbed radiation dose (Adamovics 2006, Baldock

et al. 2010). These changes can be changes in nuclear magnetic resonance (NMR) properties, changes in optical properties (e.g., color, transparency) or changes in density (Hurley *et al.* 2006, Nasr *et al.* 2013). The response of an ideal 3D dosimeter should be measurable, reproducible, and stable (De Deene 2004). Ideally, the response should not be sensitive to environmental conditions that may vary during irradiation and scanning such as humidity, light, temperature, pressure, and atmospheric gases. The response of the 3D dosimeter should depend on the total radiation dose delivered, but should not be influenced by the radiation dose rate or energy. Tissue-equivalence for the kind of radiation used is also an important characteristic that an ideal 3D dosimeter should have. Examples of current 3D dosimeters are Fricke gel dosimeters, polymer gel dosimeters, PRESAGE plastic dosimeters, and micelle gel dosimeters (Gore *et al.*, 1984, Appleby *et al.* 1987, Maryanski *et al.* 1993, Maryanski *et al.* 1994, Schreiner 2004, Adamovics 2006, Adamovics and Maryanski 2006, Guo *et al.* 2006, Hurley *et al.* 2006, Babic *et al.* 2009, Jordan and Avvakumov 2009, Baldock *et al.* 2010, Vandecasteele *et al.* 2011). Imaging techniques that are used to read out current 3D dosimeters include Magnetic Resonance Imaging (MRI), optical Computed Tomography (CT) and x-ray CT (Maryanski *et al.* 1993, Maryanski *et al.* 1994, Jirasek *et al.* 2010, Olding *et al.* 2011).

3D gel and plastic dosimeters are currently not routinely used in radiation clinics because of limitations and difficulties associated with the different 3D phantoms and the associated readout techniques (Baldock *et al.* 2010, Vandecasteele *et al.* 2011). Fricke gel dosimeters suffer from post-irradiation spatial stability problems due to rapid diffusion of iron ions, which limits the permissible time between irradiation and readout of these gels to a few hours. Addition of chelating agents to Fricke gel recipes has led to minor

improvements in spatial stability (Gore *et al.* 1984, Appleby *et al.* 1987, Schreiner 2004, Hurley *et al.* 2006, Baldock *et al.* 2010, Penev *et al.* 2013). Polymer gel dosimeters, especially polyacrylamide gels (PAG) and related gels that use N-isopropyl acrylamide (NIPAM), show relatively better post irradiation stability (Maryanski *et al.* 1993, Maryanski *et al.* 1994, De Deene *et al.* 2002a, Senden *et al.* 2006, Koeva *et al.* 2009a, Baldock *et al.* 2010, Jirasek *et al.* 2010, Chain *et al.* 2011a Olding *et al.* 2011), but polymer gels experience problems due to diffusion of unreacted monomers and are sensitive to oxygen contamination (De Deene *et al.* 2002b, McAuley 2004, Vergote *et al.* 2004, Fuxman *et al.* 2005, Jirasek *et al.* 2006, Koeva *et al.* 2009b, Baldock *et al.* 2010, Chain *et al.* 2011b, Sedaghat *et al.* 2011, Nasr *et al.* 2012).

Fricke gel and PAG are examples of dosimeters that are traditionally read out by magnetic resonance imaging (MRI). Use of MRI scanners for read out of clinical phantoms is limited due to cost, accessibility, and special skills required for quantitative MRI (Vandecasteele *et al.* 2011). Optical CT scanners are a promising alternative to MRI because they are cheaper, easier to use, and more accessible in most clinical environments (Doran 2009, Olding *et al.* 2011, Vandecasteele *et al.* 2011). These advantages of optical CT scanners have stimulated the development of optically clear radiochromic 3D dosimeters such as PRESAGE and radiochromic micelle gel dosimeters (Adamovics 2006, Adamovics and Maryanski 2006, Babic *et al.* 2009, Jordan and Avvakumov 2009, Vandecasteele *et al.* 2011, Nasr *et al.* 2013).

PRESAGE dosimeters contain leuco-dye, halogenated hydrocarbons (e.g., carbon tetrachloride and chloroform) along with other components dissolved in a solid polyurethane matrix (Adamovics 2006, Adamovics and Maryanski 2006, Guo *et al.*

2006). Upon irradiation, the colourless leuco-dye is converted to a coloured dye. Depending on the recipe used, PRESAGE dosimeters may show post-irradiation spatial stability for ~2 days. They are insensitive to oxygen and environmental conditions (Babic *et al.* 2009, Baldock *et al.* 2010). Unfortunately, tissue equivalence of PRESAGE has been an issue for this type of dosimeter (Brown *et al.* 2008).

Radiochromic micelle gel dosimeters, developed by Jordan and coworkers for optical readout, contain a colourless leuco-dye solubilized (using a surfactant) in a gelatin matrix (Babic *et al.* 2009, Jordan and Avvakumov 2009, Vandecasteele *et al.* 2011). Upon irradiation, free radicals react with the leuco-dye molecules and change them from colourless to deeply coloured. The colour deepens with increasing absorbed dose. Micelles in these phantoms help to solubilize the leuco-dye molecules, which are only sparingly soluble in water, and to distribute them throughout the 3D gel volume (Babic *et al.* 2009). Diffusion of leuco-dye molecules solubilized in micelles is considerably slower than diffusion of individual reporter molecules in micelle-free gel dosimeters because micelles are relatively large. Consequently, post-irradiation spatial stability of micelle gel dosimeters is better than ferrous xylenol-orange Fricke gel (FX) dosimeters, which are currently the most popular optical gel dosimeters (Jordan and Avvakumov 2009). The two micelle gel dosimeters introduced by Jordan and his coworker use leuco malachite green (LMG) and leuco crystal violet (LCV), respectively, as reporter molecules. Micelle gel dosimeters using diacetylenes as reporter molecules were also investigated but were found to be unsuitable for accurate optical readout (Nasr *et al.* 2013).

Leuco-dye micelle gels are promising because they have the potential to produce accurate 3D dosimetry results with excellent spatial stability (Babic *et al.* 2009, Jordan

and Avvakumov 2009, Vandecasteele *et al.* 2011, Nasr *et al.* 2013). Tissue equivalence and manufacturing simplicity gives micelle gels considerable advantages compared polyurethane-based PRESAGE dosimeters and polymer gel dosimeters for implementation in clinical environments and for use in complex anthropomorphic phantoms (Vandecasteele *et al.* 2011). However, current micelle gel dosimeters have relatively lower dose sensitivity compared to FX gels. Leuco dye micelle gels are also sensitive to temperature during irradiation and sensitive to light during storage (Babic *et al.* 2009, Jordan and Avvakumov 2009). There is some uncertainty about whether leucodye micelle gels have significant dose-rate dependence (Babic *et al.* 2009, Vandecasteele *et al.* 2011).

Babic *et al.* (2009) recommended LCV micelle gels over LMG micelle gels because LCV gel dosimeters exhibited linear dose response, lower effective diffusion, and higher dose sensitivity compared with the LMG micelle gels developed earlier by the same research group (Babic *et al.* 2009, Jordan and Avvakumov 2009). The recommended LCV micelle gel recipe reported by Babic *et al.* (2009) is composed of five components: 4.0 wt% gelatin, 4.0 mM Triton x-100 (Tx100) surfactant, 25.0 mM trichloro acetic acid (TCAA), 1.0 mM LCV, and approximately 96.0 wt% water. This particular recipe will be referred to as Jordan's standard LCV gel throughout this article.

An essential component of this standard LCV gel is the Tx100 surfactant. Surfactants are categorized as nonionic, anionic or cationic (Evans and Wennerstrom 1999). The nonionic surfactant Tx100 was chosen by Jordan and Avvakumov (2009) to make radiochromic leuco-dye micelle gels because of its compatibility with gelatin hydrogels and its ability to form stable and optically-clear gels. Vandecasteele *et al.*

(2011) reported difficulties in making LCV micelle gels using Tx100 and replaced it with the anionic surfactant sodium dodecyl sulfate (SDS). When attempting to make radiochromic micelle gels using diacetylenes as reporter molecules, Nasr *et al.* (2103) tested Tx100, SDS and the cationic surfactant Cetyl Trimethyl Ammonium Bromide (CTAB). Precipitation problems were observed for several diacetylene gels produced using Tx100 and SDS. Transparent stable gels were obtained using CTAB. Note that different surfactants begin to aggregate to form micelles at different critical micelle concentrations (e.g., ~0.3 mM for Tx100, ~8.4 mM for SDS and ~0.92 mM for CTAB in deionized water at 25 ^{o}C) (Cui *et al.* 2008). Below the critical micelle concentration, all surfactant molecules are dissolved individually in the aqueous phase. Different surfactants also produce micelles of different sizes (e.g., ~5.5 nm for Tx100, ~1.84 nm nm for SDS, and ~ 3.0 nm for CTAB in deionized water at 25 ^{o}C) due to the different sizes of the individual surfactant molecules and the number of molecules that aggregate to form the micelles (e.g., ~140 molecules per micelle for TX100, ~60 for SDS and ~61 for CTAB in deionized water at 25 ^{o}C) (Paradies 1980, Neugebauer 1990, Duplatre *et al.* 1996, Storm *et al.* 2013).

Vandecasteele *et al.* (2011) studied the performance of LMG micelle gel dosimeters using SDS as the surfactant. They showed that addition of chloroform to the recipe resulted in improved dose sensitivity. This result was not surprising because chloroform is an important component used as a sensitizer in some PRESAGE gels (Adamovics 2006, Adamovics and Maryanski 2006) and McLaughlin has shown that chloroform and other chlorinated molecules are effective in increasing dose sensitivity in a variety of dosimetry applications. (McLaughlin 1970).

Babic *et al.* (2009) studied the effects of varying the concentrations of Tx100, LCV, and TCAA on dose sensitivity when developing the recipe for Jordan's standard LCV gel. They found that sensitivity can be improved by increasing the Tx100 concentration and by increasing the LCV concentration up to 2.0 mM, which was the maximum concentration reported in their study. They also showed that a concentration of 25.0 mM TCAA maximizes the dose sensitivity. The influence of TCAA on dose sensitivity may arise from two factors, which were discussed by Vandecasteele *et al.* (2011); TCAA contains chlorine atoms and is an acid that influences pH. Note that the solubility of LCV in pure water depends strongly on pH (Scifinder 2013) and that pH may also influence the radiochemistry of LCV gels. Babic *et al.* did not report the pH of their LCV micelle gels, but Vandecasteele *et al.* (2011) endeavored to match the pH when testing several LMG micelle gel recipes.

The purpose of the current study is to develop improved recipes for radiochromic LCV micelle gel dosimeters and to gain a deeper understanding of interactions between the various gel components. First, a reproducibility study using Jordan's standard LCV gel is described along with a modified manufacturing procedure that enables easier and faster gel preparation. Next, the dose rate dependency of Jordan's standard LCV gel is tested and the effects of changing the concentrations of LCV, Tx100, and TCAA on dose sensitivity and initial gel colour are reported. Tests are performed to investigate the influence of pH, separate from the concentration of TCAA, on dose sensitivity, gel transparency and initial gel colour. Two surfactants (SDS and CTAB) are investigated as replacements for Tx100. Effects of three halogenated hydrocarbons (i.e., chloroform, 2,2,2-Trichloroethanol (TCE) and 1,1,1-Trichloro-2-methyl-2-propanol hemihydrate

(TCMPH)) on dose sensitivity are also investigated. Interaction effects between the components of LCV micelle gel dosimeters are quantified and an improved recipe that contains water, gelatin, LCV, CTAB, TCAA, and TCE is proposed.

4.4 Materials and methods

4.4.1 Gel manufacturing procedure

Jordan's standard LCV gels were produced in the initial experiments using the following procedure (Babic *et al.* 2009, Jordan and Avvakumov 2009, Jordan 2013):

1) Sprinkle gelatin (Type A, 300 Bloom porcine skin, Sigma-Aldrich, Oakville, On, Canada) onto ~85 wt% of the total deionized water in the recipe at room temperature. Let swell for 20 minutes then stir the mixture at 40 ^{o}C until the gelatin dissolves completely. Filter the gelatin mixture then cool to 30 to 32 ^{o}C.
2) Add Tx100 (Sigma-Aldrich, Oakville, On, Canada) to ~ 5 wt% of the total deionized water and stir at room temperature.
3) Add TCAA (Sigma-Aldrich, Oakville, On, Canada) onto ~ 10 wt% of the total deionized water at room temperature and stir to dissolve. Add LCV powder (Sigma-Aldrich, Oakville, On, Canada) and stir.
4) Pour the LCV mixture from step 3 into the surfactant mixture from step 2 and stir for ~1 min.
5) Add the LCV-micelle mixture from step 4 slowly (drop-wise) to the filtered gelatin mixture from step 1 at 32 ^{o}C while stirring (~5-12 min depending on the amount of the gel that is being prepared)

Because this initial procedure was lengthy and needed special care during the drop-wise addition in step 5, the following modified manufacturing procedure was developed and followed in manufacturing all gels in this study unless otherwise mentioned:

1- Sprinkle gelatin into 75 wt% of the total deionized water in the recipe and let swell for ~ 20 minutes, and then stir while heating to 45 ^{o}C until gelatin dissolves completely.
2- Add the surfactant and TCAA to the remaining 25 wt% of the deionized water and stir at room temperature for ~5 minutes until completely dissolved. Add the LCV and stir for ~ 5 minutes until completely dissolved.
3- Pour LCV mixture (at room temperature) into the gelatin mixture at 45 ^{o}C and stir for ~ 2 minutes.

The resulting mixtures prepared using both procedures were poured into 4.5 ml polystyrene cuvettes with 10 mm light path (Fisher scientific, Ottawa, On, Canada) and sealed using a cap and parafilm. Some samples were poured into 500 mL or 1 L jars (for optical CT scanning) that were also sealed using parafilm. A few samples were poured into 23×85 mm clear glass cylindrical vials for visual evaluation and photography to assess initial colour and turbidity. pH was measured using a pH electrode (Denver Instrument Company, Colorado, USA). All gels were refrigerated at 4 ^{o}C for ~ 24 h and then heated to room temperature before irradiation.

4.4.2 Irradiation procedure

A Varian Clinac 6EX linear accelerator (Varian Medical Systems, Palo Alto, CA, USA) was used to irradiate the cuvettes to different doses of 0, 5, 10, 15, 20, and 40 Gy at a dose rate of 400 cGy/min. In preliminary experiments, all cuvettes were taken out of the

fridge and left at room temperature for ~ 1 h prior to irradiation. In later experiments, the cuvettes were immersed in a water bath at 22 ^{o}C for 20 minutes to ensure uniform temperature. Cuvettes were irradiated using an isocentric setup, with a 100 cm source-to axis distance (SAD), 2 cm of plastic water buildup, 10 cm of plastic water backscatter, and 15×15 cm^2 field size. The long dimension (height) of the cuvettes was perpendicular to the beam axis.

4.4.3 Optical transmission spectrometer measurements

Absorption spectra for cuvettes irradiated to different doses were measured ~ 20 minutes after irradiation. All samples were at room temperature (20-23 ^{o}C) when the spectra were measured using a SpectroVis Plus spectrophotometer (Vernier Software & Technology, OR, USA) over the wavelength region of 380-900 nm. All absorbance measurements were calibrated using a reference cuvette filled with deionized water. The change in the optical attenuation coefficient between the irradiated and un-irradiated vials was calculated from:

$$\Delta\mu = \frac{ln(10)}{x}(A_I - A_U) \tag{4.1}$$

where X=1 cm is the length of the light path through the vial, A_I is the measured absorbance of the irradiated sample and A_U is the absorbance of the un-irradiated sample. Equation (4.1) contains the factor of ln(10) because the measured absorbance is defined using a base 10 logarithm and attenuation is defined using a natural logarithm (Laidler *et al.* 2003).

4.4.4 Dose rate dependence of LCV micelle gels

Dose rate dependency of Jordan's standard LCV gels, manufactured according to the modified recipe, was tested by irradiating gel cuvettes to different doses at different dose

rates. 24 cuvettes, divided into four sets, were filled from the same LCV gel batch. Cuvettes from the first set were irradiated using a dose rate of 100 cGy/min to final doses of 0, 5, 10, 15, 20, and 40 Gy, respectively. Cuvettes from the other three sets were irradiated to the same final doses using dose rates of 200, 400 and 600 cGy/min, respectively. The optical response for each gel cuvette was measured using the optical transmission spectrometer.

4.4.5 Effect of different surfactants and surfactant concentrations on gel transparency

The objective of these experiments was to explore the effect of surfactant on the amount of LCV that can be added to the gel recipe before the gels become turbid. Surfactants used were SDS (Fisher Scientific, Ottawa, On, Canada), Tx100, and CTAB (both from Sigma-Aldrich, Oakville, On, Canada). Surfactant concentrations were selected so that the number of micelles per unit volume would be roughly 1 and 10 times the number of micelles in Jordan's standard LCV gels. Three different LCV concentrations were tested (1.0, 1.5, and 2.0 mM) for each surfactant concentration. Gelatin and TCAA concentrations were fixed at 4.0 wt% and 25.0 mM, respectively, to match the concentrations in Jordan's standard LCV gel. Gels in this set of experiments were not irradiated. Turbidity, or lack thereof, was determined visually.

4.4.6 Effect of TCAA concentration on gel transparency

The objective of these experiments was to explore the effect of TCAA concentration on gel turbidity. Gels were manufactured using 12.5, 25.0, 38.0, and 50.0 mM TCAA. Gelatin, LCV, and Tx100 concentrations were kept at 4.0 wt%, 1.0 mM and 4.0 mM, respectively, to match the recipe in Jordan's standard LCV gel. Gels in this set of experiments were not irradiated.

4.4.7 Effect of surfactant type and concentration on dose sensitivity of LCV micelle gels

This set of experiments was used to investigate the effects of different surfactants and surfactant concentrations on dose sensitivity of LCV micelle gels. TCAA, LCV, and gelatin concentrations were fixed at 25.0 mM, 1.0 mM, and 4.0 wt%, respectively, as in Jordan's standard LCV gel. Surfactants used in this set of experiments were Tx100 (at 4.0, 19.0, and 39.0 mM), SDS (at 2.5, 9.0, and 17.0 mM), and CTAB (at 2.5, 9.0, and 17.0 mM).

4.4.8 Effect of different acids and acid concentrations on dose sensitivity of LCV micelle gels

The effect of acid concentration on dose sensitivity was studied using the halogenated acid TCAA and sulfuric acid, which is not halogenated. Gelatin and Tx100 concentrations were fixed at 4.0 wt% and 4.0 mM, respectively, as in Jordan's standard LCV gel. The LCV concentration was fixed at 0.25 mM. The TCAA concentrations used were 14.5, 21.5, 25.0, 27.5, and 33.5 mM and the sulfuric acid concentrations tested were 7.5, 11.5, 13.5, 15.0, and 19.5 mM. These sulfuric acid concentrations were selected to match the pH of the gels made using TCAA. Subsequent experiments were conducted using TCAA concentrations of 18.0 and 23.0 mM in an effort to maximize the dose sensitivity.

Additional experiments were conducted to investigate the potential of improving dose sensitivity by simultaneously adding more acid and more LCV to the recipe. Two LCV micelle gels were manufactured using a TCAA concentration of 38.0 mM and LCV concentrations of 1.0 and 2.5 mM, respectively.

4.4.9 Effect of altering TCAA concentration and pH on dose sensitivity of LCV micelle gels

A series of experiments was conducted to determine whether TCAA concentration or pH had a more important effect on dose sensitivity and gel turbidity. A set of gels was manufactured with a fixed concentration of 25.0 mM TCAA, using two different gelatin concentrations of 2.0 wt% and 6.0 wt% because gelatin concentration influenced the pH. A second set of gels was made using the same gelatin concentrations (i.e., 2.0 wt% and 6.0 wt%), but the TCAA concentrations were adjusted to match the pH of Jordan's standard LCV gels.

4.4.10 Effect of halogenated species on dose sensitivity of LCV micelle gels

Three different halogenated compounds (i.e., chloroform (Fisher Scientific, Ottawa, On, Canada), TCE, and TCMPH (both from Sigma-Aldrich, Oakville, On, Canada)) were evaluated for their effectiveness in improving the dose sensitivity of LCV micelle gels. TCE and TCMPH were selected because of their lower volatility and lower toxicity, compared to chloroform. LCV micelle gels were made at two different concentrations (10.0 and 90.0 mM) of each of the three halogenated species. All gels were manufactured according the modified procedure except that, in step 2, the halogenated compound is added to the surfactant and TCAA in 25 % of the total deionized water and mixed for ~10 minutes before LCV is added. Concentrations of gelatin, Tx100, LCV, and TCAA were kept at 4.0 wt%, 4.0 mM, 1.0 mM, and 25.0 mM, respectively as in Jordan's standard LCV gel.

4.4.11 Designed experiments to optimize LCV micelle gels made with Tx100 and TCE

As shown in Table 4.1, a full factorial designed experiment was conducted using two-levels of three factors (Tx100, LCV and TCE). Three additional runs (9-11) were conducted near the centre point. Simple linear regression models were estimated with dose sensitivity and initial gel colour as the response variables.

Table 4.1: Concentrations of Tx100, LCV, and TCE in designed experiment. Measured response variables were initial colour of the un-irradiated LCV-Triton TCE gels and the dose sensitivity. Concentrations of gelatin and TCAA were fixed at 4.0 wt% and 25.0 mM, respectively, in all gels.

#	Tx100 [mM]	LCV [mM]	TCE [mM]
1	1.6	0.75	40.0
2	1.6	0.75	80.0
3	1.6	1.25	40.0
4	1.6	1.25	80.0
5	10.0	0.75	40.0
6	10.0	0.75	80.0
7	10.0	1.25	40.0
8	10.0	1.25	80.0
9	4.0	1.0	60.0
10	4.0	1.0	60.0
11	4.0	1.0	60.0

Table 4.2: Concentrations of CTAB, LCV, and TCE in full factorial experiment with replicates at central point and subsequent experiments used to optimize the gel response. Concentrations of gelatin and TCAA were fixed at 4.0 wt% and 25.0 mM, respectively.

#	CTAB [mM]	LCV [mM]	TCE [mM]
1	9.0	0.75	40.0
2	9.0	0.75	80.0
3	9.0	1.25	40.0
4	9.0	1.25	80.0
5	25.0	0.75	40.0
6	25.0	0.75	80.0
7	25.0	1.25	40.0
8	25.0	1.25	80.0
9	17.0	1.0	60.0
10	17.0	1.0	60.0
11	17.0	1.0	60.0
12	17.0	1.0	60.0
13	17.0	1.0	60.0
14	25.0	1.25	120.0
15	33.0	1.25	100.0
16	33.0	1.5	100.0
17	33.0	1.25	120.0
18	15.5	0.75	80.0
19	17.0	0.75	120.0
20	33.0	1.25	120.0

4.4.12 Experiments to optimize LCV micelle gels made with CTAB and TCE

Preliminary experiments were conducted to explore the possibility of improving dose sensitivity of LCV micelle gels made with CTAB surfactant when TCE is added to the recipe. Three LCV micelle gels were made using 17.0 mM CTAB and different TCE concentrations (60.0, 90.0, and 120.0 mM). Concentrations of gelatin, LCV, and TCAA were fixed at 4.0 wt%, 1.0 mM, and 25.0 mM, respectively. A second round of experiments was conducted to find a suitable pH to obtain high dose sensitivity of LCV

gels. These LCV micelle gels were made without TCE and with gelatin, LCV, and CTAB concentrations fixed at 4.0 wt%, 0.25 mM, and 17.0 mM, respectively, and the following TCAA concentrations 14.5, 18.0, 21.5, 23.0, 25.0, 27.5, and 33.5 mM.

Results from the preliminary experiments were used to select the settings for a full factorial design with five replicates at the central point (experiments 1-13 in Table 4.2) was used to estimate parameters in linear regression models with dose sensitivity and initial colour as response variables. Subsequent experiments (14-20) were conducted to optimize the recipe.

4.4.13 Preliminary experiments in large-jar phantoms

To examine the response of LCV micelle gel to spatially non-uniform radiation, two 1 L polyethylene terephthalate jars were filled with gel using the optimized gel recipe of 0.75 mM LCV, 17 mM CTAB, 120 mM TCE, 25.0 mM TCAA and 4 wt% gelatin, and subsequently irradiated. Irradiations were performed using a Varian Trilogy linear accelerator with RapidArc (Varian Medical Systems, Palo Alto, California). One gel was irradiated with a single arc VMAT prostate treatment plan, up to a maximum dose of 1795.3 cGy in the gel. The second gel was used for calibration and was irradiated with a 1850 MU, 12 MeV 6 x 6 cm^2 field electron beam (SSD=100 cm) delivered to the top surface of the gel (jar lid removed).

Gel dosimeters were imaged using a Vista Optical CT scanner (Modus Medical Devices Inc., London, ON, Canada) under 590 nm LED illumination. Reference scan images were taken of each gel before irradiation. After irradiation, data scan images were also taken. Each gel was carefully timed to ensure that post-irradiation imaging times were consistent. To convert optical density values to dose, calibration central-axis depth-

dose data were obtained from the gel and compared to Wellhofer ionization-chamber water-tank measurements. This calibration was applied to the VMAT plan gel irradiation.

4.5 Results and Discussion:

4.5.1 Reproducibility of Jordan's standard LCV gels and Assessment of the Modified Manufacturing Procedure

Jordan's standard LCV gel was reproduced several times during the course of this study using the original manufacturing procedure and the revised manufacturing procedure. Plots of the change in optical attenuation ($\Delta\mu$) vs. absorbed dose are linear over the dose range from 0 to 40 Gy. Slopes of these plots are dose sensitivities. In preliminary experiments, the vials were removed from the fridge and left at room temperature for ~ 1 h prior to irradiation so that they could equilibrate to room temperature. For these samples, produced using either the original manufacturing procedure or the modified procedure, reproducibility of the dose sensitivity was poor with a standard deviation of $2.2 \cdot 10^{-3}$ $Gy^{-1}cm^{-1}$ determined using 15 dose response curves. In 25 later experiments, all conducted using the revised manufacturing procedure, a five-fold improvement (standard deviation = $4.5 \cdot 10^{-4}$ $Gy^{-1}cm^{-1}$) in reproducibility was achieved by immersing the vials in a water bath at 22 ^{o}C for 20 minutes prior to irradiation. These results confirm the conclusion of Babic *et al.* (2009) that careful control of temperature at the time of irradiation is crucial for obtaining reliable results from LCV micelle gels. The mean dose sensitivity obtained from the 25 replicates was $7.6 \cdot 10^{-3}$ Gy^{-1} cm^{-1}, indicating that reproducibility of dose sensitivity was typically within ~5.9%. Sources of variability include batch-to-batch variation in concentrations of chemical species, minor variability in the temperature at the time of radiation, and variability associated with optical readout.

Note that the average dose sensitivity measured in the current study (~$7.6 \cdot 10^{-3}$ Gy^{-1} cm^{-1}) is in good agreement with the value (~ $7.5 \cdot 10^{-3}$ Gy^{-1} cm^{-1}) reported by Babic *et al.* (2009) in Figure 5 of their article.

The modified manufacturing procedure for Jordan's standard LCV gels involved several changes compared to the original procedure (i.e., changing temperatures during manufacturing steps, changing the order of addition of gel components and skipping the gel filtration step). Using the revised procedure cuts the typical manufacturing time in half, without any noticeable change in the quality of the results. Figure 4.1 shows dose responses of three gels manufactured using Jordan's standard LCV gel recipe, which were manufactured using: i) the original procedure, ii) the original procedure without the filtering step and iii) the new procedure.

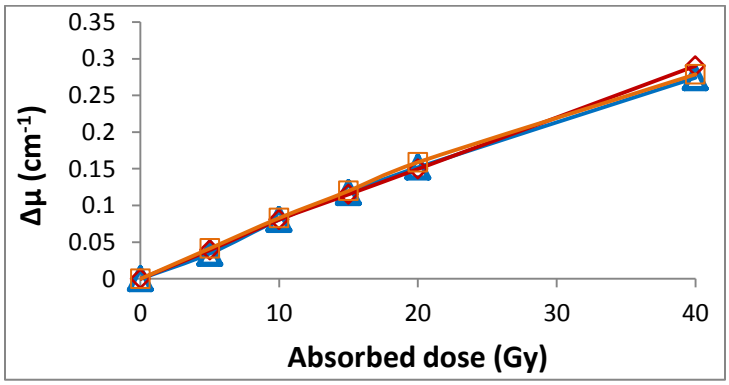

Figure 4.1: Dose response of three Jordan standard LCV gels manufactured using the old procedure (—Δ—), the old procedure without filtration (—◊—), and the new procedure (—□—). All gels were at 22 °C at the time of irradiation. Lines between symbols are added to guide the eye.

4.5.2 Dose rate dependence

Figure 4.2 shows that varying the dose rate from 100 to 600 cGy.min^{-1} has no noticeable influence on the dose response of Jordan's standard LCV gel. Dose sensitivities calculated from these data do not show any trend with dose rate. These results confirm the conclusion by Babic *et al.* (2009) that LCV micelle gels are relatively insensitive to dose rate.

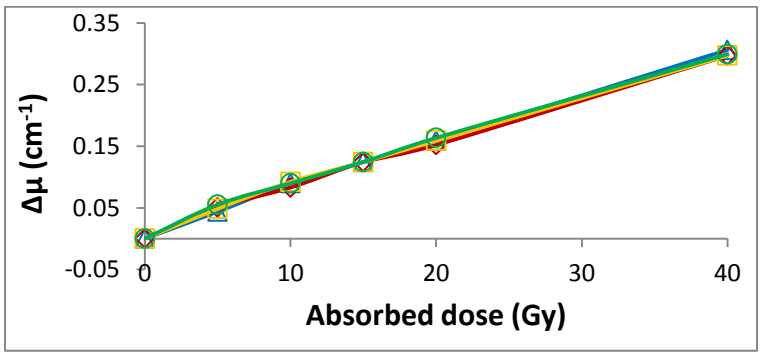

Figure 4.2: Dose response of Jordan's standard LCV gel irradiated at four different dose rates including: 100 (—Δ—), 200 (—◊—), 400 (—□—), and 600 (—○—) cGy.min^{-1}. All gels were at 22 ^{o}C at the time of irradiation. Lines between symbols are added to guide the eye.

4.5.3 Effect of different surfactants and surfactant concentrations on gel transparency

Babic *et al.* (2009) showed that increasing the LCV concentration in micelle gels increased the dose sensitivity. In the current study, experiments were performed to determine whether additional increases in LCV beyond the range of concentrations studied by Babic *et al.* could lead to further sensitivity improvements. Unfortunately turbid gels, which would be unsuitable for optical CT readout, were obtained (experimental results not shown) when LCV concentrations were increased beyond 1.5 mM, with other components fixed at their concentrations in Jordan's standard LCV gel

recipe. Presumably, the turbidity results from precipitation of LCV, which is a solid at room temperature.

To determine whether surfactants can alleviate problems with gel turbidity, three different surfactants at different concentrations were tested and the results are shown in table 4.3. Transparent LCV gels were obtained from the first two recipes which did not contain any surfactant. When 4.0 mM Tx100 was added (i.e., the concentration in Jordan's standard LCV gel) transparent gel was obtained at 1 mM LCV and turbid gels were obtained at 1.5 and 2.0 mM. Increasing the Tx100 concentration to 38.0 mM resulted in transparent gels at 1.0 and 1.5 mM LCV and turbid gels at 2.0 mM LCV. The 38.0 mM concentration of Tx100 was selected so that the number of micelles per liter would be approximately 10 times the number in Jordan's standard LCV gel (using the critical micelle concentration and the number of molecules per micelle). These results indicate that surfactant concentration has only a minor effect on the turbidity of LCV micelle gels. Using CTAB at two different concentrations (in experiments 10 to 15) did not resolve the turbidity problem for LCV concentrations of 1.5 and 2.0 mM. LCV micelle gels produced using SDS resulted in very viscous, turbid and sticky mixtures that would not be suitable for optical scanning. Note that gels 4 to 9, which were produced using Tx100 had noticeable blue colour prior to irradiation, but that the other gels in Table 4.3 had no initial colour that was observable to the naked eye.

4.5.4 Effect of trichloroacetic acid concentration on gel transparency

Gels were manufactured using different TCAA concentrations to study the relationship between acid concentration (or pH) and gel turbidity. As shown in table 4.4 the gel made with 12.5 mM TCAA (pH = 3.98) resulted in a turbid gel, and the gels made with higher

TCAA concentrations (resulting in lower pH) were transparent. The TCAA concentration also influenced the colour of the gel prior to irradiation, with low acid concentrations leading to coloured gels.

Table 4.3: Results from experiments conducted to determine the influence of surfactant type and concentration on the maximum amount of LCV that can be used to produce transparent LCV micelle gels. All experiments were conducted using 25 mM TCAA and 4 wt% gelatin. Gel 4 is a replicate of Jordan's standard LCV gel.

#	surfactant	Conc. [mM]	LCV [mM]	~ Multiple of micelles in Jordan's standard LCV gel	Turbidity	Initial Colour	pH
1	--	0.0	1.0	0	Clear	No	3.39
2	--	0.0	1.5	0	Clear	No	3.54
3	--	0.0	2.0	0	Turbid	No	3.39
4	Tx100	4.0	1.0	1	Clear	Light blue	3.38
5	Tx100	4.0	1.5	1	Turbid	Light blue	3.37
6	Tx100	4.0	2.0	1	Turbid	Light blue	3.37
7	Tx100	38.0	1.0	10	Clear	Dark blue	3.38
8	Tx100	38.0	1.5	10	Clear	Dark blue	3.45
9	Tx100	38.0	2.0	10	Turbid	Dark blue	3.48
10	CTAB	2.5	1.0	1	Clear	No	3.39
11	CTAB	2.5	1.5	1	Turbid	No	3.39
12	CTAB	2.5	2.0	1	Turbid	No	3.38
13	CTAB	17.0	1.0	10	Clear	No	3.44
14	CTAB	17.0	1.5	10	Turbid	No	3.43
15	CTAB	17.0	2.0	10	Turbid	No	3.38
16	SDS	2.5	1.0	1			
17	SDS	2.5	1.5	1			
18	SDS	2.5	2.0	1	Very turbid, viscous and sticky mixtures		
19	SDS	17.0	1.0	10			
20	SDS	17.0	1.5	10			
21	SDS	17.0	2.0	10			

Table 4.4: Results from experiments conducted to determine the influence of TCAA concentration on the transparency of LCV micelle gels. Gel 2 is a replicate of Jordan's standard LCV gel.

#	TCAA [mM]	Tx100 [mM]	LCV [mM]	Gelatin wt%	Turbidity	Initial Colour	pH
1	12.5	4.0	1.0	4.0	Turbid	Light Blue	3.98
2	25.0	4.0	1.0	4.0	Clear	Light Blue	3.30
3	38.0	4.0	1.0	4.0	Clear	No	2.25
4	50.0	4.0	1.0	4.0	Clear	No	1.88

4.5.5 Effect of surfactant type and concentration on dose sensitivity and initial colour of LCV micelle gels

Dose sensitivity of LCV micelle gels was tested at different concentrations of Tx100, CTAB and SDS as shown in table 4.5. Dose sensitivity of LCV gel with no added surfactant was $5.50 \cdot 10^{-3}$ $Gy^{-1}cm^{-1}$ and increased with increasing Tx100 concentration. For example, when 38.0 mM Tx100 was used (to make the number of micelles roughly ten times that in Jordan's standard LCV gel) dose sensitivity increased to ~1.8 times that of Jordan's standard LCV gel. Unfortunately, the initial colour of the un-irradiated gels also increased with increasing Tx100 concentration. Using CTAB at different concentrations did not seem to improve the dose sensitivity of LCV micelle gels nor influence the initial colour. All gels that were attempted using SDS at different concentrations resulted in very viscous, turbid and sticky mixtures that are not suitable for optical scanning.

Table 4.5: Dose sensitivity of LCV micelle gels made using Tx100, CTAB, and SDS. Surfactant concentrations were selected such that the number of micelles formed in the gels would be, roughly, 1, 5.5, and 10 times the number of micelles in Jordan's standard LCV gel. Gelatin, TCAA, and LCV concentrations were fixed at 4.0 wt%, 25 mM, and 1.0 mM, respectively. Gel 2 is a replicate of Jordan's standard LCV gel. Absorbance values were measured using a wavelength of 590 nm

#	surfactant	Conc. [mM]	Turbidity	Initial Colour	Initial Absorbance	Dose Sensitivity [$Gy^{-1}.cm^{-1}$]	pH
1	--		clear	No	0.020	$5.50 \cdot 10^{-3}$	3.40
2	Tx100	4.0	clear	Light Blue	0.049	$7.65 \cdot 10^{-3}$	3.36
3	Tx100	19.0	clear	Dark Blue	0.116	$1.09 \cdot 10^{-2}$	3.44
4	Tx100	38.0	clear	Dark Blue	0.207	$1.37 \cdot 10^{-2}$	3.43
5	CTAB	2.5	clear	No	0.020	$5.62 \cdot 10^{-3}$	3.37
6	CTAB	9.0	clear	No	0.025	$5.57 \cdot 10^{-3}$	3.39
7	CTAB	17.0	clear	No	0.026	$5.80 \cdot 10^{-3}$	3.39
8	SDS	2.5	V. turbid		Very turbid, viscous		3.37
9	SDS	9.0	V. turbid		and sticky mixtures		3.39
10	SDS	17.0	V. turbid				3.39

4.5.6 Effect of different acids, acid concentrations and pH on dose sensitivity of LCV micelle gels

The purpose of the experiments involving gels 1 to 12 in Table 4.6 was to study the effect of acid concentration on dose sensitivity and to isolate effect of halogen atoms in TCAA from the effect of pH on dose sensitivity. The LCV micelle gels manufactured using TCAA (gels 1 to 7 in Table 4.6) show higher sensitivity than the corresponding gels made with sulfuric acid (gels 8 to 12) at matched pH, suggesting that the chlorine atoms in TCAA had a sensitizing effect. The concentration of TCAA strongly influences dose sensitivity in a nonlinear fashion, with the highest dose sensitivity obtained using a TCAA concentration of 21.5 mM (gel 3). A similar maximum in dose sensitivity was

observed by Babic *et al.* (2009) who prepared LCV gels with different concentrations of TCAA. LCV micelle gels manufactured at low acid concentration (high pH) were turbid regardless of the type of acid used, as shown by gels 1, 2, and 8 in Table 4.6. This result confirms that transparency of LCV micelle gels is influenced by acid concentration or pH.

Table 4.6: Dose sensitivity of LCV micelle gels at different concentrations of TCAA and H_2SO_4. Concentrations of gelatin and Tx100 in gels 1 to 12 were fixed at 4 wt% and 4 mM, respectively. Gels 13-15 were produced to investigate the potential of improving dose sensitivity by simultaneously increasing the concentrations of TCAA and LCV. Gel 13 is a replicate of Jordan's standard LCV gel. Absorbance values were measured using a wavelength of 590 nm

#	Acid	Conc. [mM]	LCV [mM]	Turbidity	Initial Colour	Initial Absorbance	Dose Sensitivity [$Gy^{-1}.cm^{-1}$]	pH
1	TCAA	14.5	0.25	Turbid	----	0.185	$3.87 \cdot 10^{-3}$	4.04
2	TCAA	18.0	0.25	Turbid	----	0.122	$5.37 \cdot 10^{-3}$	3.75
3	TCAA	21.5	0.25	Clear	No	0.030	$6.38 \cdot 10^{-3}$	3.63
4	TCAA	23.0	0.25	Clear	Light Blue	0.036	$5.64 \cdot 10^{-3}$	3.43
5	TCAA	25.0	0.25	Clear	No	0.030	$4.79 \cdot 10^{-3}$	3.36
6	TCAA	27.5	0.25	Clear	No	0.019	$4.33 \cdot 10^{-3}$	3.15
7	TCAA	33.5	0.25	Clear	No	0.018	$1.93 \cdot 10^{-3}$	2.63
8	H2SO4	7.5	0.25	Turbid	----	0.044	$1.19 \cdot 10^{-3}$	4.07
9	H2SO4	11.5	0.25	Clear	No	0.019	$1.11 \cdot 10^{-3}$	3.62
10	H2SO4	13.5	0.25	Clear	No	0.015	$1.15 \cdot 10^{-3}$	3.37
11	H2SO4	15.0	0.25	Clear	No	0.012	$9.21 \cdot 10^{-4}$	3.11
12	H2SO4	19.5	0.25	Clear	No	0.017	$-1.82 \cdot 10^{-4}$	2.56
13	TCAA	25.0	1.0	Clear	Light blue	0.052	$7.72 \cdot 10^{-3}$	3.38
14	TCAA	38.0	1.0	Clear	No	0.020	$2.49 \cdot 10^{-3}$	2.62
15	TCAA	38.0	2.5	Clear	No	0.012	$4.58 \cdot 10^{-3}$	2.63

Gels 13 to 15 in table 4.6 were produced to investigate the potential for increasing dose sensitivity of LCV micelle gels by increasing the LCV concentration while simultaneously increasing the TCAA concentration to avoid LCV precipitation. The dose sensitivity of LCV gel 14 in table 4.6, made with 1.0 mM LCV and 38.0 mM TCAA, was lower than that of Jordan's standard LCV gel (gel 13). Dose sensitivity improved when the LCV concentration increased to 2.5 mM at fixed TCAA concentration (gel 15 in table 4.6) but the dose sensitivity was still below that of Jordan's standard LCV gel (gel 13). These results show that increasing the LCV concentration in LCV micelle gels by adding more TCAA (to avoid LCV precipitation) reduced rather than increased the dose sensitivity compared to Jordan's standard LCV gel. Using the additional TCAA to prevent precipitation of the LCV reduced the pH, which seems to be the cause of the poor sensitivity.

Experimental results discussed so far show that the concentration of TCAA strongly affects both dose sensitivity and gel transparency (LCV solubility) in LCV micelle gels. The purpose of experiments in table 4.7 was to isolate effects of pH from the effect of acid concentration on both dose sensitivity and transparency of LCV micelle gels. To do so, the gelatin concentration (which affects pH) was changed in a careful way such that some gels (i.e., gels 1, 2 and 3) have different pH values at constant TCAA concentration and other gels (i.e., gels 1, 4 and 5) have nearly constant pH at different TCAA concentrations. When the gelatin concentration was decreased from 4.0 wt% in gel 1 to 2.0 wt% in gel 2, the pH dropped to 2.36 and, consequently, the dose sensitivity decreased. When the gelatin concentration increased to 6.0 wt% (gel 3), the pH increased to 3.89 and the gel became turbid. When pH was kept constant at ~ 3.45, dose sensitivity

and transparency of the LCV micelle gels was relatively constant (gels 1, 4 and 5). So it can be concluded that pH, rather than TCAA concentration, is the dominant factor for achieving high dose sensitivity and transparency of LCV micelle gels. Note, however, that using TCAA rather than a non-halogenated acid like H_2SO_4 is also important for achieving high dose sensitivity (see table 4.6).

Table 4.7: Influence of gelatin concentration and TCAA concentration on the dose sensitivity and transparency of LCV micelle gels. LCV and TX100 concentrations were fixed at 1 mM and 4 mM, respectively, to match Jordan's standard LCV gel. Gel 1 is a replicate of Jordan's standard LCV gel. Absorbance values were measured using a wavelength of 590 nm

#	Gelatin wt%	TCAA [mM]	Turbidity	Initial Colour	Initial Absorbance	Dose Sensitivity [$Gy^{-1}.cm^{-1}$]	pH
1	4	25.0	clear	Light Blue	0.050	$7.46 \cdot 10^{-3}$	3.41
2	2	25.0	clear	No	0.011	$3.04 \cdot 10^{-3}$	2.36
3	6	25.0	Turbid	----	----	----	3.89
4	2	12.5	Clear	Light Blue	0.085	$8.06 \cdot 10^{-3}$	3.45
5	6	35.0	clear	No	0.024	$7.37 \cdot 10^{-3}$	3.50

4.5.7 Effect of halogenated hydrocarbons on dose sensitivity of LCV micelle gels

Vandecasteele *et al.* (2011) reported that adding chloroform and carbon tetrachloride, which are halogenated hydrocarbons, to their LMG micelle gels improved the dose sensitivity. To study the effect of halogenated compounds on dose sensitivity of LCV micelle gels, three different halogenated species (chloroform, TCE, and TCMPH) were tested at different concentrations. Chloroform was chosen because it was used by Vandecasteele *et al.* (2011) to improve dose sensitivity in their LMG micelle gels and because it is an important component in PRESAGE plastic dosimer recipe (Adamovics

2006, Adamovics and Maryanski 2006). TCE and TCMPH were chosen because, like chloroform, they have three chlorine atoms. Also, they are widely available and are less volatile and less toxic than chloroform (Sigma-Aldrich, 2013). Results in table 4.8 show that dose sensitivities of LCV micelle gels were the highest for gels manufactured with TCE. Moreover, dose sensitivity of LCV micelle gels increased with increasing TCE concentration. Using chloroform did not seem to affect the dose sensitivity of LCV micelle gels very much compared to gel (7) which is a standard Jordan LCV gel. When TCMPH was used at the low concentration of 10.0 mM, dose sensitivity became higher than that of Jordan's standard LCV gel. However, when the TCMPH concentration increased to 90.0 mM, the dose sensitivity decreased to a value lower than that of Jordan's standard LCV gel. TCE was selected for further testing as a possible additive to LCV micelle gels because it gave the best dose sensitivity results in table 4.8.

Table 4.8: Effects of adding three different halogenated compounds on dose sensitivity of LCV micelle gels. Concentrations of LCV, TCAA, Tx100, and gelatin are the same as in Jordan's standard LCV gel. Gel 7 is a replicate of Jordan's standard LCV gel. Absorbance values were measured using a wavelength of 590 nm

#	Halogenated hydrocarbon	Conc. [mM]	Turbidity	Initial Colour	Initial Absorbance	Dose Sensitivity [$Gy^{-1}.cm^{-1}$]	pH
1	Chloroform	10.0	Clear	Light Blue	0.048	$8.08 \cdot 10^{-3}$	3.40
2	Chloroform	90.0	Clear	No	0.017	$7.09 \cdot 10^{-3}$	3.34
3	TCE	10.0	Clear	Light Blue	0.054	$9.07 \cdot 10^{-3}$	3.34
4	TCE	90 .0	Clear	Light Blue	0.088	$1.25 \cdot 10^{-2}$	3.39
5	TCMPH	10.0	Clear	Light Blue	0.055	$9.26 \cdot 10^{-3}$	3.42
6	TCMPH	90.0	Clear	Light Blue	0.041	$7.32 \cdot 10^{-3}$	3.43
7	----	----	Clear	Light Blue	0.055	$7.74 \cdot 10^{-3}$	3.48

4.5.8 Designed experiments to optimize LCV micelle gels made with Tx100 and TCE

Based on promising results obtained for LCV micelle gels made with TCE and Tx100 in Table 4.8, a factorial experiment was designed to aid in gel recipe optimization. The goal was to find an improved gel with higher dose sensitivity and low initial colour, since the background colour of some of the gels in Tables 4.3 to 4.8 prior to irradiation may cause complications during optical scanning of larger jars. Table 4.9 shows results from a two-level three-factor full factorial design (gels 1 to 8) along with three replicates near the centre point (gels 9 to 11) and one replicate of Jordan's standard LCV gel (gel 12). A photograph of the unirradiated gels 1 to 12 is provided in Figure 4.3, which indicates that all of the gels were transparent and that gels 4 to 8 have a darker blue colour than the other gels.

Table 4.9: Influence of Tx100, LCV, and TCE on initial colour and dose sensitivity of LCV micelle gels. Absorbance values were measured using a wavelength of 590 nm. Concentrations of gelatin and TCAA were fixed at 4.0 wt% and 25.0 mM, respectively, as in Jordan's standard LCV gel. Gel 12 is a replicate of Jordan's standard LCV gel.

#	Tx100 [mM]	LCV [mM]	TCE [mM]	Initial Colour	Initial Absorbance	Dose Sensitivity [$Gy^{-1}.cm^{-1}$]	pH
1	1.6	0.75	40.0	No	0.024	$7.74 \cdot 10^{-3}$	3.41
2	1.6	0.75	80.0	Light Blue	0.052	$9.10 \cdot 10^{-3}$	3.39
3	1.6	1.25	40.0	Light Blue	0.033	$8.98 \cdot 10^{-3}$	3.37
4	1.6	1.25	80.0	Light Blue	0.059	$1.10 \cdot 10^{-2}$	3.36
5	10	0.75	40.0	Dark Blue	0.102	$1.02 \cdot 10^{-2}$	3.39
6	10	0.75	80.0	Dark Blue	0.144	$1.20 \cdot 10^{-2}$	3.36
7	10	1.25	40.0	Dark Blue	0.138	$1.20 \cdot 10^{-2}$	3.41
8	10	1.25	80.0	Dark Blue	0.254	$1.52 \cdot 10^{-2}$	3.41
9	4.0	1.0	60.0	Light Blue	0.070	$1.01 \cdot 10^{-2}$	3.41
10	4.0	1.0	60.0	Light Blue	0.082	$9.79 \cdot 10^{-3}$	3.42
11	4.0	1.0	60.0	Light Blue	0.072	$1.01 \cdot 10^{-2}$	3.36
12	4.0	1.0	0	Light Blue	0.057	$8.48 \cdot 10^{-3}$	3.32

Linear regression was used to estimate parameters in the following empirical models for dose sensitivity (*DS*) and absorbance (*A*) at 590 nm as a function of the Tx100, LVC and TCE concentrations:

$$DS = \mathbf{5.03 \cdot 10^{-3}} + \mathbf{2.64 \cdot 10^{-4}}[Tx100] + \mathbf{1.24 \cdot 10^{-3}}[LCV] + \mathbf{1.23 \cdot 10^{-5}}[TCE]$$
$$- 2.68 \cdot 10^{-5}[Tx100][LCV] - 1.67 \cdot 10^{-6}[Tx100][TCE]$$
$$+ 2.56 \cdot 10^{-5}[LCV][TCE] + 4.05 \cdot 10^{-6}[Tx100][LCV][TCE] \quad (4.2)$$

$$A = \mathbf{-4.71 \cdot 10^{-2}} + \mathbf{1.64 \cdot 10^{-2}}[Tx100] + \mathbf{4.07 \cdot 10^{-2}}[LCV] + \mathbf{1.25 \cdot 10^{-3}}[TCE]$$
$$\mathbf{- 1.17 \cdot 10^{-2}}\ [Tx100][LCV] \mathbf{- 2.98 \cdot 10^{-4}}[Tx100][TCE]$$
$$\mathbf{- 8.24 \cdot 10^{-4}}[LCV][TCE] + \mathbf{4.52 \cdot 10^{-4}}\ [Tx100][LCV][TCE] \quad (4.3)$$

Units for *DS*, *A*, [*Tx*100], [*LCV*] and [*TCE*] in equations (4.2) and (4.3) are provided in Table 4.9. Bolded parameter values are those that are statistically different from zero at the 95% confidence level (see Appendix A). The bolded positive values of $2.64 \cdot 10^{-4}$ Gy^{-1} cm^{-1} mM^{-1}, $1.24 \cdot 10^{-3}$ Gy^{-1} cm^{-1} mM^{-1} and $1.23 \cdot 10^{-5}$ Gy^{-1} cm^{-1} mM^{-1} for parameters in the linear terms in equation (4.2) indicate that the concentrations of Tx100, LCV and TCE all have a positive influence on dose sensitivity, as expected. None of the interaction terms in equation (4.2) are statistically significant, which may be a result of the limited amount of experimental data used to fit this model. In equation (4.3), all of the parameters for the linear terms are positive and significant at the 95% confidence level, indicating that Tx100, LCV and TCE all contribute to darker initial colour. It is somewhat surprising that all of the interaction terms are also significant, suggesting that interactions among the different species may influence the initial colour of the gels.

The following objective function was used to search for an optimized recipe for LCV micelle gels made with TCE and Tx100:

$$J = \omega\, DS - A \tag{4.4}$$

where ω is a positive weighting factor introduced to control the relative importance of achieving high dose sensitivity and low initial absorbance. Selecting a large value of ω will cause the optimizer to select gel recipes with high dose sensitivity at the expense of dark initial colour and low values of ω will result in the selection of less-coloured gels at the expense of dose sensitivity. Bounds on the species concentrations (i.e., 1.6 mM $\leq$ [*Tx*100] $\leq$10 mM, 0.75mM $\leq$ [*LCV*] $\leq$ 1.25 mM, 40 mM $\leq$ [*TCE*] $\leq$ 80 mM) were enforced during optimization to ensure that reasonable recipes would be selected. The optimization was performed using two different values of ω (i.e., ω= 7.478 Gy cm and ω = 74.78 Gy cm). The lower value of ω was selected so that the two terms in the objective function would be similar in size, so that the optimizer would pay approximately equal attention to dose sensitivity and absorbance. The larger value of ω was selected so that the optimizer would pay more attention to achieving high dose sensitivity. The optimization study was conducted twice for each value of ω, once using only the significant terms in equations (4.2) and (4.3) and once using all of the terms, regardless of whether the corresponding parameters were statistically significant or not.

When the lower value of ω was used, with both versions of equations (4.2) and (4.3), the recipe for gel 3 in Table 4.9 was selected. This gel had the lowest permissible concentration of Tx100 and TCE and the highest permissible concentration of LCV. The

dose sensitivity of this gel is only marginally better than that of Jordan's standard LCV gel but the initial colour is significantly better. As a result, we considered making some gels with higher LCV concentrations and lower concentrations of Tx100 and TCE, but these gels are expected to be turbid due to LCV precipitation.

When the higher value of ω was selected, using both versions of equations (4.2) and (4.3), the optimizer chose the recipe for gel 8 in Table 4.9, which has the highest permissible concentrations of LCV, Tx100 and TCE. As shown in Figure 4.3, this gel is dark blue and would likely not be suitable for use in large jars. The results from this optimization study suggest that producing LCV gels with substantially higher dose sensitivity and better initial colour than Jordan's standard LCV gel would not be possible using TCE and Tx100.

Figure 4.3: photograph of un-irradiated vials (23×85 mm clear glass) of gels manufactured using different concentrations of Tx100, LCV, and TCE. Vial numbers correspond to the gel numbers in table 4.9.

4.5.9 Experiments to optimize LCV micelle gels made with CTAB and TCE

Results in Table 4.5 show that LCV micelle gels made with CTAB had poor dose sensitivity but were nearly colourless prior to irradiation, over the range of CTAB concentrations that were tested. As a result, a series of experiments was conducted to explore whether better LCV gels could be produced using CTAB and TCE. Figure 4.4 shows that the dose sensitivity of LCV micelle gels made with CTAB increases with increasing [*TCE*] and that gels with substantially better dose sensitivity than Jordan's standard LCV gel can be obtained. Note that all of the gels in Figure 4.4 were nearly colourless, except for Jordan's standard LCV gel.

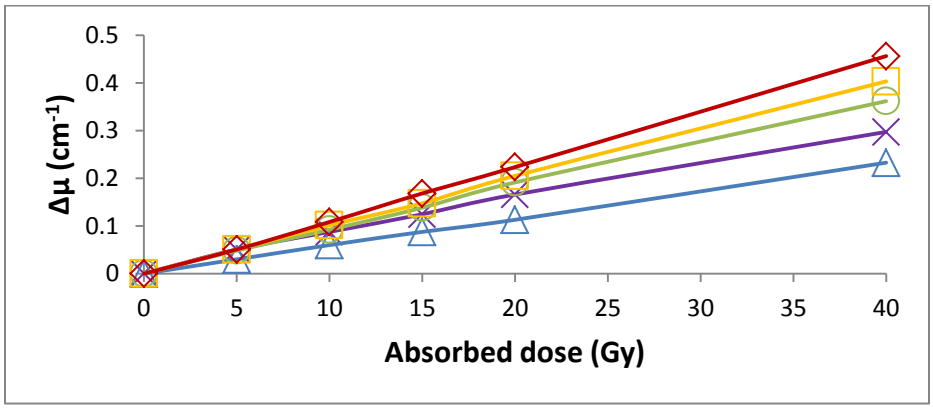

Figure 4.4: Effect of TCE at: 0 mM (—△—), 60 mM (—○—), 90 mM (—□—), and 120 mM (—◊—) on dose response of LCV micelle gels produced using CTAB as the surfactant. Concentrations of gelatin, LCV, CTAB, and TCAA were fixed at 4 wt%, 1 mM, 17 mM, and 25 mM, respectively. A replicate of Jordan's standard LCV gel (—×—) is shown for comparison. All gels were at 22 ºC at the time of irradiation. Lines between symbols are added to guide the eye.

A second round of experiments was conducted to study the effect of pH on the dose sensitivity of LCV micelle gels made with CTAB (with no TCE added) to find a suitable pH to obtain high dose sensitivity. Results in Table 4.10 confirm that the concentration of TCAA strongly affects the pH and the dose sensitivities of LCV micelle gels. The maximum dose sensitivity of these gels occurred at pH ~ 3.3 which is similar to the pH value of ~ 3.6 that gave the best dose sensitivity for gels made with Tx100 (see Table 4.6). LCV micelle gels made using CTAB that had low acid concentration (and high pH) were turbid, which confirms that transparency of LCV micelle gels is influenced by pH. As a result, a TCAA concentration of 25.0 mM was selected for further experimentation to obtain a pH that is near to best pH for achieving high dose sensitivity and to avoid potential LCV precipitation.

Table 4.10: Dose sensitivity of LCV micelle gels made with 17.0 mM CTAB, 0.25 mM LCV, and 4 wt% gelatin at different concentrations of TCAA. Absorbance values were measured using a wavelength of 590 nm

#	TCAA [mM]	Turbidity	Initial Colour	Initial Absorbance	Dose Sensitivity [$Gy^{-1}.cm^{-1}$]	pH
1	14.6	Turbid	---	0.189	$2.86 \cdot 10^{-3}$	3.85
2	18.0	Turbid	---	0.073	$4.51 \cdot 10^{-3}$	3.62
3	21.5	Clear	No	0.026	$4.84 \cdot 10^{-3}$	3.42
4	23.0	Clear	No	0.021	$5.25 \cdot 10^{-3}$	3.29
5	25.0	Clear	No	0.02	$4.91 \cdot 10^{-3}$	3.16
6	27.5	Clear	No	0.018	$4.35 \cdot 10^{-3}$	2.96
7	33.5	Clear	No	0.017	$2.83 \cdot 10^{-3}$	2.47

The full factorial design shown in Table 4.11 (runs 1 to 8) and five replicates at the central point (runs 9 to 13) were conducted to investigate the influence of [*CTAB*], [*LCV*] and [*TCE*] on dose sensitivity and initial colour. Linear regression models similar to equations (4.2) and (4.3) were fitted using the data (see Appendix B). Results from this set of experiments were promising so additional experiments (runs 14 to 17) were conducted so that quadratic terms could be included in the model equations. Note that gel 16 was slightly cloudy (see Figure 4.5) and was not used in the parameter estimation:

$$DS = \mathbf{5.39 \cdot 10^{-3}} + \mathbf{2.13 \cdot 10^{-4}}[CTAB] - 1.44 \cdot 10^{-3}[LCV] + \mathbf{3.16 \cdot 10^{-5}}[TCE] + \mathbf{1.16 \cdot 10^{-4}}[CTAB][LCV] - 1.26 \cdot 10^{-6}[CTAB][TCE] + 3.72 \cdot 10^{-5}[LCV][TCE] + 8.99 \cdot 10^{-7}[CTAB][LCV][TCE] - 6.08 \cdot 10^{-6}[CTAB]^2 - 1.44 \cdot 10^{-3}[LCV]^2 - 1.71 \cdot 10^{-7}[TCE]^2 \quad (4.5)$$

$$A = \mathbf{-6.04 \cdot 10^{-3}} + \mathbf{1.23 \cdot 10^{-3}}[CTAB] + \mathbf{2.32 \cdot 10^{-2}}[LCV] - 7.41 \cdot 10^{-5}[TCE] - \mathbf{5.41 \cdot 10^{-3}}[CTAB][LCV] + 2.97 \cdot 10^{-6}[CTAB][TCE] - 1.21 \cdot 10^{-4}[LCV][TCE] + 4.37 \cdot 10^{-6}[CTAB][LCV][TCE] + 7.94 \cdot 10^{-5}[CTAB]^2 + 6.42 \cdot 10^{-2}[LCV]^2 + 1.00 \cdot 10^{-6}\,[TCE]^2 \quad (4.6)$$

The statistically significant parameters are bolded, and units are consistent with those in Table 4.11. As expected, [*TCE*] has a positive and significant influence on dose sensitivity, as does [*CTAB*]. The parameter corresponding to [*LCV*] is not statistically significant, but the interaction term between CTAB and LCV is significant, indicating that simultaneously increasing [*LCV*] and [*CTAB*] improves the dose sensitivity,

presumably due to a higher number of CTAB micelles that contain an appropriate number of LCV molecules.

Equations 4.5 and 4.6 were used to search for an optimized recipe using the objective function in equation 4.4. The following bounds were enforced during optimization: 9 mM ≤ [*CTAB*] ≤ 33 mM, 0.75mM ≤ [*LCV*] ≤1.25 mM, 40 mM ≤ [*TCE*] ≤ 120 mM. When ω= 3.362 Gy·cm selected so that the two terms in the objective function would have similar sizes, the recipe for gel 18 in Table 4.11 was selected when all parameters (significant and non-significant) in Equations (4.5) and (4.6) were used. The recipe for gel 19 was selected when only the significant parameters were used in the optimization. These two gels recipes are similar in that they have intermediate [*CTAB*], the lowest permissible value of [*LCV*] and high [*TCE*]. When ω= 33.62 Gy·cm was selected so that dose sensitivity would be more important to the optimizer than initial colour, the recipe for gel 20 was selected using both versions of the models in Equations (4.5) and (4.6). Gel 20 has the highest permissible values of [*CTAB*], [*LCV*] and [*TCE*]. Gels 18 to 20 were prepared and irradiated. As expected, gel 20 had the highest dose sensitivity obtained in the current study, but this gel was noticeably light blue in colour as shown in Figure 4.5. Gel 19 had high dose sensitivity and was nearly colourless, which makes it promising for 3D gel dosimetery. As a result, we recommend that this gel recipe should receive further study in large jars so that dose resolution, temporal and spatial stability and dose-rate sensitivity can be assessed.

Figure 4.5: Photograph of un-irradiated vials (23×85 mm clear glass) containing LCV-CTAB-TCE gels manufactured at varying concentrations of CTAB, LCV, and TCE as described in table 4.11. Vial numbers correspond to the sample numbers in table 4.11.

Table 4.11: Influence of CTAB, LCV and TCE on initial colour and dose sensitivity of LCV micelle gels. Concentrations of gelatin and TCAA were fixed at 4.0 wt% and 25.0 mM, respectively. Absorbance values were measured using a wavelength of 590 nm

#	CTAB [mM]	LCV [mM]	TCE [mM]	Turbidity	Initial Colour	Initial Absorbance	Dose Sensitivity [$Gy^{-1}.cm^{-1}$]	pH
1	9.0	0.75	40.0	Clear	No	0.026	$7.46 \cdot 10^{-3}$	3.32
2	9.0	0.75	80.0	Clear	No	0.026	$9.10 \cdot 10^{-3}$	3.31
3	9.0	1.25	40.0	Clear	No	0.025	$6.59 \cdot 10^{-3}$	3.29
4	9.0	1.25	80.0	Clear	No	0.025	$9.44 \cdot 10^{-3}$	3.32
5	25.0	0.75	40.0	Clear	No	0.028	$8.59 \cdot 10^{-3}$	3.30
6	25.0	0.75	80.0	Clear	No	0.028	$9.86 \cdot 10^{-3}$	3.29
7	25.0	1.25	40.0	Clear	No	0.029	$9.37 \cdot 10^{-3}$	3.29
8	25.0	1.25	80.0	Clear	Light Blue	0.042	$1.15 \cdot 10^{-2}$	3.33
9	17.0	1.0	60.0	Clear	No	0.030	$9.17 \cdot 10^{-3}$	3.27
10	17.0	1.0	60.0	Clear	No	0.029	$1.00 \cdot 10^{-2}$	3.22
11	17.0	1.0	60.0	Clear	No	0.030	$9.60 \cdot 10^{-3}$	3.30
12	17.0	1.0	60.0	Clear	No	0.030	$9.37 \cdot 10^{-3}$	3.29
13	17.0	1.0	60.0	Clear	No	0.029	$1.00 \cdot 10^{-2}$	3.30
14	25.0	1.25	120.0	Clear	Light Blue	0.045	$1.28 \cdot 10^{-2}$	3.30
15	33.0	1.25	100.0	Clear	Light Blue	0.04	$1.19 \cdot 10^{-2}$	3.30
16	33.0	1.5	100.0	Turbid	---	0.207	----	3.31
17	33.0	1.25	120.0	Clear	Light Blue	0.05	$1.30 \cdot 10^{-2}$	3.31
18	15.5	0.75	80.0	Clear	No	0.028	$1.03 \cdot 10^{-2}$	3.34
19	17.0	0.75	120.0	Clear	No	0.031	$1.13 \cdot 10^{-2}$	3.31
20	33.0	1.25	120.0	Clear	Light Blue	0.048	$1.38 \cdot 10^{-2}$	3.31

4.5.10 Results for preliminary experiments in large-jar phantoms

Calibration was performed by plotting depth dose optical density values from the calibration gel against ion-chamber water-tank dose measurements for the 12 MeV electron beam irradiation. Calibration data were fitted using a linear fit function (Figure 4.6a). The calibrated optical CT measurements are shown in Figure 4.6b. This calibration was applied to the VMAT prostate-plan gel irradiation (Figure 4.7a). Dose measurements for the VMAT plan gel showed that dose distribution information is maintained over more than two weeks (Figures 4.7b-d).

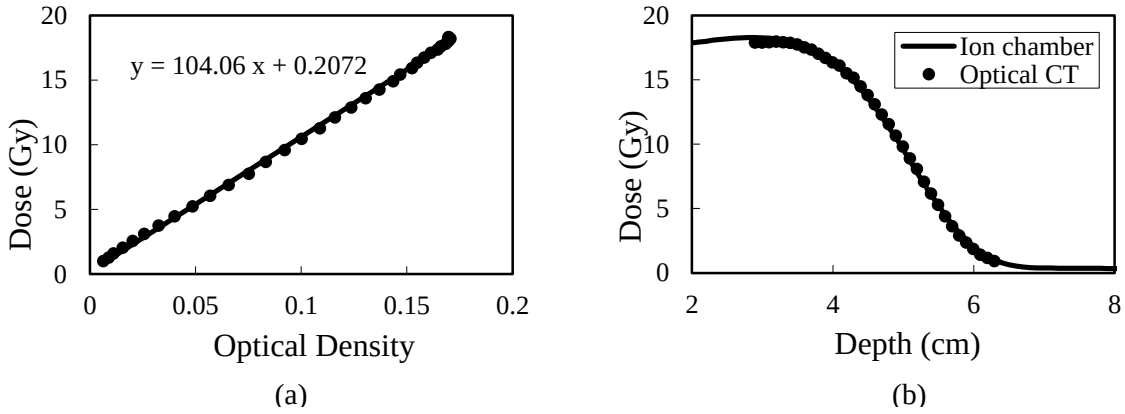

Figure 4.6: (a) Calibration data and fit function, which was applied to the VMAT plan gel. (b) Electron-beam depth-dose curve showing the Wellhofer ion chamber water tank measurements and data from the calibrated gel dosimeter.

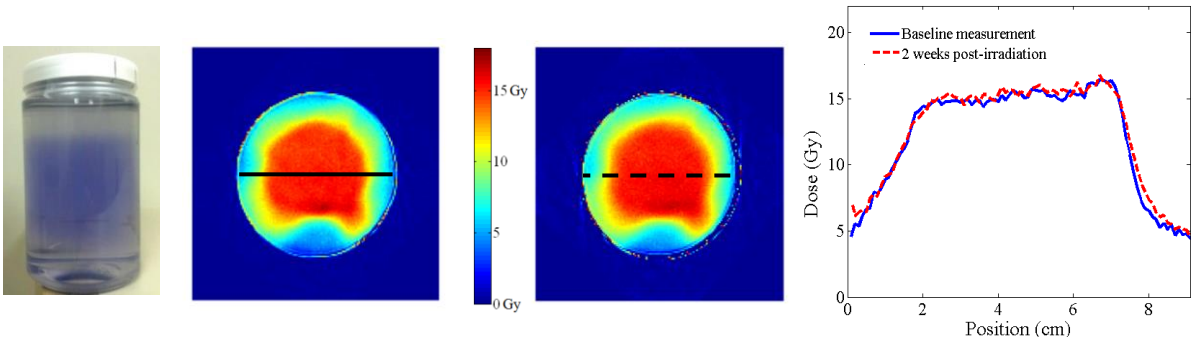

(a) (b) (c) (d)

Figure 4.7: (a) Photograph of a VMAT prostate plan irradiation in a LCV micelle jar of gel. (b) Dose map of one slice of the gel dosimeter, imaged 30 min. after irradiation (baseline measurement). (c) Dose map of the same slice of the gel dosimeter, imaged 2 weeks after irradiation. (d) Cross-plane profiles of the gel slices in (b) and (c) showing gel dosimeter stability after two weeks.

4.6 Conclusions

Radio-chromic leuco dye micelle gels (Jordan and Avvakumov 2009, Babic *et al.* 2009) are promising because they are suitable for optical readout and because they have superior spatial stability compared to FX Fricke gels. Jordan's standard LCV gel (Babic *et al.* 2009) was reproduced multiple times following the original manufacturing procedure and a modified procedure that cuts the manufacturing time in half, with no significant effect on dose sensitivity. The average dose sensitivity measured in the current study is in good agreement with the value reported by Babic *et al.* (2009) in Figure 5 of their article. Tests confirmed that Jordan's standard LCV gel has negligible dose-rate dependency over the range from 100 to 600 cGy min^{-1}.

A study on LCV micelle gels was conducted to gain a deeper understanding of the interactions between the various gel components in an effort to develop recipes with improved dose sensitivity. Dose sensitivity increased with increasing Tx100

concentration but the initial colour of the un-irradiated gels also increased, which may cause complications during optical scanning. When the Tx100 surfactant was replaced by CTAB, lower dose sensitivity was obtained and gels were colourless prior to irradiation.

Dose sensitivity of LCV micelle gels was compared using two different acids (TCAA and H_2SO_4) at a variety of concentrations. Gels produced using TCAA had higher dose sensitivities, presumably because of the sensitizing effect of the chlorine atoms in TCAA. Maximum dose sensitivity was obtained using 21.5 mM TCAA, which corresponded to a pH of 3.6. Turbid gels were produced when high LCV concentrations were used along with low concentrations of TCAA.

The effects of three halogenated compounds (chloroform, TCE, and TCMPH) on dose sensitivity were tested. TCE was the most effective at improving the dose sensitivity and is preferable to chloroform because it is less volatile and less toxic. Optimization of the recipe for LCV micelle gels made with Tx100 and TCE was aided by a two-level three-factor designed experiment. The resulting empirical model was used to select a recipe that improved the dose sensitivity by a factor of two, but the un-irradiated gel had a noticeable blue colour, which might be too dark for optical readout in larger phantoms. Optimized LCV gels made with CTAB and TCE showed improved dose sensitivities and were almost colourless gels before irradiation. The proposed optimal recipe contains 0.75 mM LCV, 17 mM CTAB, 120 mM TCE, 25.0 mM TCAA and 4 wt% gelatin. The dose sensitivity for this recipe is 1.5 times that of Jordan's standard LCV gel and the initial colour is lower. Preliminary experiments were conducted to examine the response of the optimized gel to spatially non-uniform radiation in 1 L jars and the results showed that dose distribution information is maintained for over two weeks. Further testing in large

phantoms is required to quantify the spatial and temporal stability of the proposed gel, along with its dose resolution and dose-rate behaviour.

4.7 Acknowledgments

This work was funded by the Canadian Institutes for Health Research (CIHR). The authors would like to thank Dr. Kevin Jordan from the London Health Sciences Centre for providing his detailed description of the manufacturing procedure for LCV micelle gels and for useful discussions.

4.8 Nomenclature

Abbreviation	
3D	three-Dimensional
CT	Computed Tomography
CTAB	Cetyl Trimethyl Ammonium Bromide
FX	Ferrous Xylenol-orange Fricke gel
LCV	Leuco Crystal Violet
LMG	Leuco Malachite Green
MRI	Magnetic Resonance Imaging
NIPAM	N-isopropyl acrylamide
NMR	Nuclear Magnetic Resonance
PAG	PolyAcrylamide Gels
SDS	Sodium Dodecyl Sulfate
TCAA	TriChloro Acetic Acid
TCE	2,2,2-TriChloroEthanol
TCMPH	1,1,1-TriChloro-2-Methyl-2-Propanol Hemihydrate
Tx100	Triton x-100

4.9 References for chapter 4

Adamovics JA 2006 three dimensional dosimeter for penetrating radiation and method of use *United States Patent # US 7098463B2*.

Adamovics J and Maryanski M 2006 Charaterisation of PRESAGE: a new 3D radio chromic solid polymer dosimeter for ionizing radiation *Radiation Protection Dosimetry.* **120** 107–112

Appleby A, Christman EA and Leghrouz A 1987 Imaging of spatial radiation dose distribution in agarose gels using magnetic resonance. *Med. Phys.* **14** 382-384.

Babic S, Battista J and Jordan K 2009 Radiochromic leuco dye micelle hydrogels: II. Low diffusion rate leuco crystal violet gel *Phys. Med. Biol.* **54** 6791–6808.

Baldock C, De Deene Y, Doran S, Ibbott G, Jirasek A, Lepage M, McAuley KB, Oldham M, and Schreiner LJ 2010 Polymer gel dosimetry *Phys. Med. Biol.* **55** 1–63.

Brown S, Venning A, De Deene Y, Vial P, Oliver L, Adamovics J, Baldock C 2008 Radiological properties of the PRESAGE and PAGAT polymer dosimeters. *Applied Radiation and Isotopes* **66** 1970–1974.

Chain JNM, Jirasek A, Schreiner LJ and McAuley KB 2011a Cosolvent-free polymer gel dosimeters with improved dose sensitivity and resolution for x-ray CT dose response *Phys. Med. Biol.* **56** 2091-2102.

Chain JNM, Nasr AT, Schreiner LJ and McAuley KB 2011b Mathematical Modeling of Depth-Dose Response of Polymer-Gel Dosimeters *Macromol. Theory Simul.* **20** 735–751.

Ceberg S, Gagne I, Gustafsson H, Scherman JB, Korreman SS, Kjaer-Kristoffersen F, Hilts M, and Back SJ 2010 RapidArc treatment verification in 3D using polymer gel dosimetry and Monte Carlo simulation *Phys. Med. Biol.* **55** 4885–4898

Cui X, Mao S, Liu M, Yuan H, and Du Y 2008 Mechanism of Surfactant Micelle Formation *Langmuir* **24** 10771-10775

De Deene Y, Venning A, Hurley C, Healy BJ and Baldock C 2002a Dose–response stability and integrity of the dose distribution of various polymer gel dosimeters *Phys. Med. Biol.* **47** 2459–2470

De Deene Y, Hurley C, Venning A, Vergote K, Mather M, Healy BJ and Baldock C 2002b A basic study of some normoxic polymer gel dosimeters *Phys. Med. Biol.* **47** 3441–3463.

De Deene Y 2004 Essential characteristics of polymer gel dosimeters J. Physics. Conference Series 3, 34–57.

Doran SJ 2009 The history and principles of optical computed tomography for scanning 3-D radiation dosimeters:2008 update *Journal of Physics:Conference Series* **164**, 012020.

Duplatre G, Marques F, and da Gracüa M 1996 Size of Sodium Dodecyl Sulfate Micelles in Aqueous Solutions as Studied by Positron Annihilation Lifetime Spectroscopy *J. Phys. Chem.* **100** 16608-16612

Evans DF and Wennerstrom H 1999 The Colloidal Domain, 2nd edition, *Wiley-VCH, NY, USA.*

Fuxman AM, McAuley KB and Schreiner LJ 2005 Modeling of polyacrylamide gel dosimeters with spatially non-uniform radiation dose distributions *Chem. Eng. Sci.* **60**, 1277-9337.

Gore JC, Kangt YS and Schulz RJ 1984 Measurement of radiation dose distributions by nuclear magnetic resonance (NMR) imaging *Phys. Med. Biol.* **29** 1189-1197.

Guo PY, Adamovics JA and Oldham M 2006 Characterization of a new radiochromic three-dimensional dosimeter *Med. Phys.* **33** 1338-1345.

Hurley C, McLucas C, Pedrazzini G and Baldock C 2006 High-resolution gel dosimetry of a HDR brachytherapy source using normoxic polymer gel dosimeters: Preliminary study *Nuclear Instruments and Methods in Physics Research A* **565** 801–811.

Jirasek A, Hilts M, Shaw C and Baxter P 2006 Investigation of tetrakis hydroxymethyl phosphonium chloride as an antioxidant for use in x-ray computed tomography polyacrylamide gel dosimetry *Phys. Med. Biol.* **51** 1891–1906.

Jirasek A, Hilts M and McAuley KB 2010 Polymer gel dosimeters with enhanced sensitivity for use in x-ray CT polymer gel dosimetry *Phys. Med. Biol.* **55** 5269-5281.

Jordan K and Avvakumov N 2009 Radiochromic leuco dye micelle hydrogels: I. Initial investigation *Phys. Med. Biol.* **54** 6773–6789.

Jordan K 2013 (January) Private communication.

Koeva VI, Olding T, Jirasek A, Schreiner LJ and McAuley KB 2009a Preliminary investigation of the NMR, optical and x-ray CT dose–response of polymer gel

dosimeters incorporating cosolvents to improve dose sensitivity *Phys. Med. Biol.* **54** 2779-2790.

Koeva VI, Daneshvar S, Senden RJ, Imam AHM, Schreiner LJ and McAuley KB 2009b Mathematical Modeling of PAG- and NIPAM Based Polymer Gel Dosimeters Contaminated by Oxygen and Inhibitor *Macromol. Theory Simul.* **18** 495-510.

Laidler KJ, Meiser JH, and Sanctuary BC 2003 Physical Chemistry, 4th edition, *Houghton Mifflin company, Boston, NY, USA.*

Mans A, Remeijer P, Olaciregui-Ruiz I, Wendling M, Sonke JJ, Mijnheer B, van Herk M, and Stroom JC 2010 3D Dosimetric verification of volumetric-modulated arc therapy by portal dosimetry *Radiotherapy and Oncology* **94** 181–187

Maryanski MJ, J. C. Gore JC, Kennan RP and Schulz RJ 1993 NMR relaxation enhancement in gels polymerized and cross-linked by ionizing radiation: a new approach to 3D dosimetry by MRI *Magn. Reson. Imaging.* **11** 253–258.

Maryanski MJ, Schulz RJ, Ibbott GS, Gatenby JC, Xie J, Horton D and Gore JC 1994 Magnetic resonance imaging of radiation dose distributions using a polymer-gel dosimeter *Phys. Med. Biol.* **39** 1437–1455.

McAuley KB 2004 The chemistry and physics of polyacrylamide gel dosimeters: why they do and don't work *Journal of Physics:Conference Series* **3** 29–33.

McLaughlin W 1970 Films, Dyes, and Photographic Systems *Manual on Radiation Dosimetry* ed. Holm NW and Berry RJ (Marcel Dekker INC. New York) p 129

Mijnheer B, Mans A, Olaciregui-Ruiz I, Sonke JJ, Tielenburg R, van Herk M, Vijlbrief R, Stroom J 2010 2D AND 3D dose verification at The Netherlands Cancer

Institute-Antoni van Leeuwenhoek Hospital using EPIDs *Journal of Physics: Conference Series* **250** 012020

Nasr AT, Schreiner LJ and McAuley KB 2012 Mathematical Modeling of the Response of Polymer Gel Dosimeters to HDR and LDR Brachytherapy Radiation *Macromol. Theory Simul.* **21** 36–51.

Nasr AT, Olding T, Schreiner LJ, and McAuley KB 2013 Evaluation of the potential for diacetylenes as reporter molecules in 3D micelle gel dosimetry *Phys. Med. Biol.* **58** 787–805

Neilson C, Klein M, Barnett R, and Yartsev S 2013 Delivery quality assurance with ArcCHECK *Medical Dosimetry* **38** 77-80

Neugebauer J 1990 Detergents: an overview *Methods in Enzymology* **182** 239-253

Olding T, Holmes O, DeJean P, McAuley KB, Nkongchu K, Santyr G and Schreiner LJ 2011 Small field dose delivery evaluations using cone beam optical computed tomography-based polymer gel dosimetry *Journal of Medical Physics.* **36** 3-14.

Olding T, Garcia L, Alexander K, Schreiner LJ, and Joshi C 2013 Stereotactic body radiation therapy delivery validation *Journal of Physics: Conference Series* **444** 012073

Pappas E 2009 On the role of polymer gels in the dosimetry of small photon fields used in radiotherapy *Journal of Physics: Conference Series* **164** 012060

Paradies H 1980 Shape and Size of a Nonionic Surfactant Micelle. Triton X-100 in Aqueous Solution *J. Phys. Chem.* **84** 599-607

Penev K.I. and K. Mequanint 2013 Controlling sensitivity and stability of ferrous-xylenol orange-gelatin 3D gel dosimeters by doping with phenanthroline-type ligands and glyoxal *Phys. Med. Biol.* **58** 1823–1838

Schreiner LJ 2004 Review of Fricke gel dosimeters *J. Physics. Conference Series* **3**, 9-21.

Schreiner LJ 2009 Where does gel dosimetry fit in the clinic? *Journal of Physics: Conference Series* **164** 012001

Schreiner LJ 2011 On the quality assurance and verification of modern radiation therapy treatment *Journal of Medical Physics*, **36-4** 189-91

Schreiner LJ, Olding T, and Darko J 2011 Development of in-house process QA in modern radiation therapy *Proc. Internat. Symp. Standards, Applications and Quality Assurance in Medical Radiation Dosimetry (IDOS) (IAEA Vienna, Austria November 9–12 2010)* **2** 197-205

SciFinder website (Nov. 2013) Leucocrystal Violet, CAS Registry Number: 603-48-5 *https://scifinder.cas.org/scifinder/view/scifinder/scifinderExplore.jsf*

Sedaghat M, Bujold R and Lepage M 2011 Severe dose inaccuracies caused by an oxygen-antioxidant imbalance in normoxic polymer gel dosimeters *Phys. Med. Biol.* **56** 601–625

Senden RJ, De Jean P, McAuley KB and Schreiner LJ 2006 Polymer gel dosimeters with reduced toxicity: a preliminary investigation of the NMR and optical dose–response using different monomers *Phys. Med. Biol.* **51**, 3301–3314.

Sigma-Aldrich (Nov. 2013) MSDS for chloroform, 2,2,2-Trichloroethanol and 1,1,1-Trichloro-2-methyl-2-propanol hemihydrate. http://www.sigmaaldrich.com/canada-english.html

Storm S, Jakobtorweihen S, Smirnova I, and Panagiotopoulos AZ 2013 Molecular Dynamics Simulation of SDS and CTAB Micellization and Prediction of Partition Equilibria with COSMOmic *Langmuir* **29** 11582−11592

Vandecasteele J, Ghysel S, Baete SH and De Deene Y 2011 Radio-physical properties of micelle leucodye 3D integrating gel dosimeters *Phys. Med. Biol.* **56** 627–651.

Vergote K, De Deene Y, Vanden Bussche E and De Wagter C 2004 On the relation between the spatial dose integrity and the temporal instability of polymer gel dosimeters *Phys. Med. Biol.* **49** 4507-4522.

Chapter 5

Conclusions and Recommendations

5.1 Conclusions

In Chapter 2 of this thesis, a dynamic model was developed to simulate the response of PAG dosimeters to a single spherical brachytherapy seed. Simulations were conducted for a HDR seed using ^{192}Ir implanted for one minute and for a LDR seed using ^{125}I implanted permanently. Responses of PAG dosimeters were expressed in terms of the amount of polymer formed, crosslink density, and volume fraction of aqueous phase as a function of radial distance and time. To study the effect of diffusion of monomer and crosslinker molecules on the responses of PAG dosimeters to HDR and LDR seeds, simulations were also conducted for a series of uniformly-irradiated calibration vials. Concentration gradients in uniformly-irradiated vials are zero and no diffusion occurs. Consequently, the response of PAG in uniformly-irradiated vials will account for the time-varying kinetic response of polymer gels, but not the variation caused by diffusion. Simulation results show that:

- Monomer and crosslinker concentration profiles are much flatter in the LDR simulations than in the HDR simulations because acrylamide and bisacrylamide are consumed more slowly in LDR brachytherapy dosimetry and have more time to diffuse.
- There are large deviations between the phantom irradiated by the LDR brachytherapy seed and simulated calibration vials in terms of the amount of polymer formed per Gy, the crosslink density, and the volume fraction of aqueous phase at a particular absorbed dose. Consequently, it is not recommend

to use PAG dosimeters or any other polymer gel dosimeter with diffusing monomers for application to LDR brachytherapy

- There is a very good match between simulation results for the phantom containing the HDR seed and the uniformly-irradiated vials in the three responses (amount of polymer, crosslink density and volume fraction of aqueous phase) for all distances larger than 4 mm from the centre of the seed.
- Closer to the seed, deviations between the simulated HDR phantom and the vials increase due to the large dose rate near seed and the diffusion that occurs.

In Chapter 3 of this thesis, the use of the diacetylene PCDA as a potential reporter molecule in radiochromic micelle gel dosimeters was evaluated. Gels containing PCDA and SDS changed from colourless to blue in response to irradiation. Unfortunately, all gels that changed colour in response to radiation were turbid prior to and after irradiation, which makes them unsuitable for optical CT readout. SDS precipitation at temperatures below its Kraft temperature was investigated as a potential cause for turbidity of PCDA gels. It was concluded that the addition of gelatin stopped or postponed the SDS precipitation and that the turbidity of PCDA gels appears to be caused by PCDA precipitation. Different techniques were used successfully to increase the gel stability and prevent PCDA precipitation, but unfortunately none of the gels that remained transparent responded to radiation. These results suggest that the colour change observed in PCDA micelle dosimeters is due to oligomerization within solid PCDA particles, rather than oligomerization of PCDA molecules solubilized in micelles. Note that gels were also prepared using two additional diacetylenes (DPBD and HD) and that poor results were also obtained using these potential reporter molecules. Since turbid gels are undesirable

for optical CT readout, the use of PCDA as the reporter molecule in micelle gels is not promising.

In Chapter 4 of this thesis, a new recipe for an improved LCV micelle gel dosimeter was developed. Experiments were conducted to gain deeper understanding of the interactions between the components of LCV micelle gel dosimeters in order to develop the improved recipe. Gel reproducibility and dose rate dependence of Jordan's standard LCV gel was tested. Effects of surfactant type, surfactant concentration, acid type, and acid concentration on dose sensitivity and turbidity of LCV micelle gels were studied. Sensitizing effects of chlorinated compounds were also investigated in this chapter. Empirical models were developed to optimize the recipe of LCV micelle gels. Experimental results show that:

- The average dose sensitivity obtained was about half of the highest value reported by Babic *et al.* (2009) in Figure 5 of their article. The reason for this discrepancy is unclear and may be related to temperature at the time of irradiation, which is important for obtaining reproducible dose sensitivity.
- Jordan's standard LCV gel has negligible dose rate dependency over the range of 100 to 600 cGy.min-1.
- Turbidity of LCV micelle gels appears to be related to solubility of LCV which is strongly affected by the pH of the gel. Surfactant type and concentration appear to have less influence on the turbidity of LCV micelle gels for the recipes tested.
- Dose sensitivity increased with increasing Tx100 concentration, but the initial blue colour of the un-irradiated gels also increased with increasing Tx100

concentration, which may cause complications during optical scanning of larger phantoms.

- Replacing Tx100 with CTAB at different concentrations reduced the dose sensitivity of LCV micelle gels. However, all gels manufactured with CTAB showed no noticeable initial colour.
- All gels attempted with SDS at different concentrations (when the concentrations of the other components were fixed at that in Jordan's standard LCV gel) were turbid and sticky, which makes them unsuitable for optical readout
- LCV micelle gels manufactured using TCAA showed higher dose sensitivity than gels made with H2SO4, presumably because of the sensitizing effect of the chlorine atoms in TCAA. Moreover, the concentration of TCAA strongly influenced dose sensitivity in a nonlinear fashion, with a maximum dose sensitivity obtained at a pH of 3.6, which corresponds to a concentration of 21.5 mM TCAA.
- An experiment was carefully planned (using different gelatin concentrations) to separate the effect of TCAA concentration from the effect of pH on dose sensitivity and gel turbidity. Results show that pH, rather than TCAA concentration, is the dominant factor for achieving high dose sensitivity and transparency of LCV micelle gels.
- Among the three tested halogenated compounds (chloroform, TCE, and TCMPH), TCE was the most effective at improving the dose sensitivity and is also preferable to chloroform because it is less volatile and less toxic.

- The optimized recipe of LCV micelle gels made using TCE and Tx100 resulted in noticeably coloured gel prior to irradiation, which may cause some complications for optical readout of larger phantoms.
- Gels made with LCV, TCE and CTAB showed improved dose sensitivities and were almost colourless gels prior to irradiation.
- The suggested optimized recipe contains 17 mM CTAB, 0.75 mM LCV, 120 mM TCE, 25.0 mM TCAA and 4 wt% gelatin. This recipe gives a dose sensitivity that is 1.5 times higher than the sensitivity of Jordan's standard LCV gel. The optimized gel has no noticeable blue colour prior to irradiation.
- Preliminary results showed that the dose distribution information was maintained for over two weeks when the optimized gel, made in a 1 L jar, was exposed to spatially non-uniform irradiation.

5.2 Recommendations

The following recommendations are made for further research on modeling the response of polymer gels dosimeters to radioactive brachytherapy seeds:

- The model should be extended to simulate the response of polymer gel dosimeters to cylindrical brachytherapy seeds because commercial seeds tend to be more cylindrical than spherical in shape.
- Experiments and simulations should be performed using a variety of clinical HDR radioactive brachytherapy seeds and the results should be compared to further verify the model predictions so that additional information can be obtained regarding the effectiveness of polymer gels for practical quality assurance of brachytherapy treatments.
- For the same reasons, the model should be further extended to simulate the response of polymer gel dosimeters to multiple HDR brachytherapy seeds.
- Further experiments could be conducted to investigate the possibility of developing empirical models that relate the amount of polymer formed to the usual clinical read-out variables such as R_2. If such correlations are possible then the fundamental model should be extended to include them.

Results in Chapter 3 show that the use of PCDA and other diacetylenes as reporter molecules in micelle gel dosimeters is not recommended. However, we recommend that other radiochromic reporter molecules should be evaluated for use in micelle gel dosimeters. Unlike traditional gel dosimeters in which the reporter molecules need to be water soluble, introducing micelles to the gel phantom enables the use of wider range of hydrophobic reporter molecules. In fact, reporter molecules that have very low or

negligible water solubility will help to reduce diffusion and to improve spatial stability. Reporter molecules that require close packing or a special orientation in the solid phase to produce a dosimetric response will likely not be suitable for use in micelle gel dosimeters.

Based on the results in Chapter 4, the following recommendations are made for further research on LCV micelle gels:

- Further testing of LCV micelle gels made with CTAB and TCE in large phantoms is required to check the spatial stability (in terms of diffusion of coloured molecules) and temporal stability (in terms of colour fading of uniformly irradiated vials and colour formation in un-irradiated vials) of the proposed gel, along with its dose resolution, tissue equivalence, and dose-rate behaviour.
- The effect of the manufacturing procedure on the proposed gel behavior should be tested in terms of temperature during manufacturing and the order of addition of the different components.
- Other leuco-dye reporter molecules should be tested because they may result in better gels than the proposed LCV micelle gel.
- A more extensive search should be done of the suitability of other surfactants for radiochromic micelle gel dosimeters.
- More experiments could be conducted to study the effect of using bovine gelatin versus porcine gelatin on the performance of micelle gel dosimeters. Also, there may be an opportunity to reduce the gelatin concentration to below 4 wt% if low gelatin levels are associated with better optical readout.

- Experimental evaluation of the response of LCV micelle gels to HDR and LDR brachytherapy irradiation should be conducted.

Appendix A

Decision on parameter statistical significance

Statistical significance of parameters was judged based on the calculated 95% confidence interval for each parameter. Parameter confidence intervals were calculated using (Montgomery and Runger 2007):

$$\hat{\beta}_i \pm t_{\nu,\alpha/2} s_{\hat{\beta}_i}$$

Where:

$\hat{\beta}_i$ is the i-th parameter estimate,

$t_{\nu,\alpha/2}$ is a coefficient obtained from t distribution with α=0.05 and ν degrees of freedom.

$s_{\hat{\beta}_i}$ is the standard deviation of the parameter estimate.

Standard deviations of the parameter estimates were obtained from the square roots of the corresponding diagonal elements of the parameter covariance matrix, which was determined from:

$$(X^T X)^{-1}\sigma^2$$

using an estimate of the noise variance σ^2. The noise variance was calculated as a pooled variance using two different replicate data sets: Jordan's standard LCV gel replicates (25 experiments) and replicates at or near the central point (3 for Tx100 gels and 5 for CTAB gels) of the factorial designed experiments. The X matrix that corresponds to the Tx100 experiments (gels 1-11 in Table 4.9) is:

$$X = \begin{bmatrix} 1 & -1 & -1 & -1 & 1 & 1 & 1 & -1 \\ 1 & -1 & -1 & 1 & 1 & -1 & -1 & 1 \\ 1 & -1 & 1 & -1 & -1 & 1 & -1 & 1 \\ 1 & -1 & 1 & 1 & -1 & -1 & 1 & -1 \\ 1 & 1 & -1 & -1 & -1 & -1 & 1 & 1 \\ 1 & 1 & -1 & 1 & -1 & 1 & -1 & -1 \\ 1 & 1 & 1 & -1 & 1 & -1 & -1 & -1 \\ 1 & 1 & 1 & 1 & 1 & 1 & 1 & 1 \\ 1 & -0.43 & 0 & 0 & 0 & 0 & 0 & 0 \\ 1 & -0.43 & 0 & 0 & 0 & 0 & 0 & 0 \\ 1 & -0.43 & 0 & 0 & 0 & 0 & 0 & 0 \end{bmatrix}$$

and the X matrix that corresponds to the CTAB experiments (gels 1-15 and 17 in Table 4.11) is:

$$X = \begin{bmatrix} 1 & -1 & -1 & -1 & 1 & 1 & 1 & -1 \\ 1 & -1 & -1 & 1 & 1 & -1 & -1 & 1 \\ 1 & -1 & 1 & -1 & -1 & 1 & -1 & 1 \\ 1 & -1 & 1 & 1 & -1 & -1 & 1 & -1 \\ 1 & 1 & -1 & -1 & -1 & -1 & 1 & 1 \\ 1 & 1 & -1 & 1 & -1 & 1 & -1 & -1 \\ 1 & 1 & 1 & -1 & 1 & -1 & -1 & -1 \\ 1 & 1 & 1 & 1 & 1 & 1 & 1 & 1 \\ 1 & 0 & 0 & 0 & 0 & 0 & 0 & 0 \\ 1 & 0 & 0 & 0 & 0 & 0 & 0 & 0 \\ 1 & 0 & 0 & 0 & 0 & 0 & 0 & 0 \\ 1 & 0 & 0 & 0 & 0 & 0 & 0 & 0 \\ 1 & 0 & 0 & 0 & 0 & 0 & 0 & 0 \\ 1 & 1 & 1 & 3 & 1 & 3 & 3 & 3 \\ 1 & 2 & 1 & 2 & 2 & 4 & 2 & 4 \\ 1 & 2 & 1 & 3 & 2 & 6 & 3 & 6 \end{bmatrix}$$

The parameters were estimated using these coded experimental settings and then the models were transformed into the versions shown in equations 4.2 and 4.3 for Tx100 gels and equations 4.5 and 4.6 for CTAB gels.

References for appendix A

Montgomery DC and Runger GC 2007 Applied Statistics and Probability for Engineers *John Wiley & Sos, Inc USA*

Appendix B

Preliminary models for LCV gels made with TCE and CTAB

Preliminary models were fitted for dose sensitivity and initial absorbance at 590 nm as functions of [*CTAB*], [*LCV*], and [*TCE*] using the data from the full factorial design shown in Table 4.11 (runs 1 to 8) and five replicates at the central point (runs 9 to 13). The resulting model equations are:

$$DS = \mathbf{1.02 \cdot 10^{-2}} - \mathbf{9.89 \cdot 10^{-5}}[CTAB] - 6.57 \cdot 10^{-3}[LCV] - \mathbf{8.48 \cdot 10^{-6}}[TCE]$$
$$+ \mathbf{2.57 \cdot 10^{-4}}[CTAB][LCV] + 3.29 \cdot 10^{-7}[CTAB][TCE]$$
$$+ 7.28 \cdot 10^{-5}[LCV][TCE] - 1.23 \cdot 10^{-6}[CTAB][LCV][TCE] \quad (B.1)$$

$$A = \mathbf{-8.65 \cdot 10^{-2}} + 3.91 \cdot 10^{-3}[CTAB] + \mathbf{1.46 \cdot 10^{-1}}[LCV] - 1.41 \cdot 10^{-5}[TCE]$$
$$- \mathbf{5.37 \cdot 10^{-3}}[CTAB][LCV] + 1.56 \cdot 10^{-6}[CTAB][TCE]$$
$$- 5.63 \cdot 10^{-5}[LCV][TCE] + 6.25 \cdot 10^{-6}\,[CTAB][LCV][TCE] \quad (B.2)$$

Units for *DS*, *A*, [*CTAB*], [*LCV*] and [*TCE*] in equations (B.1) and (B.2) are provided in Table 4.11.